

ABSTRACT

Wen, Haifang. Fatigue Performance Evaluation of WesTrack Asphalt Mixtures Based on Viscoelastic Analysis of Indirect Tensile Test (under the direction of Dr. Y. R. Kim).

This dissertation presents the viscoelastic characterization of asphalt concrete in indirect tensile testing and the development of a simple performance test for fatigue cracking. The analytical solutions to calculate creep compliance and center strain from displacements measured on the specimen surface were developed based upon the theory of viscoelasticity. These developments were verified by 3-D finite element viscoelastic analysis and tests. A simple performance test was developed based on these solutions and work potential theory. To evaluate its validity, the indirect tensile tests were performed on WesTrack asphalt mixtures varying aggregate gradations, asphalt contents, and air void contents. Fracture energy obtained from indirect tensile strength testing and creep testing was highly correlated with field performance of these mixtures at WesTrack. A combination of indirect tensile creep and strength testing was proposed as a simple performance test for fatigue cracking. Recommendations for expanding the applicability of the simple performance test developed are provided.

**FATIGUE PERFORMANCE EVALUATION OF
WESTRACK ASPHALT MIXTURES BASED ON
VISCOELASTIC ANALYSIS OF INDIRECT TENSILE TEST**

by

HAFIANG WEN

A dissertation submitted to the Graduate Faculty of
North Carolina State University
in partial fulfillment of the
requirements for the degree of
Doctor of Philosophy

DEPARTMENT OF CIVIL ENGINEERING

Raleigh, North Carolina

2001

APPROVED BY

Dr. Y.R. Kim
Chair of Advisory Committee

Dr. A.A. Tayebali

Dr. T. Hassan

Dr. M. N. Guddati

BIOGRAPHY

Haifang Wen was born in 1974 in Dongying, Shandong, CHINA where he spent his happy childhood. At the age of 14 years old, Haifang Wen joined Dongying High School, living far from his parents. In 1991, Haifang graduated from high school and was admitted to Shangdong University of Technology, Jinan, ShanDong, majoring in civil engineering with emphasis on highway engineering. In 1995, Haifang Wen attended the graduate school of Southeastern University, Nanjing, Jiangsu for his Master degree. The subject of thesis is “the application of soil stabilization to pavement base courses”. Haifang Wen was awarded M.S. degree in 1998 and continued his study in America in pursuit of PhD degree under the direction of Dr. Y. R. Kim.

Acknowledgements

Special thanks go to my advisor, Dr. Y. R. Kim, for his guidance during my study and research. Special thanks also go to Dr. Tayebali, Dr. Guddati, and Dr. Hassan for providing assistance and serving as committee member and Dr. Li'an Xie for serving as Graduate School representative. I also have to acknowledge the help and support from Dr. Yiping Qiu with Textile College. The acknowledgements also go to North Carolina Department of Transportation and Federal Highway for funding the research.

Cordial thanks go to my family: Mom, Dad, three older brothers and one older sister, for their continuous support and care. Brother, Bin Wen with Northwestern University, always offers me understanding and great advices for my study and life. This dissertation is dedicated to Liying Yue who always shares my happiness and helps me pass the tough time during the study at NC State. With her, the period at Raleigh becomes valuable in my life.

I really appreciate the time of staying with Yanqing Zhao, Zhen Feng, and Bing Xu. I also appreciate the input from other members of research group. The friendship with Xiangyang Lv, Wanxi and Xinxin, and Chuyang Zhang, is so enjoyable. I will miss the time of playing basketball at NC State with basketball fans friends.

TABLE OF CONTENTS

LIST OF TABLES.....	vii
LIST OF FIGURES.....	viii
CHAPTER	
1. INTRODUCTION.....	1
1.1 Needs.....	1
1.2 Objective and Significance.....	5
2. LITERATURE REVIEW.....	7
2.1 Development of Simple Performance Test for Fatigue Cracking	7
2.2 Indirect Tensile Test	11
2.3 Mechanical Approaches for Characterizing Asphalt Concrete Fatigue Behavior	14
2.3.1 Phenomenological Approach	14
2.3.2 Mechanical Approach	15
3. THEORETICAL BACKGROUND.....	24
3.1 Elastic Solution of Stress in Indirect Tension Test	24
3.2 Theory of Viscoelasticity	30
3.3 Damage Mechanics	33
4. MATERIALS AND TESTING PROGRAMS.....	38
4.1 Material	38
4.1.1 North Carolina Mix	38

4.1.2	WesTrack Mix	43
4.1.3	Field Cores	47
4.2	Test Configuration	55
4.3	Test Program	60
5.	DETERMINATION OF VISCOELASTIC PROPERTIES	66
5.1	Development of Creep Compliance Calculation Method for Indirect Tension Specimen	67
5.2	Determination of Center Point Strain From Horizontal Deformation Measurement	73
5.3	Verification Using Finite Element Viscoelastic Analysis	75
5.3.1	Verification of Creep Compliance Calculation Method	75
5.3.2	Verification of Calculation of Center Strain Using Finite Element Method	80
5.3.3	Verification Using Uniaxial Direct Tension Test and Indirect Tension Test	81
5.4	Application of Theory of Viscoelasticity to Indirect Tension Specimen	87
5.4.1	Creep Compliance Test	87
5.4.2	Cyclic Test and Pseudo-strain Calculation	93
5.5	Effect of Specimen Geometry	100
6.	DEVLEOPMENT OF SIMPLE PERFORMNACE TEST AND VALIDATION	110
6.1	WesTrack Field Performance	110

6.2 Laboratory Investigation of Westrack Mixtures	112
6.3 Validation of Development of Simple Performance Test	124
6.3.1 Fine Gradation Mixtures.....	125
6.3.2 Coarse Gradation Mixtures	127
6.3.3 Fine and Coarse Gradation Mixtures.....	127
7. CONCLUSIONS AND RECOMMENDATIONS	134
REFERENCES.....	138
APPENDICES.....	140
A. Mixing and Compaction.....	140
B. MATLAB Codes.....	141

LISTS OF TABLES

Table 4.1	Aggregate Gradation of North Carolina Mix.....	39
Table 4.2	Factorial Experiment Design of WesTrack	46
Table 4.3	Aggregate Gradation of WesTrack Coarse Mixes.....	48
Table 4.4	Aggregate Gradation of WesTrack Fine Mixes.....	49
Table 4.5	Theoretical Maximum Specific Gravity of WesTrack Mixtures.....	49
Table 4.6	Compaction Efforts for WesTrack Mixtures Selected.....	50
Table 4.7	Comparison of Air Void Measurement Using SSD and CoreLok.....	54
Table 5.1	Coefficients Used to Calculate Poisson's Ratio and Creep Compliance...72	
Table 5.2	Coefficients in Equation (5.19).....	74
Table 5.3	Coefficients in a Prony Series Representation of E(t).....	79
Table 5.4	Creep Test Parameters.....	87
Table 5.5	Non-linear Regression Results of Equation (5.32) Coefficients of a Particular Mix	94
Table 5.6	Prony Series Coefficients of Relaxation Modulus for a Particular Mix...97	
Table 6.1	Traffic Volume Experimented by the Mixtures.....	125
Table 6.2	Regression Coefficients in Equation (6.2)	133

LISTS OF FIGURES

Figure 2.1	Haversine Loading Pattern for Triaxial Dynamic Modulus Test.....	8
Figure 3.1	Schematic of Indirect Tension Test.....	25
Figure 3.2	Stress Distribution along Horizontal and Vertical Diameters.....	26
Figure 3.3	Total Work Done in Actual Process.....	37
Figure 4.1	Aggregate Gradation of North Carolina Mix.....	40
Figure 4.2	Superpave Gyratory Compactor.....	42
Figure 4.3	Air Void Distribution in SGC Sample.....	43
Figure 4.4	WesTrack Oval Track Section Map.....	46
Figure 4.5	Design Gradation of WesTrack Coarse Mix.....	50
Figure 4.6	Design Gradation of WesTrack Fine Mix.....	51
Figure 4.7	Approach to Obtain Specimen for Testing from Field Core.....	53
Figure 4.8	CoreLok Machine Used to Measure Air Void.....	51
Figure 4.9	Planview of Apparatus Glued to Specimen.....	56
Figure 4.10	Gluing and Marking Device.....	57
Figure 4.11	Positioning Specimen on Loading Strip.....	58
Figure 4.12	Test Configuration of Indirect Tensile Test.....	59
Figure 4.13	Schematic of Creep Test.....	61
Figure 4.14	Schematic of Cyclic Test.....	63
Figure 4.15	Schematic of Tensile Strength Test.....	65
Figure 4.16	Definition of Energies.....	65
Figure 5.1	Effect of Change of Poisson's Ratio on Strain Calculation.....	75

Figure 5.2	3-D Finite Element Model Mesh of Indirect Tension Specimen.....	78
Figure 5.3	Verification of Creep Compliance Calculation.....	80
Figure 5.4	Verification of Center Strain Calculation.....	82
Figure 5.5	Preparation for Direct Tension Specimen and Indirect Tension Specimen	83
Figure 5.6	Comparison of Creep Compliance from IDT and Uniaxial Test.....	86
Figure 5.7	Strain Distribution along Axis of Uniaxial Direct Tension Specimen with End Plate.....	86
Figure 5.8	Creep Compliance at Different Temperatures before Shifting.....	88
Figure 5.9	Creep Compliance Master Curve after Shifting.....	88
Figure 5.10	Relationship between Shift Factor and Temperature.....	90
Figure 5.11	Curvefitting of Creep Compliance Using PLS.....	90
Figure 5.12	Creep Compliance and Converted Relaxation Modulus.....	93
Figure 5.13	Measured and Regressed Horizontal Displacements.....	95
Figure 5.14	Stress vs. Time for Cyclic Test.....	98
Figure 5.15	Smoothed Center Strain vs. Time.....	99
Figure 5.16	Biaxial Stress vs. Center Strain.....	99
Figure 5.17	Biaxial Stress vs. Pseudo Strain.....	100
Figure 5.18	Three Cases Studied Using Finite Element Method.....	103
Figure 5.19	Finite Element Analysis Results for Case I.....	105
Figure 5.20	Finite Element Analysis Result for Case II.....	105
Figure 5.21	Finite Element Results for Case III.....	106
Figure 5.22	Illustration of Bulging Effect.....	107

Figure 5.23	Effect of Bulging on Horizontal Measurement.....	108
Figure 5.24	Effect of Bulging on Vertical Measurement.....	109
Figure 6.1	Schematic Diagram of the Truck.....	111
Figure 6.2	Creep Compliance of Four Coarse Gradation Mixtures.....	114
Figure 6.3	Creep Compliance of Four Fine Gradation Mixtures.....	114
Figure 6.4	Poisson's Ratio in Creep Test.....	115
Figure 6.5	Poisson's Ratio in Tensile Strength Test.....	115
Figure 6.6	Stress-Strain Relationship in Indirect Tensile Strength Test.....	116
Figure 6.7	Field Performance of WesTrack Mixtures Selected.....	119
Figure 6.8	Fracture Energies of WesTrack Mixtures Selected.....	119
Figure 6.9	Creep Compliance of WesTrack Mixtures at 200 Seconds.....	122
Figure 6.10	m-value of WesTrack Mixtures.....	122
Figure 6.11	Maximum Tensile Stress of WesTrack Mixtures.....	123
Figure 6.12	Horizontal Strain of WesTrack Mixtures at Failure.....	123
Figure 6.13	Field Performance of WesTrack Sections (Fine).....	126
Figure 6.14	Fracture Energies of WesTrack Field Cores (Fine).....	126
Figure 6.15	Field Performance of Fine Gradation Mixtures.....	129
Figure 6.16	Fracture Energies of Coarse Gradation Mixtures.....	129
Figure 6.17	Field Performance of Both Fine and Coarse Gradation Mixtures.....	130
Figure 6.18	Fracture Energies of Both Fine and Coarse Gradation Mixtures.....	130
Figure 6.19	Relationship between Field Performance and Fracture Energy.....	131
Figure 6.20	Relationship between Strain Energy and Field Performance.....	132
Figure 6.21	Relationship between Damage Energy and Field Performance.....	132

CHAPTER 1

INTRODUCTION

1.1 Needs

Hot Mix Asphalt (HMA) is used extensively throughout the world as a cost-effective pavement surfacing material for highways, streets, airfields, and parking lots. Simple improvements in the life of HMA can result in a large economic saving. Asphalt mixtures have been traditionally designed with an empirical laboratory design procedure. In 1987, the Strategic Highway Research Program (SHRP) began developing a new system for specifying asphalt materials. Superior Performing Asphalt Pavements (SuperPave) is the final product of the SHRP asphalt research program. Superpave represents an improved system for specifying the asphalt binder and mineral aggregate, developing the asphalt mixture design, and analyzing and establishing pavement performance prediction. The system includes an asphalt binder specification, a hot mix asphalt design and analysis system, and computer software that integrates the system's components. The core of the Superpave system is a performance-based specification system which has a direct relationship to field performance. The Superpave design method for HMA consists of three phases: (1) materials selection for the asphalt binder and aggregate, (2) aggregate blending, and (3) volumetric analysis on specimens compacted using the Superpave Gyrotory Compactor.

However, due to the relatively short duration of the SHRP research program, only a limited amount of field performance information was used to calibrate and correlate the newly developed tests and acceptance criteria for the asphalt binder and the HMA

mixture design method. Therefore, it is imperative to define relationships among material properties and pavement performance which might be accomplished with the use of accelerated pavement testing on a full scale test track, such as WesTrack.

WesTrack is an accelerated pavement test facility under a contract to the Federal Highway Administration (FHWA) and the National Cooperative Highway Research Program (NCHRP). The objectives of the WesTrack research project are as follows:

- a. to continue the development of performance related specifications (PRS) for HMA pavements by evaluating the effect of variations in materials and construction quality (asphalt binder content, aggregate gradation, in-place air void content, etc.) on pavement performance as evaluated by a full scale accelerated field test track, and
- b. to provide early field verification of the SHRP's Superpave volumetric design procedure.

The WesTrack test track consists of 26 sections with a combination of different asphalt binder content, air void content, and aggregate gradation. Traffic was initiated in March of 1996 and was completed in February of 1999. In general, the relative performance of all the sections at the WesTrack met expectations; e.g., low asphalt content, high air void mixes are prone to show fatigue cracking, and high asphalt content mixes tend to rut first. Unexpectedly, however, the asphalt mixes with fine gradation performed better in terms of both rutting and fatigue cracking than the mixes with coarse gradation. According to the Superpave mix design method, fine aggregate in mixes is deleterious to the resistance to distresses and, hence, is not recommended to be used in the mix design.

Results from other experimental construction projects and some of the accelerated tests also questioned whether the SuperPave volumetric mixture design procedure alone is sufficient for determining the acceptance or rejection of HMA mixtures under current traffic and climatic conditions. In addition, industry demands necessitate a simple performance related test that provides reliable performance of the HMA mixture during the volumetric mixture design process using the Superpave Gyratory Compactor.

A Simple Performance Test (SPT) is defined as a test method that accurately and reliably measures a mixture response characteristic or parameter that is highly correlated to the occurrence of pavement distress (cracking and rutting) over a diverse range of traffic and climatic conditions. SPT will be included as a final stage in the Superpave volumetric design standard. One of the requirements for SPT is that it can measure a fundamental engineering property that can be linked back to the advanced material characterization methods of the detailed distress prediction models: the permanent deformation model, the fatigue cracking model, and the thermal cracking model.

The fatigue cracking of HMA pavement is based on the horizontal tensile strain at the bottom of HMA due to repeated traffic loading. Starting as microcracks, these cracks propagate, densify, and coalesce to form macrocracks, a development that is directly related to stress-strain fields in asphalt layers. Accurate prediction of fatigue behavior requires an in-depth understanding of the characteristics of asphalt concrete under realistic traffic conditions.

Numerous models of varying sophistication have been developed to predict the fatigue behavior of asphalt concrete including elastic, viscoelastic, elastoplastic, viscoplastic, and crack models. One of the keys to obtaining appropriate asphalt mixture

properties for use in one model is to use testing modes which induce stress states that are similar to those experienced by the asphalt concrete layer. The common testing modes used in the laboratory for fatigue evaluation are the:

- a. uniaxial tension and compression test,
- b. triaxial test,
- c. indirect tension test,
- d. beam flexure test, and
- e. hollow cylinder test.

The critical location for load-induced cracking is generally at the bottom of the asphalt concrete layer and directly underneath the load. The stress state therein is longitudinal and transverse tension with vertical compression. It is noteworthy that the stress state in the vicinity of the center of an indirect tension specimen is very similar to that at the bottom of the asphalt layer. Another advantage of the indirect tension testing mode over other testing modes is that the failure plane is almost always vertical. Therefore, it is easy to identify the location of microcrack initiation and to measure the material response of interest. Finally, the indirect tensile testing on Superpave Gyratory compacted specimens simulates the relationship between the compaction direction and critical tensile stress direction in the field accurately. These advantages warrant in-depth investigation of indirect tensile test as an SPT for fatigue cracking.

Another important factor of a reliable fatigue test method is the test and analysis procedure. The test procedure should be simple and practical for the method to be accepted by state highway agencies. At the same time, the analysis method must be fundamentally correct. It is noteworthy that the reliable material testing method originates

from the balance between the simplicity of the test procedure and the accuracy of analysis. That is, to achieve the same degree of reliability from a test method, one must either employ a complex test method that simulates actual loading and environmental condition with approximate analytical solutions, or use a simpler test method with more accurate analytical solutions. This balance is the key to developing a test method that is accurate and practical enough for highway agencies to adopt.

1.2 Objective and Significance

The objective of the research is to develop a simple performance test method for asphalt concrete using an indirect tension test, based upon advanced mechanistic principles. These methods employ the test and analysis procedures with varying complexities. The specific tasks needed to accomplish the objectives include:

- a. study of the stress and strain states inside the indirect tension specimen,
- b. determination of the test configuration, including specimen geometry and gauge length, using finite element analysis,
- c. derivation of viscoelastic solutions for stresses and strains in indirect tension specimens and their verification, and
- d. development of a simple performance test method and validation using field performance of WesTrack mixtures.

The resulting simple performance test will accurately and precisely measure those properties that are highly correlated to pavement fatigue cracking and will play a key role in the quality control (QC) and quality acceptance (QA) of HMA mixtures.

This dissertation is composed of seven chapters. Chapter 1 introduces the needs of this study and the objectives to be accomplished. Literature review and proposed theories are presented in Chapters 2 and 3, respectively. Chapter 4 describes the material and testing programs used in this study. Following, in Chapter 5, is the description of the theoretical development of material characterization in the indirect tension test, including creep compliance, center strain, and finite element viscoelastic analysis. In Chapter 6, the developed test method and theory are verified by the field performance of the asphalt mixture at WesTrack. The findings of the research and recommendations are presented in Chapter 7.

CHAPTER 2

LITERATURE REVIEW

A literature review was undertaken to examine the progress in the development of simple performance testing, indirect tensile testing, and the mechanistic characterization of asphalt concrete. For the simple performance test, a group of promising tests was selected as candidates, including the triaxial modulus test, the indirect tensile strength test, the indirect tensile creep test, and the indirect tensile fatigue test. The interim results and preliminary recommendations of the NCHRP 9-19 research project were briefed. The advantages and disadvantages of a variety of testing modes were evaluated so that the optimum one would be selected and used to characterize the fatigue behavior of asphalt concrete in this study. Emphasis was placed on the indirect tensile test, especially its measurement system development and analysis procedure. Finally, the mechanistic approaches to characterize asphalt concrete were summarized.

2.1 Development of a Simple Performance Test for Fatigue Cracking

In the NCHRP 9-19 report (2001), many tests had been proposed as a SPT, including the triaxial dynamic modulus test, the indirect tensile creep compliance test, and other test methods.

Triaxial Dynamic Modulus Tests

The test consists of applying a uniaxial (haversine) compressive stress to an unconfined or confined HMA cylindrical test specimen, as shown in Figure 2.1.

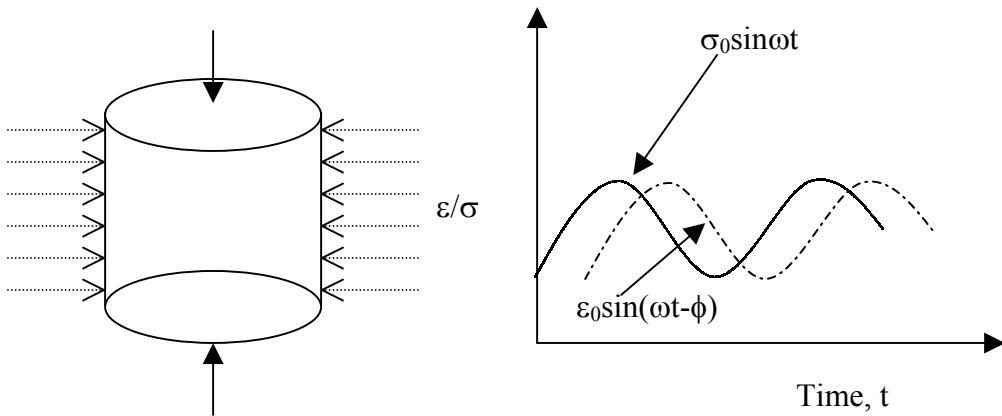


Figure 2.1 Haversine Loading Pattern for Triaxial Dynamic Modulus Test

The complex modulus is represented by the storage and the loss moduli in the following relationship:

$$E^* = E' + iE'' \quad (2.1)$$

where E' is the storage modulus or elastic component of the complex modulus and E'' is the loss modulus or the viscous component.

The dynamic modulus may be determined by calculating the ratio of the stress amplitude, σ_0 , to the strain amplitude, ϵ_0 , from the cyclic test; that is,

$$|E^*| = \frac{\sigma_0}{\epsilon_0} \quad (2.2)$$

The phase angle, ϕ , is the angle at which a cycle of strain response lags a cycle of stress input:

$$\phi = \tan^{-1} \left| \frac{E''}{E'} \right| \quad (2.3)$$

Indirect Tensile Test

The indirect tensile test is conducted by applying a compressive load to a cylindrical specimen through two diametrically opposite, arc-shaped, rigid loading strips. Four indirect tensile tests were used in the NCHRP 9-19 research project, including an indirect tensile strength test, a resilient modulus test, a fatigue test, and a creep test.

According to ASSHTO TP9-96, the indirect tensile strength is determined by applying a constant rate of ram movement to failure. The tensile strength is calculated as follows:

$$S = \frac{2P}{\pi dt} \quad (2.4)$$

where d = the diameter of the specimen,
 t = the thickness of the specimen, and
 P = the failure load.

The repeated load indirect tensile resilient modulus test of asphalt concrete is conducted through repetitive application of compressive loads in a haversine waveform. The resilient modulus is calculated using the following equation:

$$M_R = \frac{P}{t\delta_{xx}}(a + bv) \quad (2.5)$$

where M_R = resilient modulus,
 P = load amplitude,
 v = Poisson's ratio,
 δ_{xx} = horizontal deformation across the gauge length, and
 a, b = integration constants.

The fatigue test is used to determine the fatigue life of asphalt concrete, that is, the number of load cycles to failure. The fatigue life is mathematically represented by:

$$N_f = K_1\sigma^{K_2} \quad (2.6)$$

where K_1, K_2 = regression coefficients.

The tensile creep compliance is determined by applying a static load of fixed magnitude along the diametral axis of a specimen. The creep compliance is represented by the following equation:

$$D(t) = D_1t^{m_1} \quad (2.7)$$

where D_1, m_1 = material regression coefficients.

Three projects were used in the experimental plan, including MnRoad, FHWA ALF, and WesTrack. Multiple sections of each project were used to ensure a diverse range of distress magnitude between the individual test sections. The correlation between the triaxial dynamic modulus and cracking is fair, while the correlation between the response parameter from the indirect tensile test and cracking were poor to very poor and site-dependent. The triaxial dynamic modulus test under low confining pressure was recommended as the simple performance test for fatigue cracking from the NCHRP 9-19 research project.

2.2 Indirect Tensile Test

Irrespective of the recommendations of the NCHRP 9-19 research project, the indirect tensile test offers certain advantages, which have been demonstrated by many researchers. Kennedy and Hudson (1968) used the indirect tensile test to study tensile strength of asphalt concrete. In 1972, Schmidt demonstrated the suitability of the indirect tensile test for the measurement of the resilient modulus of asphalt concrete.

Wallace and Monismith (1975) stated that, for a detailed study of characteristics of asphalt concrete, the following five parameters were required for a cylinder specimen:

- a. vertical strain due to the increment of vertical stress,
- b. radial strain due to the increment of vertical stress,
- c. radial strain due to the increment of radial stress,
- d. vertical strain due to the increment of radial stress, and
- e. radial strain due to the increment of radial stress perpendicular to the strain.

In general, direct tension testing measures the first parameter while triaxial testing measures the first and the second parameters. The third and the fifth parameters may be measured by indirect tensile testing. As described in Chapter 1, the stress state in the center of an indirect tensile specimen is similar to that at the bottom of the asphalt concrete layer under traffic. If asphalt concrete were an isotropic material, each of the tests would measure the same characteristics of asphalt concrete. It has been reported, however, by Dehlen (1969) and others that the anisotropy of asphalt concrete is quite pronounced. Similar observations have been found in this study, which will be addressed in Chapter 5. Furthermore, Wallace and Monismith (1975) pointed out that the application of stress induced further anisotropy of a similar magnitude. For a cylindrical specimen taken from pavement or laboratory, the direction of load applied in a direct tension test or deviatoric stress in a triaxial test is parallel to that of the compaction. The fatigue crack, however, is initiated in a direction perpendicular to that of compaction in the asphalt concrete pavement layer, which is simulated better in an indirect tensile test.

A bending beam test involves the application of a bending load to a beam specimen. It is favored by many engineers because its loading conditions are similar to the field loading conditions of pavement materials. One major criticism of the bending beam test is that the maximum tensile stress occurs at the outer surface. Another disadvantage, which precludes the bending beam test as a candidate for the simple performance test, is that the beam specimen cannot be fabricated by the Superpave Gyrotory Compactor, which has been specified as one of prerequisites of simple performance testing.

Roque and Buttlar (1992) developed a measurement and analysis system to determine asphalt concrete properties, primarily thermal cracking, using the indirect tensile testing mode, which was incorporated in ASSHTO TP9-96, *Standard Test Method for Determining the Creep Compliance and Strength of Hot Mix Asphalt (HMA) Using the Indirect Tensile Test Device*. They proposed the Gauge-Point-Mounted device to measure horizontal and vertical deformations across a gauge length of 25.4mm (1 inch). Poisson's ratio was also obtained from the horizontal and vertical deformations instead of using assumed values. Correction factors from 3-D finite element analysis were used to account for: (1) the effect of specimen bulging on deformation measurement, and (2) approximation of 2-D plane stress assumption. Based upon the elastic analysis, creep compliance was calculated using the following equations:

$$D(t) = \frac{X \times D \times b}{P \times GL} \times C \quad (2.8)$$

where $D(t)$ = creep compliance,
 X = horizontal deformation,
 D = diameter of specimen,
 b = thickness of specimen,
 P = load applied,
 GL = gauge length, and
 C = correction factor.

Poisson's ratio was computed as:

$$\nu = -0.1 + 1.48\left(\frac{X}{Y}\right)^2 - 0.778\left(\frac{b}{D}\right)^2\left(\frac{X}{Y}\right)^2 \quad (2.9)$$

where X = horizontal deformation, and

Y = vertical deformation.

Extensive indirect tensile cyclic tests were performed on the asphalt concrete specimens, as described in the NCHRP 1-28 report (1997), *Laboratory Determination of Resilient Modulus for Flexible Pavement Design*. A representative group of indirect tensile testing devices, measurement systems, and analysis methods were carefully selected for evaluation in the testing program. The SHRP LG testing device was adopted to minimize rocking. Poisson's ratio was evaluated using a surface mounted LVDT to measure vertical deformation and externally mounted LVDT to determine horizontal deformation.

2.3 Mechanistic Approaches for Characterizing Asphalt Concrete Fatigue Behavior

Fatigue is the process of cumulative damage resulting from repeated traffic loading; fatigue cracking is its resultant distress. In general, there are two approaches to characterize the fatigue behavior of asphalt concrete, one is a phenomenological approach and the other a mechanistic approach.

2.3.1 Phenomenological Approach

Most of the tests employed the bending beam test (Deacon 1965, Franchen and Verstraeten 1974, Pell 1962). Adedimila and Kennedy (1976), however, used the

repeated load indirect tensile test. The fatigue behavior of a mixture may be defined by the relationship between the number of cycles to failure and initial tensile strain, as follows:

$$N_f = a \left(\frac{1}{\varepsilon_0} \right)^b \quad (2.10)$$

where N_f = number of cycles to failure,
 ε_0 = initial tensile strain, and
 a, b = material-dependent coefficients.

Monismith et al. (1985) improved the above equation to account for the effects of mixture stiffness for asphalt concrete:

$$N_f = a \left(\frac{1}{\varepsilon_0} \right)^b S^c \quad (2.11)$$

where S is mixture stiffness and c is the material-dependent coefficient.

2.3.2 Mechanistic Approach

The above relationships are applicable only to specific environments, materials, and traffic conditions, and are empirical. It is required, however, that the parameter obtained from a simple performance test should be linked to the advanced material characterization methods needed for detailed distress prediction models. The phenomenological approach, therefore, is not appropriate direction to pursue. Attention is

turned, then, to the mechanistic approach that explores the mechanisms of fatigue behavior fundamentally. The fracture mechanics method and the viscoelastic continuum damage mechanics method may be categorized into a mechanistic approach to study the characteristics of asphalt concrete.

Linear Elastic Fracture Mechanics

In linear elastic fracture mechanics, Paris' law is used to describe the continuous crack growth:

$$\frac{dc}{dN} = AK^n \quad (2.12)$$

where dc/dN = crack propagation rate per load cycle,

K = stress intensity factor, and

A, n = material parameters.

In linear elastic fracture mechanics, the crack propagates continuously. Jacobs (1996) investigated the applicability of fracture mechanics to asphalt concrete and showed that a crack in asphalt concrete grows discontinuously, indicating the limitation of the fracture mechanics approach for asphalt concrete. It was pointed out that the discontinuous crack propagation could be due to the inhomogeneity of asphalt concrete. Still, the measured discontinuous crack growth was treated as a continuous single crack in case the comparison was based on the maximum normal stresses occurring during the fracture process. Thus, the fracture mechanics principle was applied to describing the crack growth process. With finite element analysis, Jacobs found a relationship between the A and n value, as follows:

$$\log A = a + bn \quad (2.13)$$

where a, b = regression parameters.

The parameter n was determined using the slope of creep compliance vs. time in the log-log coordinate for a controlled-displacement test. Shapery (1973) theoretically justified the use of Paris' law for the description of the crack growth process in viscoelastic material and presented a relationship between crack growth velocity and properties of material. Jacobs compared the A and n values that were determined experimentally to those values estimated theoretically and concluded that Shapery's derivations of A and n were validated by their findings.

Read et al. (1997) presented the development and subsequent use of the indirect tensile fatigue test (ITFT) to evaluate the life to crack initiation of asphalt concrete. First, results from ITFT were compared to those of two other tests, the trapezoidal cantilever test and the uniaxial tension-compression test; a high degree of correlation was observed. They addressed the problem of compressive or shear failure in ITFT. In general, it is assumed that cracks start at the center of an indirect tensile test specimen, due to tensile stress, and then propagate towards the loading strips. Under certain conditions, such as high temperature or high load, either compressive or shear failure can occur underneath the loading strips. Shear failure will take the form of a wedge of material pushed through the specimen from the top loading strip. It was also pointed out that under the test temperature of 20°C, tensile failure occurred first in all cases. Read et al. used linear elastic fracture mechanics to describe the stress field in the vicinity of a crack, and an analytical expression was developed for additional ITFT specimen compliance due to the

presence of a crack. Finally they recommended drilling a hole at the center of the indirect tensile test specimen to increase the horizontal stress in the vicinity of the hole.

Roque and Zhang (1999) applied the principle of fracture mechanics to characterize the mixture resistance to propagation, not crack initiation. A notch, 8 mm diameter hole, was drilled at the center of the indirect tensile specimen to concentrate the stress, so that the crack was initiated and could propagate along the predetermined path. The crack length was determined using the measured response, load, and dimension of the specimen, on the basis of (1) an energy-based approach and (2) a compliance-based approach. The latter one was finally adopted. The following relationship was developed between crack length and the horizontal measurement obtained from the Superpave IDT:

$$\frac{\delta}{\delta_0} = 2\sqrt{1 + \frac{c}{L^2}} - \frac{1 + \nu}{\sqrt{a + \frac{c^2}{L^2}}} + \nu \quad (2.14)$$

where δ, δ_0 = resilient horizontal deformation with crack and without crack,
 ν = Poisson's ratio,
 c = crack length, and
 L = gauge length.

They calculated the stress intensity factor, K , using both approximate theoretical relationship and finite element analysis. Thus, fracture parameters could be obtained using Paris' law. One unique feature of this method was that the cracking length could be determined, not experimentally measured, thus reducing the measurement error. Zhang (2001) showed, however, that Paris' law did not appear to incorporate all the aspects

involved in the mechanism of cracking of asphalt mixtures subjected to generalized loading conditions and cannot be directly used for asphalt concrete because the crack growth rate failed to correlate with the field performance of asphalt concrete. After invalidation of the applicability of the principle of fracture mechanics, Zhang (2000) built a second fracture mechanics model to pursue the permanent deformation. Thereafter, the concept of “threshold” was introduced. The threshold was defined as the material’s state between micro-crack and macro-crack. If the threshold was not reached, microdamage in the specimen was healable and cracks would not propagate. Cracks would advance only if the threshold was exceeded. Finally, they considered dissipated creep strain energy as threshold.

Viscoelastic Continuum Damage Mechanics

Asphalt concrete is a history-dependent composite material. Therefore, accurate prediction of its behavior under realistic traffic loading conditions requires the application of the theory of viscoelasticity. To develop a realistic mechanistic model for asphalt concrete undergoing damage, the viscoelasticity and damage growth should be considered in the constitutive modeling. Schapery (1975) developed the theory for predicting the time-dependent size and shape of cracks in linearly viscoelastic isotropic media, followed by the derivation of relations for predicting the time of fracture initiation and crack tip velocity. A nonlinear viscoelastic constitutive theory with effects of distributed damage had been shown to provide an accurate characterization of the deformation behavior of highly-filled rubber under uniaxial loading (Schapery 1981). In this model, pseudo-strain replaced physical strain based on the correspondence principle to transform a viscoelastic problem to an elastic case. For viscoelastic materials,

Schapery (1986) showed that the local crack growth rate obeys a power law in the local J integral,

$$\frac{da}{dt} = A(J_v)^k \quad (2.15)$$

where a = crack length,
 J_v = viscoelastic J integral, and
 A, k = positive constants.

From the above equation, a damage parameter could be obtained, as follows:

$$S_p = \left(\int_0^t |\varepsilon^R|^p dt \right)^{\frac{1}{p}} \quad (2.16)$$

where ε^R = pseudo-strain, and
 p = positive constant.

Schapery (1990) applied the method of thermodynamics of irreversible processes to develop a theory applicable to describing the behavior of elastic media with growing damage and other structural changes and extended it to the viscoelastic media. The theory was proven to be successful for particular composites with damage growth under monotonic loading.

The nonlinear elastic-viscoelastic correspondence principle developed by Schapery (1984) was applied to uniaxial cyclic stress strain data of sand-asphalt as a means of reducing the viscoelastic analysis to an elastic case (Kim 1988). It was verified that the resulting constitutive model satisfactorily predicts the effects due to multilevel loading, due to the sequence of multilevel loading, and due to various durations of rest periods. Kim concluded that the correspondence principle provides a means of accurately modeling the damage growth and fracture healing of asphalt concrete under complex

cyclic loading. Kim and Little (1990) pointed out that the hysteretic behavior of asphalt concrete under traffic loading is attributed to three major mechanisms: damage growth, relaxation of stresses, and microcrack healing.

Kim, Lee, and Little (1997) presented a systematic application of viscoelasticity and continuum damage mechanics to characterize the fatigue behavior of asphalt concrete. A uniaxial viscoelastic constitutive model was developed to account for damage evolution in asphalt concrete under cyclic loading conditions. The elastic-viscoelastic correspondence principle was applied to evaluate damage growth and healing in cyclic loading separately from time-dependent characteristics of the material. The work potential theory was employed to model the damage growth during loading cycles and healing during rest periods. The constitutive model successfully predicted the damage growth of asphalt concrete under monotonic loading of varying strain rates and damage growth and recovery due to complex loading history. The work potential theory is composed of the following three relations:

$$\text{Strain Energy Density Function:} \quad W = W(\varepsilon_{ij}, S_m) \quad (2.17)$$

$$\text{Stress-Strain Relationships:} \quad \sigma_{ij} = \frac{\partial W}{\partial \varepsilon_{ij}} \quad (2.18)$$

$$\text{Damage Evolution Laws:} \quad -\frac{\partial W}{\partial S_m} = \frac{\partial W_s}{\partial S_m} \quad (2.19)$$

where σ_{ij} are stresses, ε_{ij} are strains, S_m are internal state variables (or damage parameters), and $W_s = W_s(S_m)$ is the dissipated energy due to damage growth. Schapery

generalized the theory to account for the coupling between viscoelasticity and damage, using the extended elastic-viscoelastic correspondence principle and rate-type damage evolution laws, as follows:

$$\dot{S}_m = \left(-\frac{\partial W^R}{\partial S_m} \right)^{\alpha_m} \quad (2.20)$$

where $W^R = W^R(\varepsilon_{ij}^R, S_m)$ is the pseudo-strain energy density function, α_m is the material-dependent constant, and the overdot denotes the time derivative.

The uniaxial constitutive equations for linear elastic and linear viscoelastic bodies with and without damage are presented here:

$$\text{Elastic Body without Damage:} \quad \sigma = E_R \varepsilon \quad (2.21)$$

$$\text{Elastic Body with Damage:} \quad \sigma = C(S_m) \varepsilon \quad (2.22)$$

$$\text{Viscoelastic Body without Damage:} \quad \sigma = E_R \varepsilon^R \quad (2.23)$$

$$\text{Viscoelastic Body with Damage:} \quad \sigma = C(S_m) \varepsilon^R \quad (2.24)$$

where $C(S_m)$ denotes that C is a function of damage parameters S_m .

Lee and Kim (1998) studied experimentally the types of S_m and the mathematical form of $C(S_m)$ for modeling the fatigue behavior of asphalt concrete. Several parameters were proposed as internal state variables representing time-dependent damage growth and microdamage healing of asphalt-aggregate mixtures: pseudo-strain normalized by the largest pseudo-strain up to current time ($\varepsilon^R/\varepsilon_L^R$), pseudo-strain amplitude (ε_0^R), and work potential theory-based internal state variables.

Based upon the assumption that asphalt concrete is linearly viscoelastic and that any deviation from the linear viscoelastic behavior is due to damage during loading or due to microdamage healing during rest periods, Kim et al. (1997) developed the following constitutive model:

$$\sigma = I \varepsilon_e^R (F + G + H) \quad (2.25)$$

where I = initial pseudo-stiffness,

ε_e^R = effective pseudo-strain,

F = the damage function representing the change in the slope of each σ - ε_e^R loop,

G = the hysteresis function representing the different between loading and unloading paths, and

H = the microdamage healing function representing the change in secant pseudo-stiffness due to rest periods.

This constitutive model is capable of accurately predicting fatigue behavior of asphalt concrete under (1) constant-strain-rate monotonic loading; and (2) controlled-strain and controlled-stress cyclic loading.

CHAPTER 3

THEORETICAL BACKGROUND

Unlike the uniaxial test, the stress and strain distributions in the indirect tensile specimen are complicated. Generally, the mechanical characterization of material in an indirect tensile test is based upon the elastic solution derived by Hondros (1959) in which an approximation of the plane stress problem is assumed to simplify the analysis. Recent studies (Roque et. al., 1992) show that a two-dimensional theoretical solution might not be sufficiently accurate in some cases. A three-dimensional solution to the indirect tensile test was, therefore, derived in this study on the basis of Wijk's work (1978). However, due to the viscoelastic nature of asphalt concrete, these elastic solutions are not applicable to asphalt concrete directly. In order to convert these elastic solutions into viscoelastic solutions, the elastic-viscoelastic correspondence principle is employed in this study. Finally, work potential theory developed by Schapery (1981) is introduced as a means of accounting for initiation and propagation of microcracks.

3.1 Elastic Solution of Stress in the Indirect Tension Test

Indirect tension testing is done by applying a compressive force to a cylindrical specimen along two diametrically opposite, arc-shaped loading strips, as shown in Figure 3.1. Hondros (1959) derived the stress equations, which model closely the actual test conditions, and used the test to determine Young's modulus and Poisson's ratio of material.

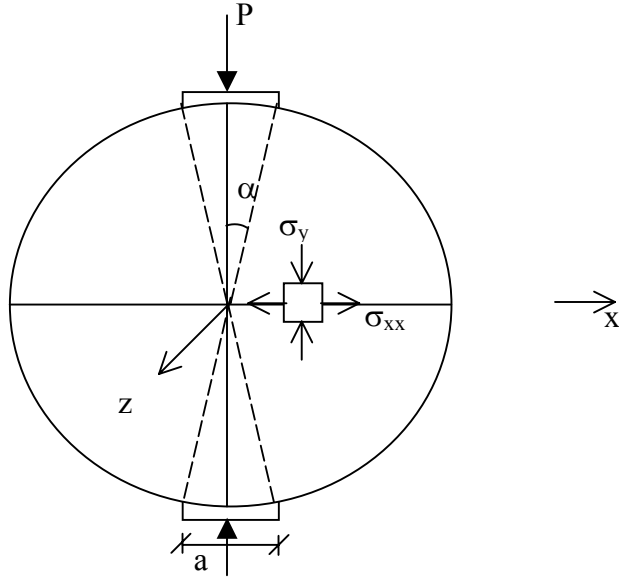


Figure 3.1 Schematic of Indirect Tension Test

In Hondros' analysis, the stresses along the horizontal diameter are:

$$\sigma_x(x) = \frac{2P}{\pi ad} \left[\frac{(1 - x^2/R^2) \sin 2\alpha}{1 + 2x^2/R^2 \cos 2\alpha + x^4/R^4} - \tan^{-1} \left(\frac{1 - x^2/R^2}{1 + x^2/R^2} \tan \alpha \right) \right] = \frac{2P}{\pi ad} [f(x) - g(x)] \quad (3.1)$$

$$\sigma_y(x) = -\frac{2P}{\pi ad} \left[\frac{(1 - x^2/R^2) \sin 2\alpha}{1 + 2x^2/R^2 \cos 2\alpha + x^4/R^4} + \tan^{-1} \left(\frac{1 - x^2/R^2}{1 + x^2/R^2} \tan \alpha \right) \right] = -\frac{2P}{\pi ad} [f(x) + g(x)] \quad (3.2)$$

The stresses along the vertical diameter are:

$$\sigma_x = \frac{2P}{\pi ad} \left[\frac{(1 - y^2/R^2) \sin 2\alpha}{1 - 2y^2/R^2 \cos 2\alpha + y^4/R^4} - \arctan \left(\frac{1 + y^2/R^2}{1 - y^2/R^2} \tan \alpha \right) \right] = \frac{2P}{\pi ad} [m(y) - n(y)] \quad (3.3)$$

$$\sigma_y = -\frac{2P}{\pi ad} \left[\frac{(1 - y^2/R^2) \sin 2\alpha}{1 - 2y^2/R^2 \cos 2\alpha + y^4/R^4} + \arctan \left(\frac{1 + y^2/R^2}{1 - y^2/R^2} \tan \alpha \right) \right] = -\frac{2P}{\pi ad} [m(y) + n(y)] \quad (3.4)$$

where P = applied load,
 a = loading strip width,
 d = thickness of specimen,
 R = specimen radius, and
 α = radial angle.

Figure 3.2 shows the stress distribution along the horizontal and vertical axes. Noteworthy is that the stresses are independent of Poisson's ratio, indicating that normalized stress distribution is only a function of specimen geometry and is material-independent.

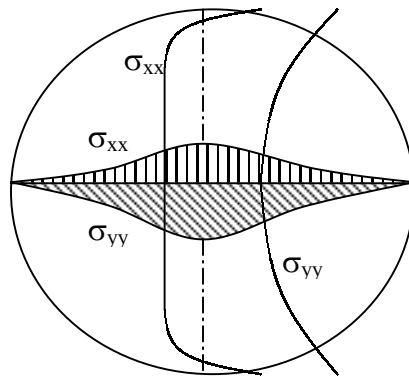


Figure 3.2 Stress Distribution along Horizontal and Vertical Diameters

In this study, an attempt was made to develop three-dimensional solutions for the indirect tensile test. The solution to a two-dimensional problem may be used to construct the solution to a certain three-dimensional problem in the case of vanishing stresses, σ_z ,

τ_{xz} , and τ_{yz} , the first being the normal stress, the other two being the shear stresses in the xy plane (Wijk 1978).

Suppose that the potential function of the two-dimensional problem is $\varphi(x, y)$, then the normal stresses are $\sigma_x(x, y)$ and $\sigma_y(x, y)$ in the following (Wijk 1998):

$$\sigma_x = \frac{\partial^2 \varphi(x, y)}{\partial y^2} \quad (3.5)$$

$$\sigma_y = \frac{\partial^2 \varphi(x, y)}{\partial x^2} \quad (3.6)$$

Three-dimensional solutions may be obtained for the indirect tensile test with the following observations:

$$\sigma_z(x, y, z) = \tau_{zx}(x, y, z) = \tau_{zy}(x, y, z) = 0 \quad (3.7)$$

Based on this observation, Wijk derived the following equations for stresses:

$$\sigma_x(x, y, z) = \sigma_x(x, y) + \frac{\partial^2 \Delta \varphi(x, y, z)}{\partial y^2} \quad (3.8)$$

$$\sigma_y(x, y, z) = \sigma_y(x, y) + \frac{\partial^2 \Delta \varphi(x, y, z)}{\partial x^2} \quad (3.9)$$

$$\Delta \varphi(x, y, z) = -\frac{z^2}{2(1/\nu + 1)} \left\{ \frac{\partial^2}{\partial x^2} + \frac{\partial^2}{\partial y^2} \right\} \varphi(x, y) \quad (3.10)$$

where ν is Poisson's ratio.

Input Equation (3.10) in Equations (3.8) and (3.9), respectively,

$$\sigma_x(x, y, z) = \sigma_x(x, y) - \frac{z^2}{2(1/\nu + 1)} \left\{ \frac{\partial^2}{\partial x^2 \partial y^2} + \frac{\partial^2}{\partial y^4} \right\} \varphi(x, y) \quad (3.11)$$

$$\sigma_y(x, y, z) = \sigma_y(x, y) - \frac{z^2}{2(1/\nu + 1)} \left\{ \frac{\partial^2}{\partial x^4} + \frac{\partial^2}{\partial x^2 \partial y^2} \right\} \varphi(x, y) \quad (3.12)$$

In order to use these stress solutions to obtain solutions for displacements, it is recongnized that at both sides of an indirect tensile test specimen, stress σ_z is completely vanished. Therefore, the stress-strain relationship in a three-dimensional problem is the same as that in the following two-dimensional problem:

$$\varepsilon_x = (\sigma_x - \nu\sigma_y) / E \quad (3.13)$$

$$\varepsilon_y = (\sigma_y - \nu\sigma_x) / E \quad (3.14)$$

where E is Young's modulus.

The three-dimensional stresses, σ_x and σ_y , from Equations (3.11) and (3.12) are input in Equation (3.13) and (3.14), thus obtaining the general expressions of three-dimensional strain distribution:

$$\varepsilon_x = \left\langle \sigma_x(x, y) - \frac{z^2}{2(1/\nu + 1)} \left\{ \frac{\partial^2}{\partial x^2 \partial y^2} + \frac{\partial^2}{\partial y^4} \right\} \varphi(x, y) - \nu \left[\sigma_y(x, y) - \frac{z^2}{2(1/\nu + 1)} \left\{ \frac{\partial^2}{\partial x^4} + \frac{\partial^2}{\partial x^2 \partial y^2} \right\} \varphi(x, y) \right] \right\rangle / E \quad (3.15)$$

$$\varepsilon_y = \left\langle \sigma_y(x, y) - \frac{z^2}{2(1/\nu + 1)} \left\{ \frac{\partial^2}{\partial x^4} + \frac{\partial^2}{\partial x^2 \partial y^2} \right\} \varphi(x, y) - \nu \left[\sigma_x(x, y) - \frac{z^2}{2(1/\nu + 1)} \left\{ \frac{\partial^2}{\partial x^2 \partial y^2} + \frac{\partial^2}{\partial y^4} \right\} \varphi(x, y) \right] \right\rangle / E \quad (3.16)$$

The horizontal and vertical displacements under a certain loading may be obtained by integrating the function of strain along the gauge length. The linear three-dimensional solutions for the vertical and horizontal displacements across a 50.8mm (2 inches) gauge length on a 100.8mm (4 inches) diameter specimen are written as follows:

$$U = \frac{P(0.23 + \nu + 0.78\nu^2 + 80.6\nu^2 d^2)}{Ed(1 + \nu)} \quad (3.17)$$

$$V = \frac{P(0.3 + 1.38\nu + 0.78\nu^2 + 222\nu^2 d^2)}{Ed(1 + \nu)} \quad (3.18)$$

where U, V = horizontal and vertical displacements, respectively,
P = load,
ν = Poisson's ratio,
d = thickness of specimen, and
E = Young's modulus.

For a specimen of 152.4mm (6 inches) diameter, the vertical and horizontal displacements across a 50.8mm (2 inches) gauge length are:

$$U = \frac{P(0.18 + 0.773\nu + 0.588\nu^2 + 30.81\nu^2 d^2)}{Ed(1 + \nu)} \quad (3.19)$$

$$V = \frac{P(0.21 + 0.89\nu + 0.68\nu^2 + 48.5\nu^2 d^2)}{Ed(1 + \nu)} \quad (3.20)$$

3.2 Theory of Viscoelasticity

As a viscoelastic material, asphalt concrete has time- or rate-dependence. The response of viscoelastic material depends not only on the current state of input, but also on all past history of input, indicating that the material has a memory for all past history of input. The theory of viscoelasticity has been successfully applied to describe the characteristics of asphalt concrete by many researchers. The response of a linear viscoelastic body to any loading history may be expressed in terms of a convolution integral. To check if the system is linear, the following two conditions should be satisfied:

a. Homogeneity: $R\{AI\} = A\{RI\}$ (3.21)

b. Superposition: $R\{I_1 + I_2\} = R\{I_1\} + R\{I_2\}$ (3.22)

where I_1, I_2 = input histories,
 R = response, and
 A = arbitrary constant.

The response of a non-aging linear viscoelastic body subjected to any loading histories may be expressed by a convolution integral, as follows:

$$\sigma = \int_0^t E(t - \tau) \frac{d\varepsilon}{d\tau} d\tau \text{ or } \varepsilon = \int_0^t D(t - \tau) \frac{d\sigma}{d\tau} d\tau \quad (3.23)$$

where $E(t)$ is the relaxation modulus and $D(t)$ is the creep compliance.

For a one-dimensional problem, the elastic constitutive equation is

$$\sigma = E\varepsilon \quad (3.24)$$

where E is Young's modulus. If one takes the Laplace transform of both sides of Equation (3.24), it can be reduced to:

$$\bar{\sigma} = \tilde{E}\bar{\varepsilon} \quad (3.25)$$

where $\bar{\sigma}$ and $\bar{\varepsilon}$ are Laplace transform of stress and strain, and \tilde{E} is the Carson transform of the relaxation modulus.

Equation (3.25) is the viscoelastic solution of non-aging linear viscoelastic materials in the Laplace domain for one-dimensional problems. It is noted that Equation (3.25) takes the same form as Equation (3.24) for linear elastic materials, except that stress and strain are Laplace transformed and the modulus is Carson transformed.

The above process is called the elastic-viscoelastic correspondence principle. Schapery (1984) proposed an extended correspondence principle which is applicable to both linear and non-linear viscoelastic materials. In this principle, stresses and strains are not physical variables in viscoelastic materials and are replaced by pseudo variables as follows:

$$\sigma^R = E_R \int_0^t D(t-\tau) \frac{d\sigma}{d\tau} d\tau \quad (3.26)$$

$$\varepsilon^R = \frac{1}{E_R} \int_0^t E(t-\tau) \frac{d\varepsilon}{d\tau} d\tau \quad (3.27)$$

where E_R is the reference modulus which is a constant.

Asphalt concrete is considered thermorheologically simple and its temperature dependence of mechanical properties is amenable to analytical description. Thus, the behavior at fast rates of loading corresponds to the behavior at cold temperature, and that of slow rates of loading to high temperatures. The long time behavior of asphalt concrete may be predicted without actually having to test the material over the extended time scale. All of the relaxation (or creep) curves can be superposed to form a single master curve by means of horizontal translation along the time axis. Assuming that the viscoelastic response of the material is to be controlled by a single function of temperature, Williams et al.(1955) developed a relationship, giving the time shift factor as:

$$\log \alpha_T = \log \frac{t_T}{t_{T_0}} = \frac{C_1(T - T_0)}{C_2 + T - T_0} \quad (3.28)$$

where α_T = shift factor that is dependent on the difference between the reference and data temperatures,

t_T, t_{T_0} = time required to reach a specific relaxation modulus or creep compliance T and T_0 , respectively,

C_1, C_2 = constants dependent on the choice of the reference temperature, T_0 , and

T = the test temperature.

This feature is called the time-temperature superposition principle.

3.3 Damage Mechanics

Schapery (1991) introduced the method of thermodynamics of irreversible processes to develop a theory applicable to describing the mechanical behavior of elastic media with growing damage and other structure changes. The theory allows for strong nonlinearities and coupling between the internal state variable and describes a variety of mechanisms including micro- and macrocrack growth in composite materials.

An appropriate constitutive model for asphalt concrete must account for the effects of viscoelasticity and damage. For elastic solids, Schapery applied the method of thermodynamics of irreversible process and the observed phenomenon of path independence of work in damage-inducing processes to develop the work potential theory applicable to describing the mechanical behavior of elastic media with growing damage.

The behavior of elastic media with changing structure will be expressed in terms of relationships between generalized forces, Q_j and independent displacement q_j ($j=1,2, \dots, J$). As is customary, these variables may be selected for any given application such that:

$$\delta W' = Q_j q_j \quad (3.29)$$

for each virtual displacement δq_j , where $\delta W'$ is virtual work. q_j could be strain, displacement, or rotation, and Q_j a stress force or moment. Also, $\delta W'$ could be the work done on a material element of initial unit volume or on an entire body. In this study, q_j and Q_j are considered strain and stress, respectively. Thus, $\delta W'$ is the work done on a material element of initial unit.

The basic assumption of material or structural response used here is that the strain energy function $W=W(q_j, S_m)$ exists with the property that:

$$Q_j = \frac{\partial W}{\partial q_j} \quad (3.30)$$

where S_m ($m=1,2, \dots, M$) =internal state variables. S_m are the only independent thermodynamic state variables, besides q_i , needed to account for change of structure. S_m may serve to define, among other things, change relative to some reference state in the microcrack and macrocrack states, such as the geometry of individual cracks or statistical averages pertaining to distributed microcracks, void volumes, etc.

The relationship between total work and strain energy may be derived by first noting that:

$$dW = \frac{\partial W}{\partial q_j} dq_j + \frac{\partial W}{\partial S_m} dS_m = Q_j dq_j - f_m dS_m \quad (3.31)$$

for any infinitesimal process where f_m is the thermodynamic force defined as follows:

$$f_m = -\frac{\partial W}{\partial S_m} \quad (3.32)$$

Integrate the above equation from an arbitrary state $(q_j^{(1)}, S_m^{(1)})$ at time t_1 , say, along the actual process to the current state (q_j, S_m) at time t , and then solve for the work done during the time interval $t-t_1$. This yields:

$$\Delta W_T = W - W^{(1)} + \int_1 f_m dS_m \quad (3.33)$$

If we assume that whenever $\dot{S}_m \neq 0$,

$$f_m = \frac{\partial W_s}{\partial S_m}, \quad (3.34)$$

where $W_s = W_s(S_m)$ is a state function, then the work is obviously a state function:

$$\Delta W_T = W - W^{(1)} + W_s - W_s^{(1)} \quad (3.35)$$

In order to simplify the notation, it is helpful at this point to introduce a reference state (q_i^R, S_m^R) and, without losing the general nature of the results, take $W=W_s=0$ in this state. The supposition is that the body is in this reference state at $t=0$, and takes W_T as the total work from $t=0$ up to the current time. Thus:

$$W_T = W + W_s \quad (3.36)$$

where W is strain energy and W_s is dissipated energy.

Each f_m will be viewed as a thermodynamic stress available for producing changes in the corresponding structural parameter S_m , and $\partial W_s / \partial S_m$ as that required for these changes. Thus, it is assumed that if Equation (3.34) is not satisfied for any given m , then $\dot{S}_m = 0$.

According to Shapery's theory, the above equation may be rewritten in the following form:

$$W_T = W(q_i, S_m) + W_s(S_m) \quad (3.37)$$

This theory is applicable to only linear or non-linear elastic media. However, asphalt concrete is a thermorheological material and is time- and rate-dependent at room temperature. Thus, the stress-strain curve is divided into segments. For each segment, it is assumed that the stress-strain relationship is similar to that of elastic media.

The former equation is rewritten as:

$$W_{Ti} = W_i + W_{Si} \quad (3.38)$$

The total work done on the body by stress during an actual process is denoted by W_T ,

$$W_T = \int Q dq = \sum_{i=1}^M Q_i q_i \quad (3.39)$$

Figure 3.3 shows the total work done in an actual process.

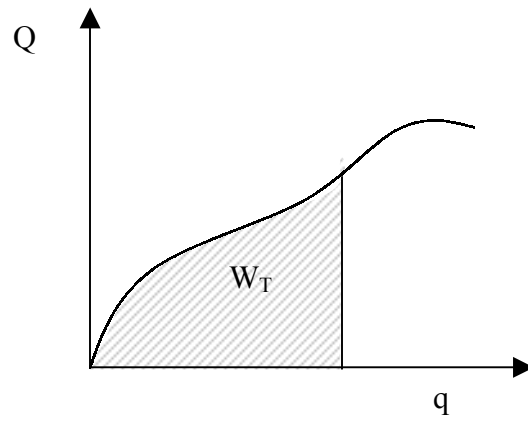


Figure 3.3 Total Work Done in Actual Process

CHAPTER 4

MATERIALS AND TESTING PROGRAMS

4.1 Materials

Asphalt mixes used in this study were obtained from two sources, North Carolina and WesTrack. The former one was used to characterize the mechanical properties of asphalt concrete in indirect tensile testing, while the latter was used to develop a simple performance test for fatigue cracking. Field cores from WesTrack were used to verify the development of the simple performance test using WesTrack field performance.

4.1.1 North Carolina Mix

For the North Carolina mix, specimens used to develop the model were fabricated using the North Carolina SPS-9 mixture which meets the Superpave specification for 12.5 mm mix design. The aggregate blend used consists of 95.5%, by mass, granite aggregates obtained from three stockpiles in Lemon Springs, NC, 3.5% natural sand (Rambeaut sand), and 1% bag house fines. The aggregate gradation is within the control points and falls below the restricted zone. The aggregate gradation of the North Carolina mix is summarized in Table 4.1. Figure 4.1 presents the design gradation of the North Carolina mix.

Table 4.1 Aggregate Gradation of North Carolina Mix

Sieve Size	Granite Aggregate %Pass (95.5%)	Sand %Pass (3.5%)	Bagfines %Pass (1.0%)	Total Percent Passing (%)
3/4	100.00	100.00	100.00	100.00
1/2	92.43	100.00	100.00	92.43
3/8	84.42	100.00	100.00	84.42
#4	44.56	100.00	100.00	44.56
#8	28.33	100.00	100.00	28.33
#16	19.71	99.81	100.00	19.53
#30	14.02	98.28	100.00	12.31
#50	10.92	96.94	100.00	7.87
#100	7.57	96.61	100.00	4.18
#200	5.71	96.52	99.95	2.18
Pan	4.50	96.50	99.00	0.00

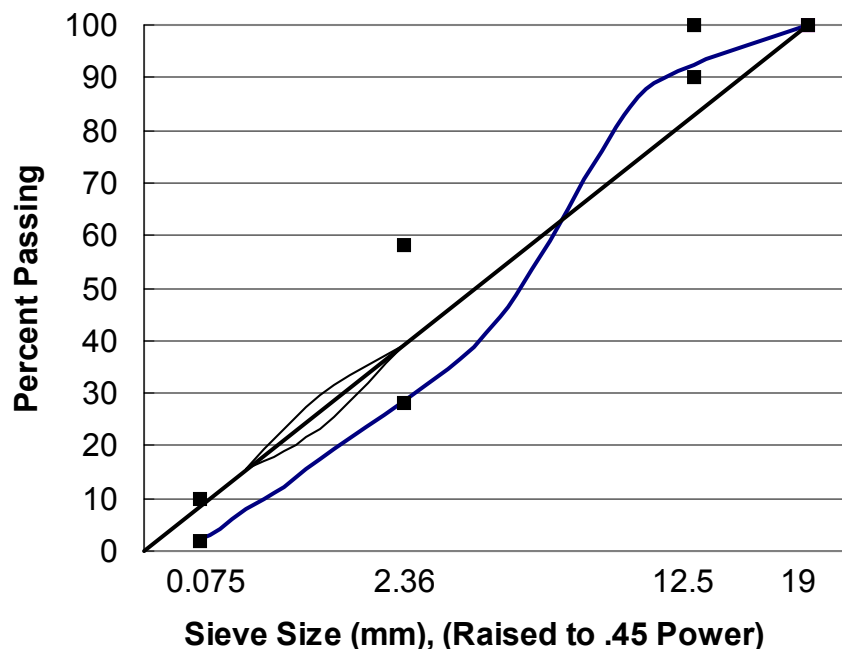


Figure 4.1 Aggregate Gradation of North Carolina Mix

Aggregates were mixed with 5.2% unmodified asphalt PG70-22 obtained from the Citgo Asphalt Company in Paulsboro, New Jersey. The theoretical maximum specific gravity of the North Carolina mixture is 2.481. Samples, 150 mm in diameter and 115 mm in height, were compacted to approximately four percent air void at a temperature of 153°C using the IPC Superpave Gyratory Compactor, ServoPac, as shown in Figure 4.2. The compaction pressure is 600 kPa and the gyration is at 1.25 degrees with 30 gyrations per minute.

The specimen selected for material characterization testing should be representative of the material being tested. Material properties, most importantly air voids, should be consistent throughout its volume (i.e., statistically homogeneous). Moreover, material responses under mechanical tests should be consistent and independent of

aggregate size and specimen boundary conditions. In that sense, if the traditionally known representative volume element (RVE) requirements are to be followed, then according to ASTM D-3497:

- the minimum ratio of maximum aggregate size to diameter should be 1:4, and
- the minimum ratio of diameter to height should be 1:2.

Figure 4.3 shows the air void distribution within the SGC sample. The top and bottom edges (15 mm thick), which were cut off from the original specimen, have very high air void contents. The remaining top and bottom sections (38 mm thick) to be used in the indirect tensile tests have comparable air voids, the bottom one having a slightly lower occurrence than the top. As for the variation along the diameter of each section, the ring has significantly more air voids than the core. This difference is larger in the top section. Therefore, it may be necessary for IDT testing that samples be cored from the 150 mm diameter specimens. It was decided that two sections 38 mm in thickness and 100 mm in diameter be cut from the original sample and be used in the IDT test (Chehab et al., 2000).



Figure 4.2 Superpave Gyrotory Compactor

4.1.2 WesTrack Mixes

WesTrack is the U.S. Department of Transportation's Federal Highway Administration (FHWA) \$15 million full scale accelerated pavement test facility project, located approximately 100 kilometers southeast of Reno, Nevada. The facility was designed, constructed, and operated by a team of private companies and universities. As originally constructed, the track consisted of 26 HMA test sections. The original test sections included both fine and coarse graded Superpave mixtures developed from locally available (Dayton, Nevada) crushed gravel and a neat PG64-22 binder. Asphalt content, in-place air voids, and gradation were systematically varied among the test sections to simulate typical construction variability.

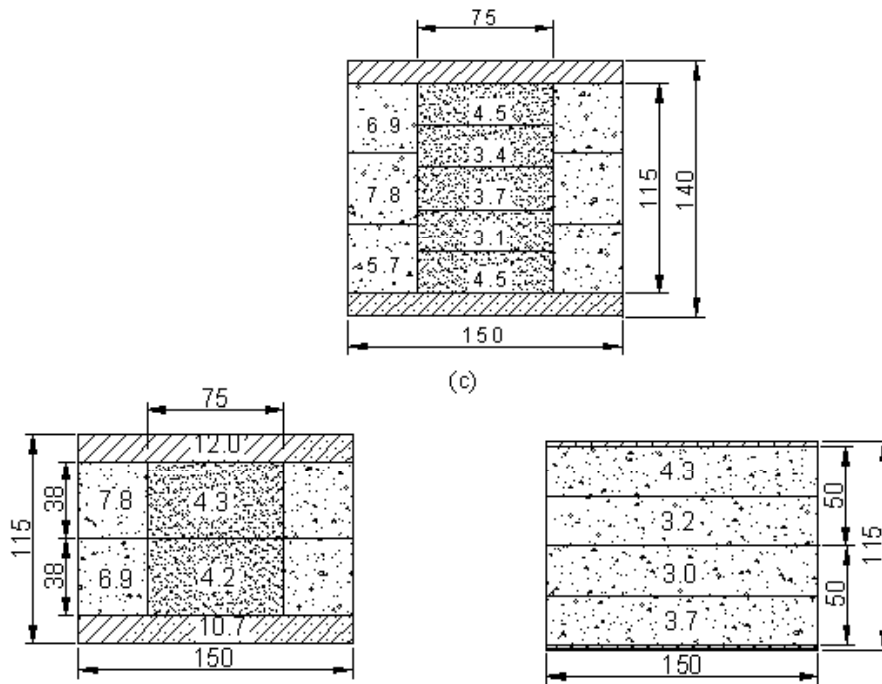


Figure 4.3 Air Void Distribution in SGC Sample (after Chehab et al., 2000)

The climatic conditions at the track are typical of the high desert, inter-mountain western portion of the United States. Total annual precipitation amounts to

approximately 100 millimeters. Summer temperature extreme approaches 40° Celsius (104° F) while winter extreme approaches minus 25° Celsius (-13°F). Frost penetration into the underlying pavement structure is unlikely in this environment.

A single asphalt binder was chosen, a PG 64-22. The asphalt binder meets the high temperature requirement at the 98% level of the Superpave specification and the low temperature Superpave requirement at the 50% level. Three levels of asphalt content were selected for study in the experiment. Optimum asphalt contents were determined for the fine and coarse gradations using the Superpave volumetric mix design method. The optimum for the fine mix was applied to the fine plus. The asphalt content was then to be varied plus and minus 0.7% from the optimum asphalt content for each of the gradations developed for evaluation. The optimum asphalt binder content for each mixture was designated at the “medium” level and the asphalt binder content 0.7% below and 0.7% above the target optimum were designated as “low” and “high”, respectively.

A single primary aggregate source combined to develop three gradations was selected for the original experiment. One fine gradation which plots above the restricted zone on the Superpave 19 mm nominal maximum size gradation chart was selected and designated as the “fine” gradation because a relatively large portion of the aggregate passed the 4.75 mm sieve. The gradation incorporated approximately 25% natural sand. A second gradation was obtained by adding approximately 2% bag house fines to the fine gradation. This gradation was designated “fine plus” as it was “fine” gradation “plus” extra bag house fines. The third gradation was developed to plot below the restricted zone on the Superpave 19 mm nominal maximum size gradation chart. This gradation was designated the “coarse” gradation because a relatively large portion of the aggregate was

retained on the 4.75 mm sieve. The coarse gradation did not contain natural sand and is typical of current Superpave recommendation.

Three in-place air void levels were selected for study in the experiment. An 8% air void was designated as the “medium” level and was considered to be typical for hot mix asphalt construction in the United States. The other target air voids selected were 4% and 12% and they were designated as “low” and “high”, respectively.

A single HMA thickness of 150 mm was selected based on structural design to provide fatigue failure for a typical hot mix asphalt at about 5 million ESALs. The complete structural section consists of 150 mm scarified and mixed subgrade soil. The HMA was constructed in two 75 mm lifts.

The combination of these three factors and their levels is depicted in the factorial experiment design shown in Table 4.2. Note that six cells out of the matrix were eliminated (because of construction impracticality), leaving 26 potential mixes. The numbers within each cell represent the randomized paving sequence of each section. In June 1997 an additional eight sections were built to replicate the coarse aggregate experiment with a different aggregate source. Figure 4.4 illustrates the oval test track.

Only fine and coarse mixes were used in this study. Field aggregate gradation, instead of design gradation, was used to fabricate specimens for testing because there is discrepancy between design gradation and field, “as built” gradation. Fine gradation consists of 73.5% WesTrack aggregate, 25% Wadsworth sand, and 1.5% hydrated lime. Coarse gradation consists of 98.5% WesTrack aggregate and 1.5% hydrated lime. The field aggregate gradations of both coarse and fine mixes are summarized in Tables 4.3 and

4.4, respectively. Figures 4.5 and 4.6 present the design gradations of coarse and fine mixes used in this study, respectively.

Table 4.2 Factorial Experiment Design of WesTrack (after WesTrack Report)

	1995 design									1998 design		
Design	Aggregate Gradation											
	Fine			Fine Plus			Coarse			Coarse		
Air Void Content (%)	Design Asphalt Contents (%)											
	4.7	5.4	6.1	4.7	5.4	6.1	5.0	5.7	6.4	5.1	5.8	6.5
Low-4%		4	18		12	21/9		23	25		39	55
Med-8%	2	1/15	14	22	19/11	13	8	5/24	7	38	35/54	37
High-12%	3/16	17		10	20		26	6		56	36	

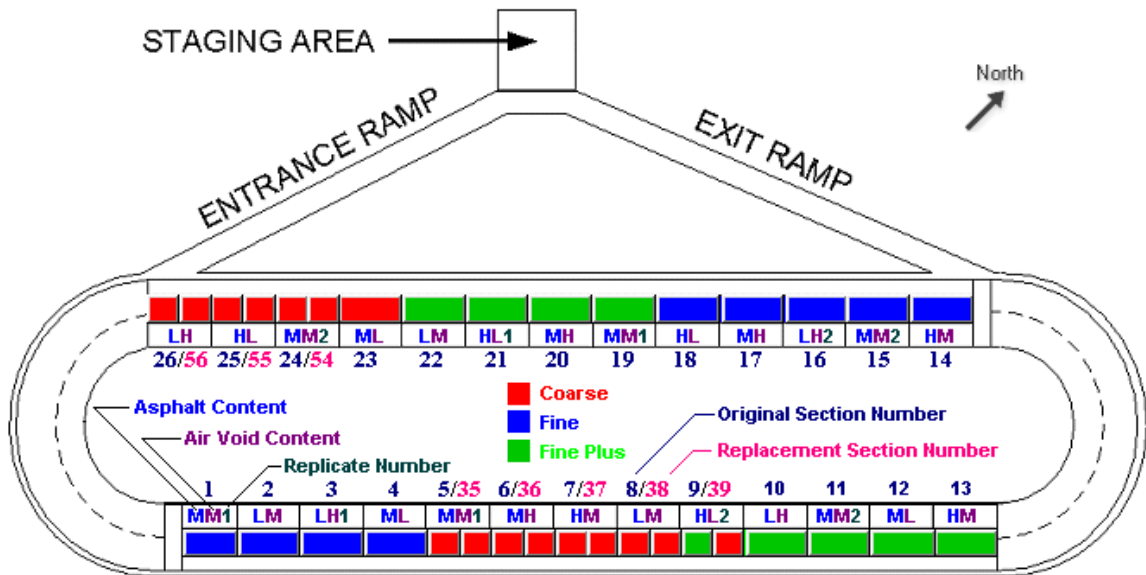


Figure 4.4 WesTrack Oval Track Section Map (WesTrack Database)

The maximum specific gravities were measured using loose batches in accordance with ASTM 2041-90 and are summarized in Table 4.5 for both fine and coarse mixes (McGraw, 2000). The mixtures were mixed at 151°C. After mixing, the mixtures were aged for four hours at 135°C. The samples were compacted using the Superpave Gyratory Compactor at 141°C and were cut into two specimens for testing in accordance with the procedure for North Carolina specimens. A trial and error procedure was used to determine the desired compaction efforts to obtain the target air void level of the specimen, at 4%, 8%, or 12 %, by adjusting the compaction height of samples from the same quantity of mixes (see Appendix A). The air voids were measured using SSD methods, with a tolerance level of +/-0.5%. It is noted that the 12% air void specimen could not be fabricated in the lab due to compaction impracticability. For convenience, three consecutive letters are designated as gradation, air void level, and asphalt content, using the following letters:

- a. *C* and *F* stand for coarse gradation and fine gradation, respectively.
- b. *L*, *M*, and *H* stand for low, medium, and high air void level, respectively, and
- c. *L*, *O*, and *H* stand for low, optimum, and high asphalt content, respectively.

For example, *CLO* represents the mix with coarse gradation, a low air void level, and optimum asphalt content. Table 4.6 summarizes the compaction effort for eight mixtures in this study. It should be noted that these designations are different from those of the original WesTrack study shown in Figure 4.4.

4.1.3 Field Cores

Field cores were sampled from the WesTrack pavements. Figure 4.7 illustrates the basic approach used to obtain test specimens for testing from a field core. Specimens were sliced from the middle of each of the two lifts to obtain the uniform mixture that predominantly controls the fatigue cracking performance of a section.

It was noted that traffic direction was marked on the field cores. Thus, arrow heads were drawn at the end of the line on the top side of the specimen to indicate the direction of load application for the indirect tensile test. The arrows thereby indicate that the tensile stresses induced in the indirect tensile test are coincidental to the longitudinal tensile stresses which cause fatigue cracking in the field.

Table 4.3 Aggregate Gradation of WesTrack Coarse Mixes

Sieve Size	Aggregate % Pass (98.5%)	Lime % Pass (1.5%)	Total Passing Percent (%)
3/4	100.00	100.00	100.00
1/2	81.46	100.00	81.74
3/8	65.71	100.00	66.22
#4	40.98	100.00	41.87
#8	26.29	100.00	27.40
#16	18.30	100.00	19.52
#30	13.06	100.00	14.37
#50	8.84	100.00	10.21
#100	4.48	100.00	5.91
#200	2.52	90.00	3.83

Table 4.4 Aggregate Gradation of WesTrack Fine Mixes

Sieve Size	Aggregate % Pass (73.5%)	Sand % Pass (25%)	Lime % Pass (1.5%)	Total Passing Percent (%)
3/4	100.00	100.00	100.00	100
1/2	84.07	100.00	100.00	88.29
3/8	67.12	100.00	100.00	75.83
#4	29.53	100.00	100.00	48.20
#8	13.84	100.00	100.00	36.67
#16	8.88	96.00	100.00	32.02
#30	7.54	79.90	100.00	27.02
#50	5.38	39.90	100.00	15.43
#100	4.67	10.51	100.00	7.56
#200	2.60	1.54	90.00	3.65

Table 4.5 Theoretical Maximum Specific Gravity of WesTrack Mixtures

Fine Mix		Coarse Mix	
Asphalt Content (%)	G _{mm}	Asphalt Content (%)	G _{mm}
4.7	2.424	5.1	2.409
5.4	2.388	5.8	2.386
6.1	2.387	6.5	2.363

Table 4.6 Compaction Efforts for WesTrack Mixtures Selected

Mix	FLO	FML	FMO	FMH	CLO	CML	CMO	CMH
Sample Height (mm)	116	119.36	121.76	119.23	115.33	121.74	121.6	121

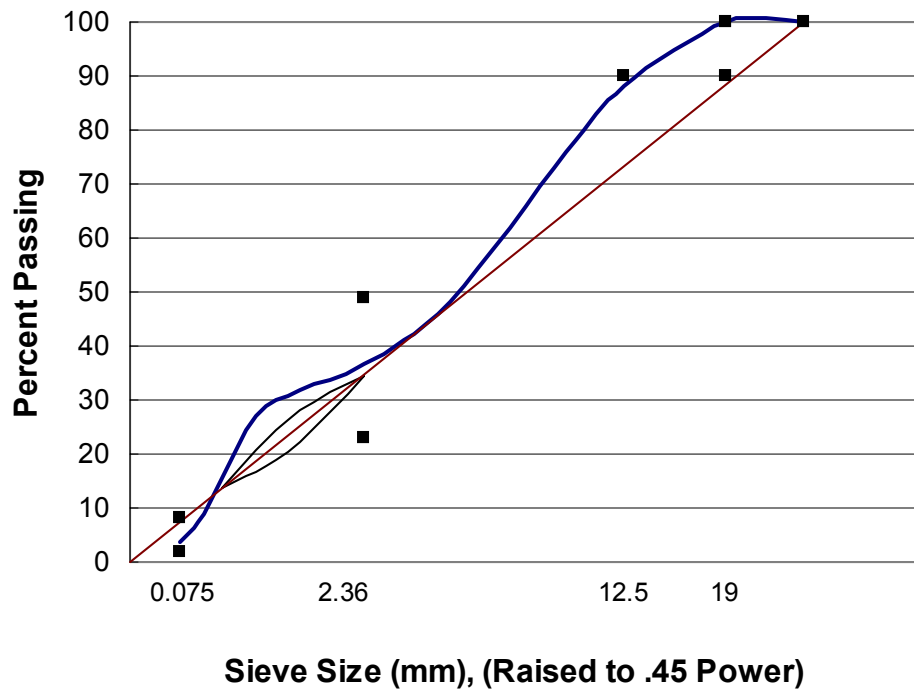


Figure 4.5 Design Gradation of WesTrack Fine Mix

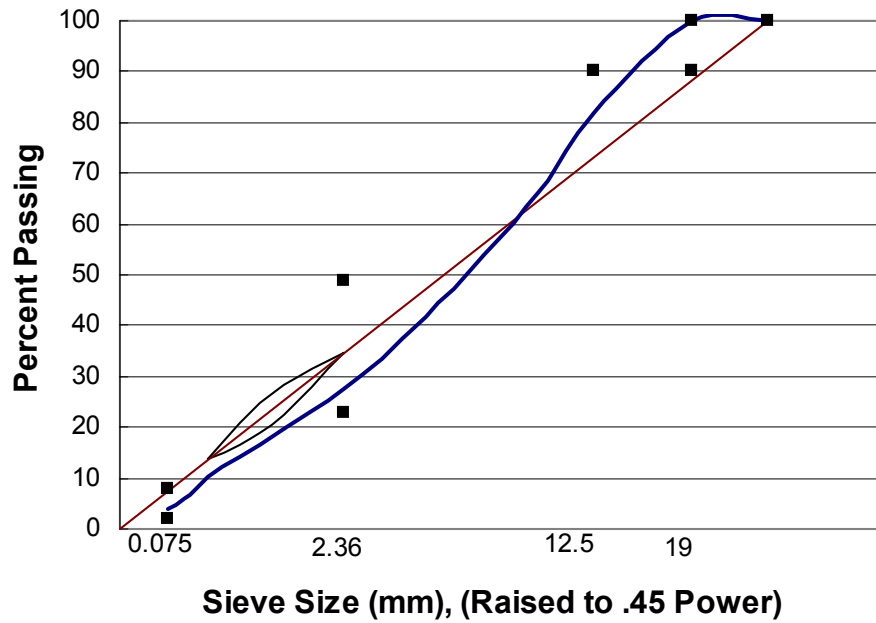


Figure 4.6 Design Gradation of WesTrack Coarse Mix

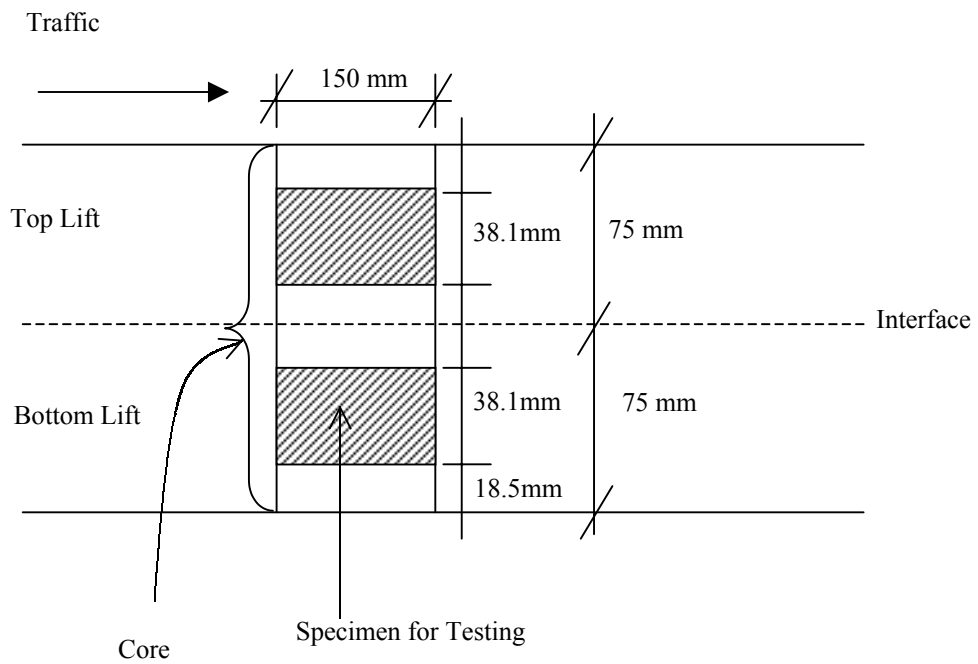


Figure 4.7 Approach to Obtain Specimen for Testing from Field Core

Upon completion of specimen preparation, CoreLok (see Figure 4.8) was available for air void measurement. CoreLok was developed due to the increase in the use of coarse and open graded mixes which created a need for a more reliable and accurate method of bulk specific gravity measurement of laboratory and field specimens. Open graded mixes readily absorb water and drain quickly when removed from the water tank. The lack of control over the penetration and drainage of water in and out of asphalt samples creates a fundamental problem with the water displacement measurement using the current principle for the determination of specific gravity.

The most efficient and accurate method of correcting for this problem is to seal the samples prior to testing in water. The current sealing methods, namely Parafilm and Paraffin, are optimized for 100 diameter samples.

CoreLok uses a 1.25 hp vacuum pump in conjunction with control electronics and a vacuum tight chamber to seal samples. The sample is placed inside a specially designed plastic polymer bag and inserted in the chamber. The door is then closed. A switch recognizes the door closure and activates the vacuum pump. The vacuum pump operates for approximately 45 seconds. At this point, the chamber and the bag are close to absolute vacuum. An automatic sealing strip heat-seals the bag at the open end and air is allowed to enter the chamber in a controlled vacuum. Since the bag is sealed and is under vacuum, the increased pressure in the chamber forces the plastic bag around the sample, creating a tightly vacuum-sealed sample (CoreLok, 2000).

The advantage of this method is that the membrane lines the outer surface closely and completely seals the specimen. Since there is minimal operator effort involved, this method has excellent repeatability.



Figure 4.8 CoreLok Machine Used to Measure Air Void

The results of the air void measurement of specimens from field cores are shown in Table 4.7. It was found that the CoreLok method yielded a close value for fine mixes, compared to the SSD method. For coarse mixtures, there is a significant difference between the result using CoreLok and that using SSD. It was expected that the CoreLok method would indicate the closest value to the actual because it followed the contour of surface pores and prevented water from penetrating inside relatively successfully.

Table 4.7 Comparison of Air Void Measurement Using SSD and Corelok

Mixture ID		Bulk Specific Gravity		Air Void (%)	
		SSD	CoreLok	SSD	CoreLok
FMO	Top	2.286	2.292	6.1	5.8
	Bottom	2.268	2.272	5.8	5.7
FML	Top	2.267	2.271	6.9	6.8
	Bottom	2.244	2.243	6.8	6.9
FHL	Top	2.190	2.192	11.6	11.6
	Bottom	2.230	2.226	8.4	8.5
FLO	Top	2.319	2.322	4.2	4.1
	Bottom	2.317	2.32	3.9	3.9
CLO	Top	2.33	2.33	3.6	3.7
	Bottom	2.300	2.308	3.9	3.6
CHOr	Top	2.153	2.114	10.9	12.5
	Bottom	2.126	2.093	13.0	14.4
CMOr	Top	2.300	2.297	5.8	5.9
	Bottom	2.277	2.273	7.1	7.3
CHLr	Top	1.999	2.099	18.5	14.4
	Bottom	2.022	2.124	17.6	13.5

One unique feature of the CoreLok method is that samples remain dry and uncontaminated for further testing purpose after measurements are taken. After the measurements are taken using the SSD method, samples of fine gradation are difficult to dry, either by an air pressure gun or by fan, blowing overnight, due to water entrapment and the dense structure within samples. The samples must be vacuumed several times.

Both the ASTM D2726 and D1188 procedures require that the specimen be placed in the oven for twenty-four hours at 110° C before measuring its mass in the dry condition. This requirement consumes a considerable amount of time and can alter the properties of the specimens. Therefore, CoreLok is an effective way to measure air void, with the exception that special care must be taken to avoid breaking the seal.

Different specimen diameters were used in the indirect tensile test. The laboratory-fabricated specimen had a 101.6mm (4 inches) diameter, which was cored out of an “as compacted” sample with a 152.4mm (6 inches) diameter, while the specimen from the field core had a 152.4mm (6 inches) diameter. The effect of specimen geometry on test results will be addressed in Chapter 5.

4.2 Test Configuration

AASHTO TP9-96 is typically used as the standard test method for indirect tensile tests. One of the major differences between the AASHTO TP9-96 setup and the setup in this study is that AASHTO TP9-96 uses a loading frame with four columns whereas this study uses a loading frame with two columns. Another difference is the gauge length used to mount the LVDTs for measurement of specimen deformation. AASHTO TP9-96 uses a GPM where the gauge length is set at 25.4 mm (one inch), whereas the gauge length used in this study is 50.8 mm (2 inches). The advantage of using this gauge length is that it minimizes the effect of large aggregates located in between the two gauge points and stress concentration in the vicinity of loading strips. The plan-view of the apparatus that holds the LVDTs is presented in Figure 4.9.

Figure 4.10 shows the gluing and marking device for the IDT specimens that secures the concentric and perpendicular LVDT mounting mirrored on the opposing flat circular faces. The perpendicular line on the sides of specimen coincide with the mark on the top end of the specimen that indicates the direction of traffic, if present. The cross marked on the cylindrical side serves to match the cross on the bottom loading strip, thus minimizing the possibility of misaligning the specimen. The approach to position the specimen is illustrated in Figure 4.11. The final test setup is presented in Figure 4.12.

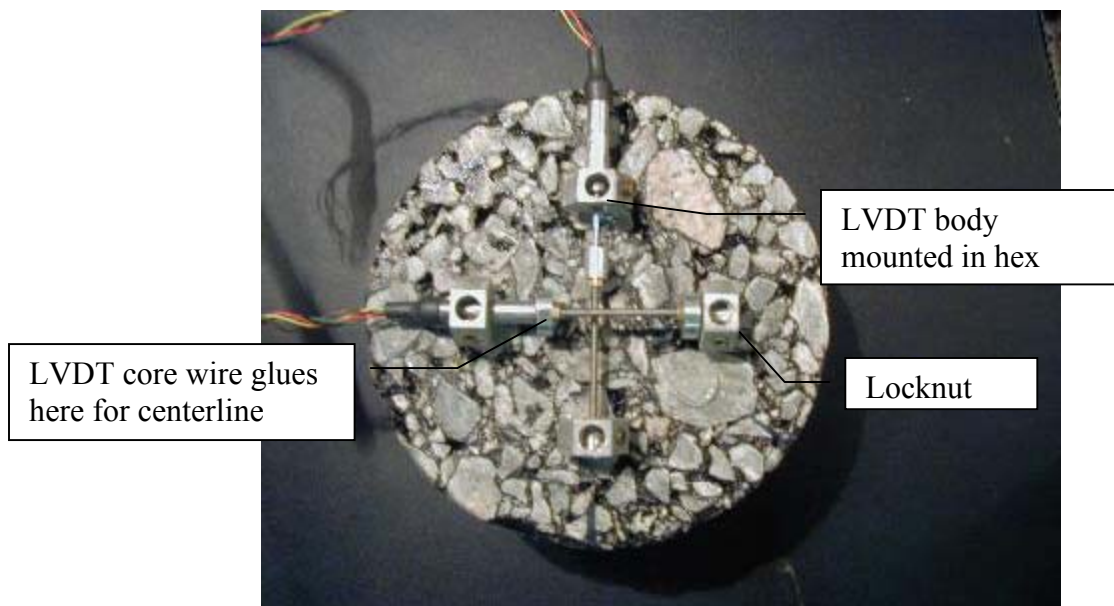


Figure 4.9 Plan View of LVDTs Glued to a Specimen



Figure 4.10 Gluing and Marking Device

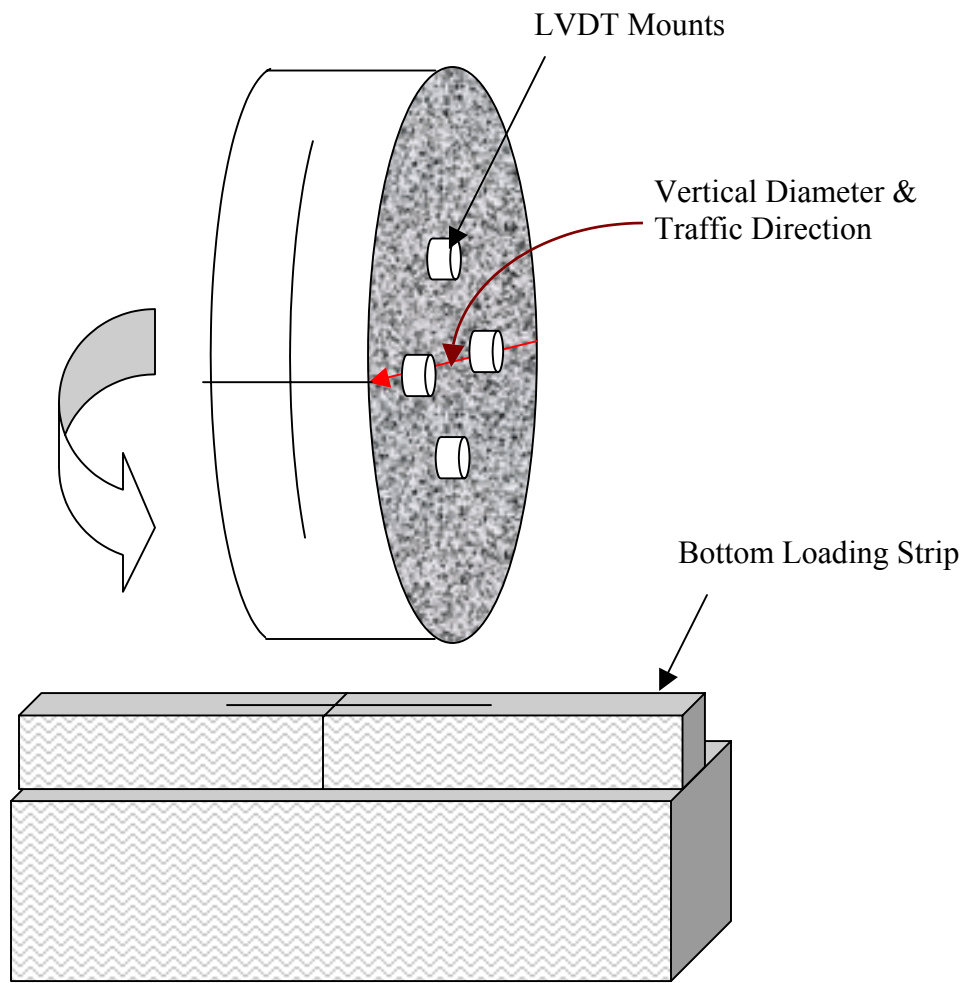


Figure 4.11 Positioning Specimen on Loading Strip

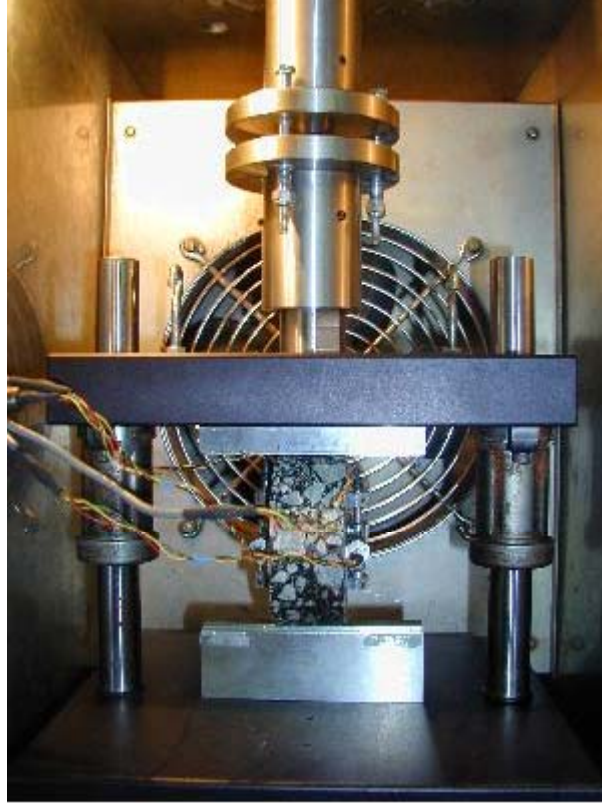


Figure 4.12 Test Configuration of Indirect Tensile Test

4.3 Test Program

All tests were performed in an indirect tensile testing mode using the MTS servo-hydraulic closed-loop testing machine. An environmental chamber was used to control the temperature of the specimens. Prior to testing, the specimen was placed into the chamber at the testing temperature for at least two hours for conditioning. Displacements were measured by XSB LVDTs and loads were measured by the MTS load cell. Test data were collected by the National Instrument LabView 16-bit data acquisition board.

In an attempt to validate the applicability of the theory of viscoelasticity to the indirect tensile testing mode, creep and cyclic loading tests were conducted on the North Carolina mixes. Creep tests at several different temperatures were performed to obtain the thermorheological properties. To minimize variation due to the inherent differences from sample to sample, a series of tests was performed on each individual specimen. Since the same specimen underwent various combinations of tests and temperatures, a relatively low stress/strain level was applied to the specimen to ensure negligible damage during the entire testing period. The loading level was reduced when testing was performed at higher temperatures. To check the extent of damage that the specimen received during a series of tests, additional creep tests were conducted at 20°C as a rheological fingerprint. All other tests were conducted at 20°C. For WesTrack specimens, a creep test was conducted first, followed by a constant-crosshead-rate monotonic test after a 30-minute rest period.

Creep Test

A creep test is designed to apply a load instantaneously, maintain the load level for a time period, and then unload instantaneously. The loading history and response in a typical creep test are shown in Figure 4.13, where the dotted line denotes the actual loading path.

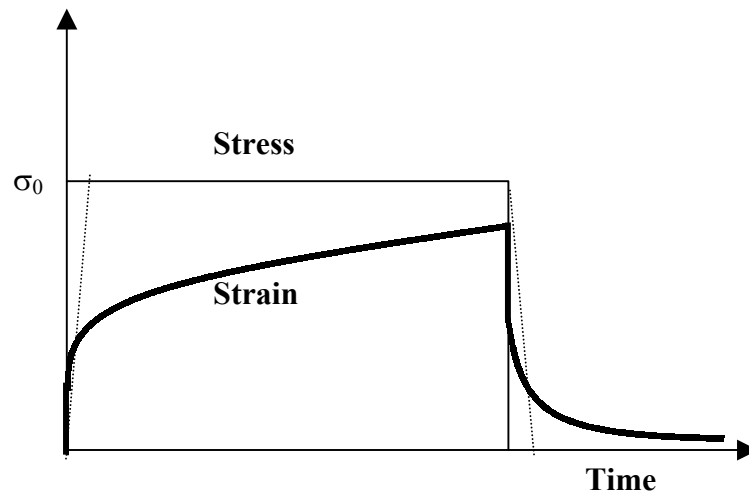


Figure 4.13 Schematic of Creep Test

The load must be small enough for the response of the asphalt concrete to be within the linear viscoelastic range. The principle of superposition in the theory of viscoelasticity is used to obtain the appropriate loading level. Creep compliance may then be calculated as follows:

$$D(t) = \frac{\varepsilon(t)}{\sigma_o} \quad (4.1)$$

where $D(t)$ = creep compliance,
 σ_0 = stress amplitude, and
 $\varepsilon(t)$ = strain.

Creep tests were conducted at $-10, 0, 10,$ and 20°C to obtain the creep compliance master curve and time-temperature shift factors. A minimum two-hour rest period was allowed between tests.

Calculation of pseudo strain requires the expression of the relaxation modulus as a function of time. The relaxation modulus test is fairly cumbersome to perform because the immediate increase in displacement input results in a large initial load response. For this practical reason it is desirable to predict the relaxation modulus from a creep test or complex modulus test, using the theory of viscoelasticity. In this study, the relaxation modulus was predicted from creep compliance.

Complex Modulus Test

The complex modulus test applies a haversine load to the specimen at a particular amplitude and frequency. Figure 4.14 shows a schematic of stress input and strain response.

The dynamic modulus and phase angle may be calculated from the complex modulus test results. The complex modulus is composed of the storage and loss moduli in the following manner:

$$E^* = E' + iE'' \quad (4.2)$$

where E^* = complex modulus,

E' = storage modulus, and
 E'' = loss modulus.

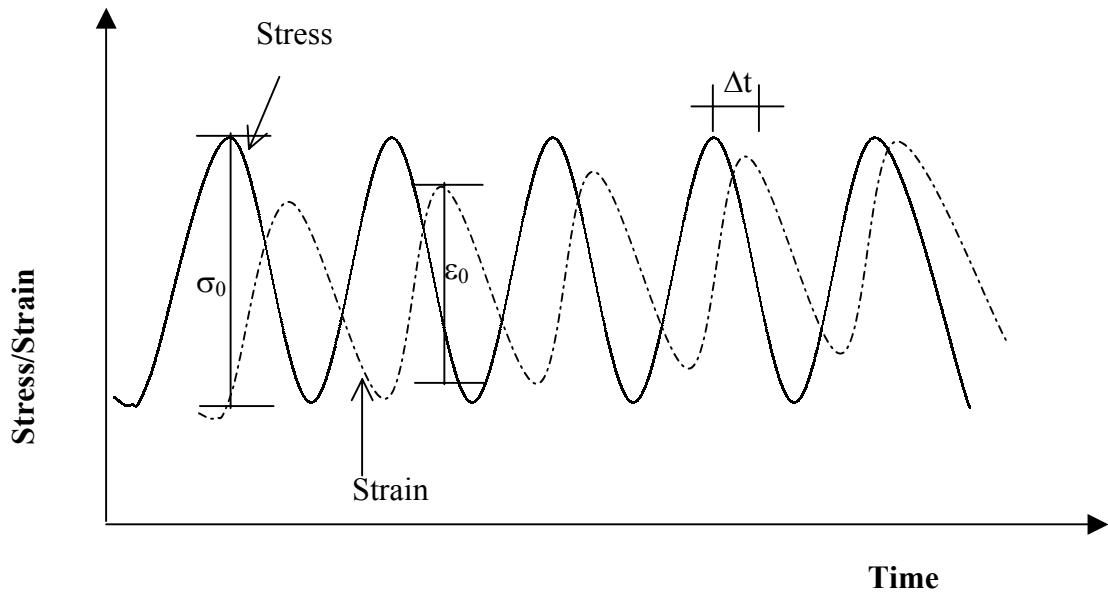


Figure 4.14. Schematic of Cyclic Test

Dynamic modulus is the amplitude of complex modulus:

$$|E^*| = \sqrt{(E')^2 + (E'')^2} = \left| \frac{\sigma_0}{\epsilon_0} \right| \quad (4.3)$$

where σ_0, ϵ_0 = the stress and strain amplitudes in the complex modulus test.

The phase angle, ϕ , is calculated from the time lag between the load and displacement:

$$\phi = 2\pi f \Delta t = \tan^{-1} \left(\frac{E''}{E'} \right) \quad (4.4)$$

where f is loading frequency and Δt is the time lag between load and displacement.

For an purely elastic material the phase angle is 0° , and 90° is for purely viscous material. The same specimens tested in creep tests were used in the cyclic tests. A computer program has been developed to regress the measured strain and stress that were used to calculate pseudo strain. This program not only saved analysis time, but also minimized the possible error due to the signal noise in the measured data.

Tensile Strength Test

The tensile strength test is designed to apply a load to the specimen at a constant rate of ram movement. Figure 4.15 shows a schematic of a tensile strength test. Ideally, it is desirable to have a constant-strain-rate input. Since the strain is calculated using the measured displacement across the 50.8 (2 inches) gauge length, it is difficult to conduct such a test. Instead, a constant-crosshead-rate monotonic test was performed, controlling the movement of ram at 50.8 mm/minute. The maximum level of ram movement was selected so that the resulting load level reached its peak value and was decreasing. However, the test should be finished or be stopped before the specimen is split completely. Otherwise, LVDTs, especially the vertical ones, may be damaged. Tensile strength, total energy (TE), strain energy (SE), and damage energy (DE) may be obtained from the test results. The definitions of these energies are shown in Figure 4.16.

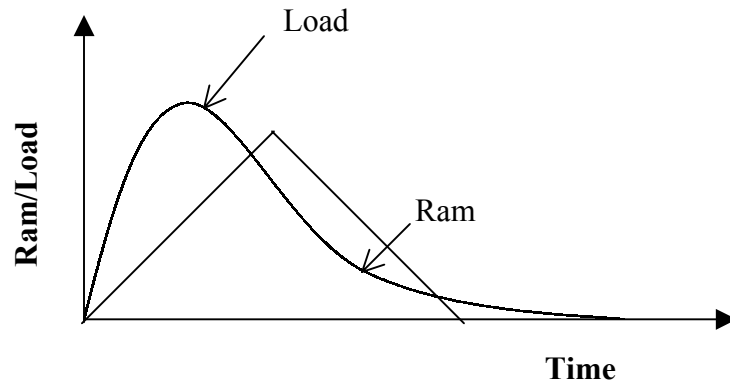


Figure 4.15. Schematic of Tensile Strength Test

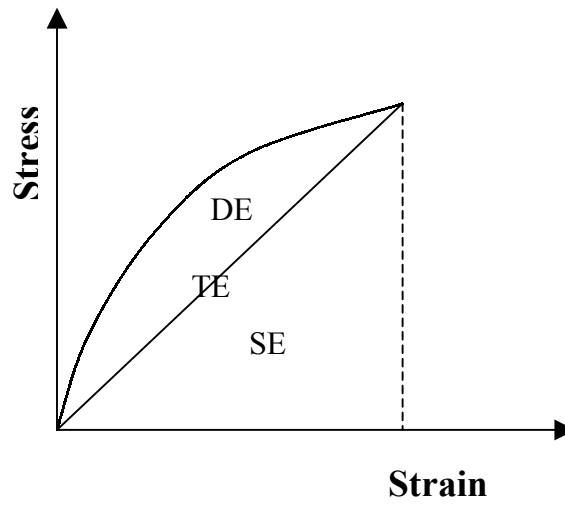


Figure 4.16 Definition of Energies

CHAPTER 5

DETERMINATION OF VISCOELASTIC PROPERTIES

Creep compliance is one of the essential mechanical properties in the study of fatigue behavior of asphalt concrete. The relaxation modulus also can be predicted from creep compliance through the theory of viscoelasticity. AASHTO TP9-96 provides the method to determine creep compliance. However, the method is not applicable to the displacement measurement across the 50.8mm gauge length that is used in this study. Moreover, the method is based on the approximation of elastic analysis. In this study, the theory of viscoelasticity was used to develop a method for determination of creep compliance from deformations measured from a 50.8mm gauge length.

In indirect tension testing, a microcrack is initiated at the center of the specimen and propagates towards the loading strips along the vertical diameter due to the tensile stress. Therefore, the response of the material at the center of the testing specimen is of interest. Since the stress and strain distribution in the indirect tension specimen is non-uniform, the strain at the center of the specimen is not equal to the average strain which is obtained by dividing measured displacement by gauge length used. Therefore, the relationship between center strain and measured displacement was derived based on the theory of viscoelasticity.

Several approaches were combined to verify the relationships derived. First, viscoelastic finite element analysis was used to check the theoretical derivations. However, after this finite element analysis verification, the applicability of these relationships to asphalt concrete remains unknown. Secondly, considering the relatively

simple expression of stress and strain in the uniaxial direct tension specimen, creep compliance obtained from an indirect tension test was compared to that from a direct tension test. To eliminate the effects of sample variation on the comparison, both the direct tension test and the indirect tension test were conducted on specimens taken from one Superpave Gyratory Compactor sample. Thirdly, pseudo strain was determined to check the applicability of the theory of viscoelasticity to asphalt concrete in the indirect tension testing mode. On the other hand, pseudo strain could be used to verify the theoretical developments. To calculate pseudo strain, the relaxation modulus needs to be predicted from creep compliance. The interrelationship between creep compliance and the relaxation modulus was presented and the methods to convert creep compliance into a relaxation modulus were studied.

As previously described in Chapter 4, different specimen geometries were used in this study. The effects of specimen geometry on the characterization of asphalt concrete were studied using finite element analysis and experiment.

5.1 Development of Creep Compliance Calculation Method for Indirect Tension Specimen

As discussed in Chapter 3, two-dimensional and three-dimensional solutions are available for the analysis of an indirect tension specimen. The three-dimensional solution theoretically provides more accurate results. However, it is cumbersome to operate the complicated equations. It was documented (Zhang 2000) that plane stress conditions are approximated fairly closely for a relatively thin (around 25.4mm) specimen. Since the

thickness of specimen used in this study was 38.1 mm, a creep compliance calculation method was developed based on Hondros' two-dimensional elastic solution of stresses.

In Hondros's analysis, the stresses along the horizontal diameter are expressed as follows:

$$\sigma_x(x) = \frac{2P}{\pi ad} \left[\frac{(1-x^2/R^2) \sin 2\alpha}{1+2x^2/R^2 \cos 2\alpha + x^4/R^4} - \tan^{-1} \left(\frac{1-x^2/R^2}{1+x^2/R^2} \tan \alpha \right) \right] = \frac{2P}{\pi ad} [f(x) - g(x)] \quad (5.1)$$

$$\sigma_y(x) = -\frac{2P}{\pi ad} \left[\frac{(1-x^2/R^2) \sin 2\alpha}{1+2x^2/R^2 \cos 2\alpha + x^4/R^4} + \tan^{-1} \left(\frac{1-x^2/R^2}{1+x^2/R^2} \tan \alpha \right) \right] = -\frac{2P}{\pi ad} [f(x) + g(x)] \quad (5.2)$$

where P = applied load,

a = loading strip width,

d = thickness of specimen,

R = specimen radius, and

α = radial angle.

Because of the small specimen thickness, 38.1mm, plane stress is assumed in the specimen:

$$\varepsilon_x(x) = \frac{1}{E} (\sigma_x - \nu \sigma_y) \quad (5.3)$$

where E is Young's modulus and ν is Poisson's ratio.

Due to the viscoelastic characteristics of asphalt concrete, strain is also time-dependent. The elastic-viscoelastic correspondence principle was used to solve the viscoelastic problem. The elastic-viscoelastic correspondence principle states that the viscoelastic equations are identical to the elastic equations in the Laplace transformed domain with the substitution of the Carson transformed modulus for the elastic modulus. In this study, Poisson's ratio is assumed to be constant. Thus, the transformed form of the stress-strain relationship is:

$$\bar{\varepsilon}(x, s) = \frac{1}{\tilde{E}}(\bar{\sigma}_x - \nu\bar{\sigma}_y) \quad (5.4)$$

where $\bar{\varepsilon}$, $\bar{\sigma}_x$, and $\bar{\sigma}_y$ are Laplace transformed strain and stresses while \tilde{E} is the Carson transformed modulus. According to the theory of viscoelasticity, the relationship between the relaxation modulus and creep compliance is:

$$\tilde{E} \times \tilde{D} = 1 \quad (5.5)$$

where \tilde{D} is the Carson transformed creep compliance. Substitute \tilde{E} with \tilde{D} , and Equation (5.4) becomes:

$$\bar{\varepsilon}(x, s) = \tilde{D}(\bar{\sigma}_x - \nu\bar{\sigma}_y) \quad (5.6)$$

Equations (5.1), (5.2), and (5.6) yield:

$$\bar{\varepsilon}(x, s) = \tilde{D} \frac{2\bar{P}}{\pi ad} [(1 + \nu)f(x) + (\nu - 1)g(x)] \quad (5.7)$$

where $P = P_0 H(t)$ for a creep test and

$H(t) = 0$, when $t < 0$; 1 , when $t > 0$.

Performing the inverse Laplace transform on both sides of Equation (5.7) yields:

$$\varepsilon(x, t) = \frac{(1 + \nu)f(x) + (\nu - 1)g(x)}{\pi ad} \int_0^t D(t - \tau) \frac{dP}{d\tau} d\tau \quad (5.8)$$

For the creep test, Equation (5.8) becomes:

$$\varepsilon(x, t) = 2P_0 D(t) \frac{(1 + \nu)f(x) + (\nu - 1)g(x)}{\pi ad} \quad (5.9)$$

The horizontal deformation of specimen U is obtained by integrating strain over the gauge length:

$$U(t) = \int_{-l}^l \varepsilon(x, t) dx \quad (5.10)$$

where l is half of the gauge length. Equations (5.9) and (5.10) yield:

$$U(t) = \frac{2P_0 D(t)}{\pi ad} \left[(1 + \nu) \int_{-l}^l f(x) dx + (\nu - 1) \int_{-l}^l g(x) dx \right] \quad (5.11)$$

After rearranging, creep compliance, $D(t)$, is represented as:

$$D(t) = \frac{U(t)}{2P_0 A} \quad (5.12)$$

$$\text{where } A = \frac{(1+\nu) \int_{-l}^l f(x) dx + (\nu-1) \int_{-l}^l g(x) dx}{\pi \alpha d}$$

According to Hondros' solution, the stresses along the vertical diameter are:

$$\sigma_x = \frac{2P}{\pi \alpha d} \left[\frac{(1-y^2/R^2) \sin 2\alpha}{1-2y^2/R^2 \cos 2\alpha + y^4/R^4} - \arctan\left(\frac{1+y^2/R^2}{1-y^2/R^2} \tan \alpha\right) \right] = \frac{2P}{\pi \alpha d} [m(y) - n(y)] \quad (5.13)$$

$$\sigma_y = -\frac{2P}{\pi \alpha d} \left[\frac{(1-y^2/R^2) \sin 2\alpha}{1-2y^2/R^2 \cos 2\alpha + y^4/R^4} + \arctan\left(\frac{1+y^2/R^2}{1-y^2/R^2} \tan \alpha\right) \right] = -\frac{2P}{\pi \alpha d} [m(y) + n(y)] \quad (5.14)$$

Similar to the procedure above, creep compliance is represented, in terms of vertical deformation, $V(t)$:

$$D(t) = \frac{V(t)}{2P_0 B} \quad (5.15)$$

$$\text{where } B = \frac{(\nu-1) \int_{-l}^l n(y) dy - (1+\nu) \int_{-l}^l m(y) dy}{\pi \alpha d}$$

Equating Equations (5.12) and (5.15) yields:

$$\nu = -\frac{a_1U(t) + b_1V(t)}{a_2U(t) + b_2V(t)} \quad (5.16)$$

$$D(t) = -\frac{d}{P}[cU(t) + eV(t)] \quad (5.17)$$

where a_1 , a_2 , b_1 , b_2 , c , and e are coefficients related to specimen diameter and gauge length used to measure displacements. Values of these coefficients from different diameter and gauge length as shown in Table 5.1.

Table 5.1 Coefficients Used to Calculate Poisson's Ratio and Creep Compliance

Specimen Diameter (mm)	Gauge Length (mm)	a_1	a_2	b_1	b_2	c	e
100	25.4	3.385	1.081	1	3.122	0.7874	2.2783
	50.8	4.580	1.316	1	3.341	0.4032	1.024
150	25.4	3.172	1.039	1	3.060	1.199	3.533
	50.8	3.673	1.154	1	3.192	0.611	1.685
	76.2	4.559	1.330	1	3.311	0.415	1.034

It is noteworthy that Equation (5.17) is independent of Poisson's ratio and, hence, is material-independent. This is attributed to a two-dimensional plane stress assumption. Poisson's ratio could not be removed from Equation (5.17) if the viscoelastic solution was based upon a three-dimensional elastic solution, as shown in Equations (3.15) and (3.16).

5.2 Determination of Center Point Strain from Horizontal Deformation Measurement

Given that the maximum tensile strain along the horizontal diameter occurs at the center point of the specimen and that the fatigue plane is along the vertical diameter, the measured displacement across the gauge length must be converted into the center point strain, instead of the average strain, in order to study the stress-strain relationship of the element where crack is initiated.

Based on Equation (5.9) and the theory of viscoelasticity, along the horizontal diameter of the indirect tension specimen, the center point strain, $\varepsilon_{x=0}$, in a creep test is represented as follows:

$$\varepsilon_{x=0}(t) = D(t) \frac{2P_0}{\pi ad} [(1 + \nu)f(x=0) + (\nu - 1)g(x=0)] \quad (5.18)$$

Equations (5.11) and (5.18) yield:

$$\varepsilon_{x=0} = U \frac{a + b\nu}{c + d\nu} = UA \quad (5.19)$$

where a, b, c, and d are coefficients related to specimen diameter and gauge length used.

Table 5.2 shows the values of these coefficients for specimens with different diameter and gauge length.

Table 5.2 Coefficients in Equation (5.19)

Specimen Diameter (mm)	Gauge Length (mm)	a	b	c	d
100	25.4	12.4	37.7	0.291	0.908
	50.8	12.4	37.7	0.471	1.57
150	25.4	8.48	25.6	0.207	0.634
	50.8	8.48	25.6	0.373	1.18
	76.2	8.48	25.6	0.478	1.59

It is seen from Equation (5.19) that the strain-displacement relationship is independent of stress. Therefore, Equation (5.19) is applicable to specimens subjected to any loading condition, whether constant-strain-rate loading or controlled-stress cyclic loading, etc. It is found that the strain-displacement relationship is dependent on Poisson's ratio, indicating that the relationship is material-dependent. Theoretically, the strain-displacement relationship should be independent of Poisson's ratio. Again, the dependence in Equation (5.19) is ascribed to the plane stress assumption. However, the dependence is insensitive to the change of Poisson's ratio, as shown in Figure 5.1 where the number before the hyphen stands for specimen diameter while the one after the

hyphen stands for gauge length. When Poisson's ratio increases from 0.1 to 0.5, there is only a slight change of A in Equation (5.19). Therefore, the effect of plane stress assumption on the strain calculation is negligible.

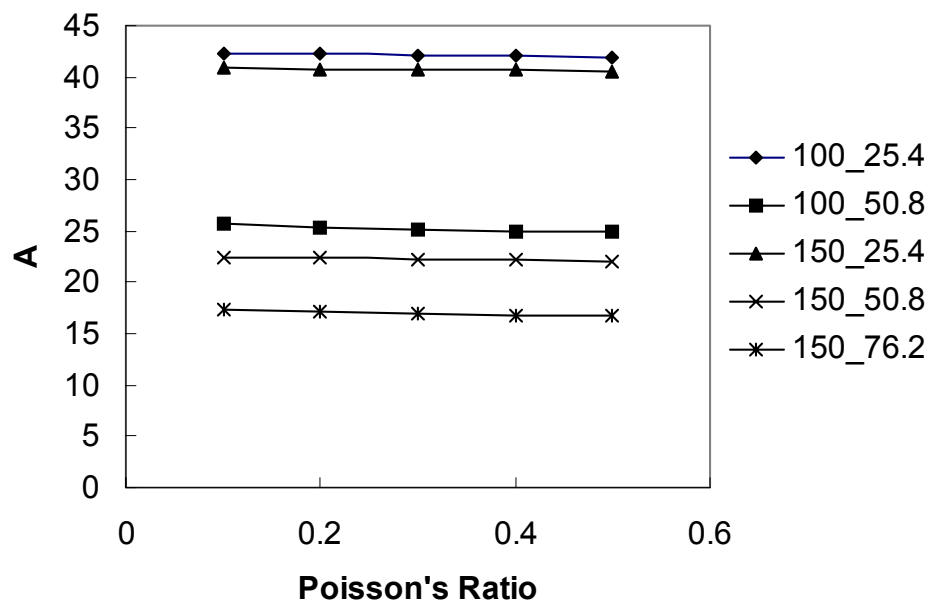


Figure 5.1 Effect of Change of Poisson's Ratio on Strain Calculation

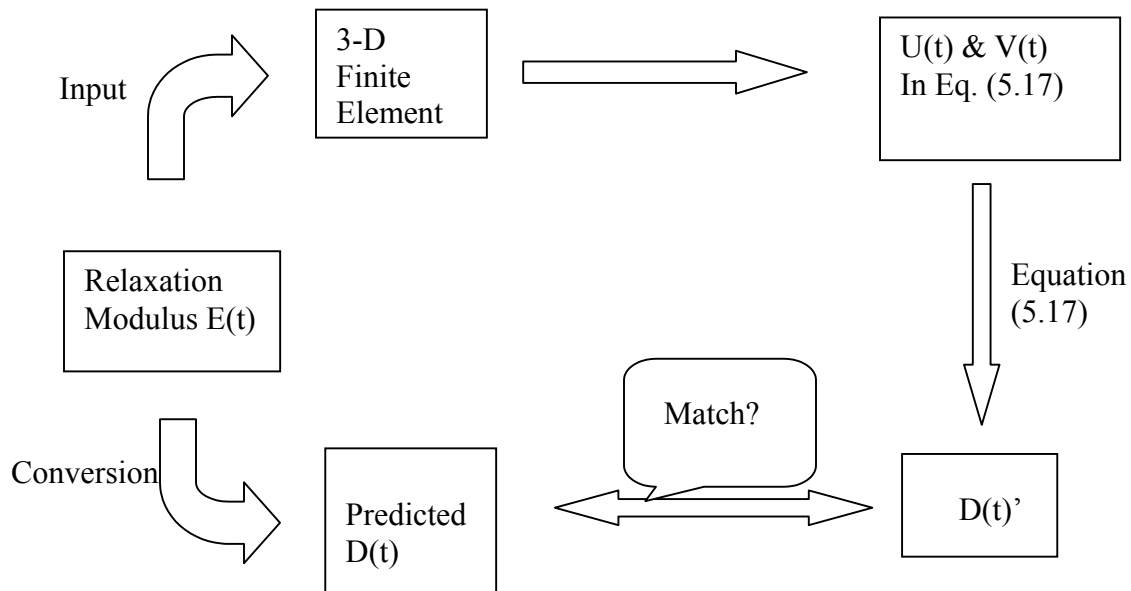
5.3 Verification Using Finite Element Viscoelastic Analysis

5.3.1 Verification of Creep Compliance Calculation Method

Three-dimensional finite element viscoelastic analysis is used to verify the creep compliance calculation in Equation (5.17). With ABAQUS computer software, the 3-D finite element model is used to analyze an IDT specimen, 100 mm in diameter and 38

mm in thickness, loaded with a 12.8 mm wide steel loading strip. Due to its symmetry, only a quarter of the specimen is used and meshed, as shown in Figure 5.2. A constant load was applied to the loading strip for 100 seconds. The step used to accomplish the analysis was controlled by automatic time incrementation.

Indirect tensile specimen deformations are obtained by using known values of creep compliance in the form of a Prony series and Poisson’s ratio. The standard test configuration described in Chapter 4 is used. The horizontal and vertical deformations across the 50.8mm gauge length are used to calculate the creep compliance using Equation (5.17). The calculated creep compliance is compared with creep compliance predicted from the relaxation modulus. The procedure of verification is shown in the following flowchart:



Material parameters needed for the ABAQUS viscoelastic model are the normalized shear modulus and bulk modulus in terms of a Prony series, whereas the modulus obtained from the laboratory in this study is the relaxation modulus. An analytical procedure is needed to convert the relaxation modulus into creep compliance and the relaxation modulus into shear and bulk moduli. The approach to convert the relaxation modulus into creep compliance will be addressed in detail later. Assuming the material is isotropic and non-aging, the relationship among the relaxation modulus, shear modulus, and bulk modulus may be represented as:

$$\tilde{K} = \frac{\tilde{E}}{3(1-2\tilde{\nu})} \quad (5.20)$$

$$\tilde{G} = \frac{\tilde{E}}{2(1+\tilde{\nu})} \quad (5.21)$$

where \tilde{K} = Carson transform of the bulk relaxation modulus,
 \tilde{G} = Carson transform of the shear relaxation modulus,
 \tilde{E} = Carson transform of the relaxation modulus, and
 $\tilde{\nu}$ = Carson transform of Poisson's ratio.

Assuming Poisson's ratio does not change with time, the Carson transform of Poisson's ratio ($\tilde{\nu}$) becomes a constant (ν). Therefore, the shear and bulk moduli may be estimated from the relaxation modulus in the following relationship:

$$K(t) = \frac{E(t)}{3(1-2\nu)} \quad (5.22)$$

$$G(t) = \frac{E(t)}{2(1+\nu)} \quad (5.23)$$

The relaxation modulus in the form of a Prony series is presented as:

$$E(t) = E_g + \sum_{i=1}^{11} E_i e^{-\frac{t}{\rho_i}} \quad (5.24)$$

where E_i and τ_i are constants and are tabulated in Table (5.3).

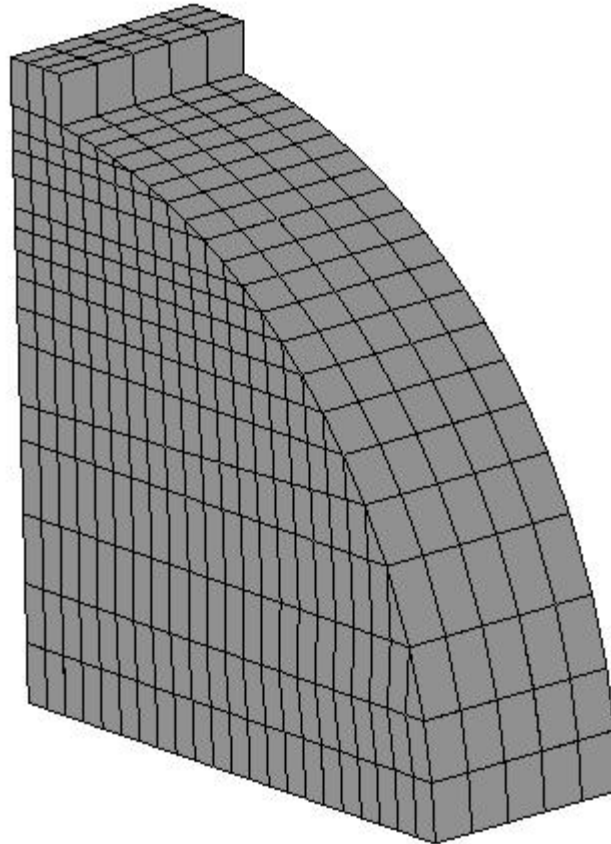


Figure 5.2 3-D Finite Element Model Mesh of Indirect Tension Specimen

Table 5.3. Coefficients in a Prony series representation $E(t)$ (After Lee, 1996)

i	ρ_i (sec)	E_i (Gpa)
1	1E-5	2.03E+02
2	1E-4	3.77E+03
3	1E-3	3.59E+03
4	1E-2	2.52E+03
5	1E-1	1.29E+03
6	1E+00	4.09E+02
7	1E+01	1.31E+02
8	1E+02	3.40E+01
9	1E+03	1.22E+01
10	1E+04	1.61E+00
11	1E+05	1.76E+00
$E_g=3.5$ Gpa		

Creep compliance was determined from the relaxation modulus using a numerical integration method (see Appendix B) based on the creep compliance and relaxation modulus convolution integral. With viscoelastic finite element analysis, the horizontal and vertical displacements across a 50 mm gauge length, $U(t)$ and $V(t)$ in Equation (5.17), were obtained and were used to calculate creep compliance.

The analysis results are shown in Figure 5.3 in which converted $D(t)$ is the creep compliance predicted from the known relaxation modulus; Equation (5.17) is the calculated creep compliance using the viscoelastic solution.

Figure 5.3 shows a good correspondence between creep compliances from Equation (5.17) and the predicted creep compliance, thus indicating the validity of the creep compliance calculation method developed for this test setup using a 50.8mm gauge length.

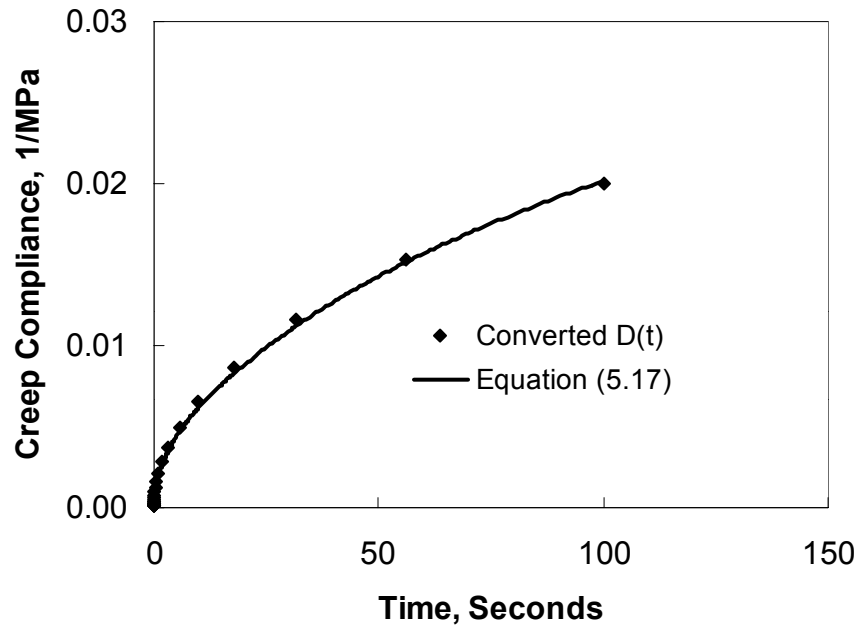
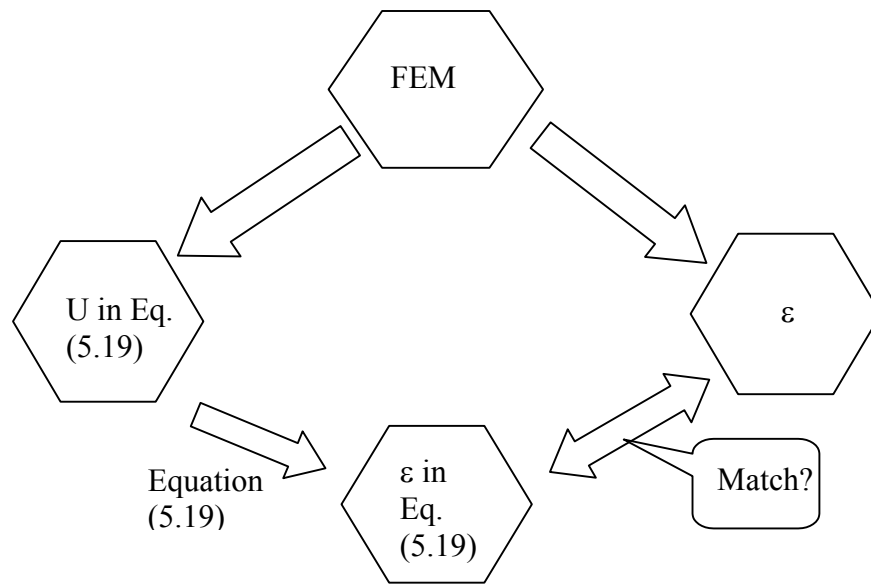


Figure 5.3 Verification of Creep Compliance Calculation

5.3.2 Verification of Calculation of Center Strain Using Finite Element Method

From the finite element analysis, the displacements across the 50.8mm gauge length and the center point strain may be obtained directly. The center point strain may also be calculated from Equation (5.19) with the known displacement. The procedure of verification is shown in the following flowchart:



The elastic analysis of this finite element model was used to warrant the accuracy of finite element mesh by checking with the known elastic theoretical IDT stress/strain solution while viscoelastic analysis of uniaxial finite element model was used to check the viscoelastic material and loading input based upon theoretical viscoelastic uniaxial stress/strain solutions. The strain at the center of IDT specimen can be obtained from finite element analysis output using the nodal strain.

Figure 5.4 compares strain obtained from the finite element analysis to calculated strain using Equation (5.19). The average strain (measured deformation divided by gauge length) is also shown in Figure 5.4 for comparison. It is seen from Figure 5.4 that the calculated center strain is very close to that obtained from the finite element analysis, indicating that Equation (5.19) calculates center strain from the displacement accurately.

5.4 Verification Using Uniaxial Direct Tension Testing and Indirect Tension Testing

Finite element analysis indicates that the theoretical developments accurately represent the properties of materials in indirect tensile tests. However, because asphalt concrete is a complicated material, the applicability of the derivations to asphalt concrete is unknown and needs to be proven experimentally.

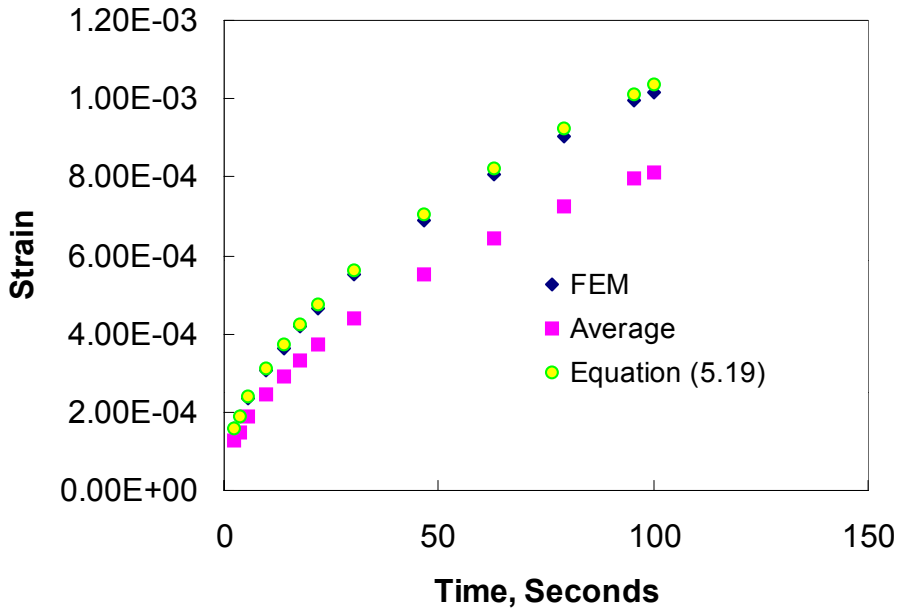


Figure 5.4 Verification of Center Strain Calculation

Considering the relatively simple stress and strain state in a direct tension specimen, the test result from the uniaxial test may provide the reference to that of indirect tension tests. Thus, creep compliance obtained from an indirect tension creep test was compared to that obtained from a direct tension creep test.

In a direct tension test, the stress and strain are represented as:

$$\sigma = \frac{P(t)}{A}, \quad \varepsilon = \frac{L(t)}{GL} \quad (5.25)$$

where P = load applied,
 A = circular cross-section area,
 L = measured displacement, and
 GL = gauge length.

Creep compliance from a direct tension creep test is calculated, as follows:

$$D(t) = \frac{\sigma(t)}{\varepsilon(t)} \quad (5.26)$$

To eliminate the effects of sample variation on the comparison, both a direct tension test and an indirect tension test were conducted on specimens out of one Superpave Gyratory Compactor sample. A direct tension creep test was first conducted on the specimen out of an “as-compacted” SGC sample. The specimen used in the direct tension test was cut into two indirect tension specimens. Figure 5.5 illustrates the procedure to prepare the direct tension specimens and indirect tension specimens.

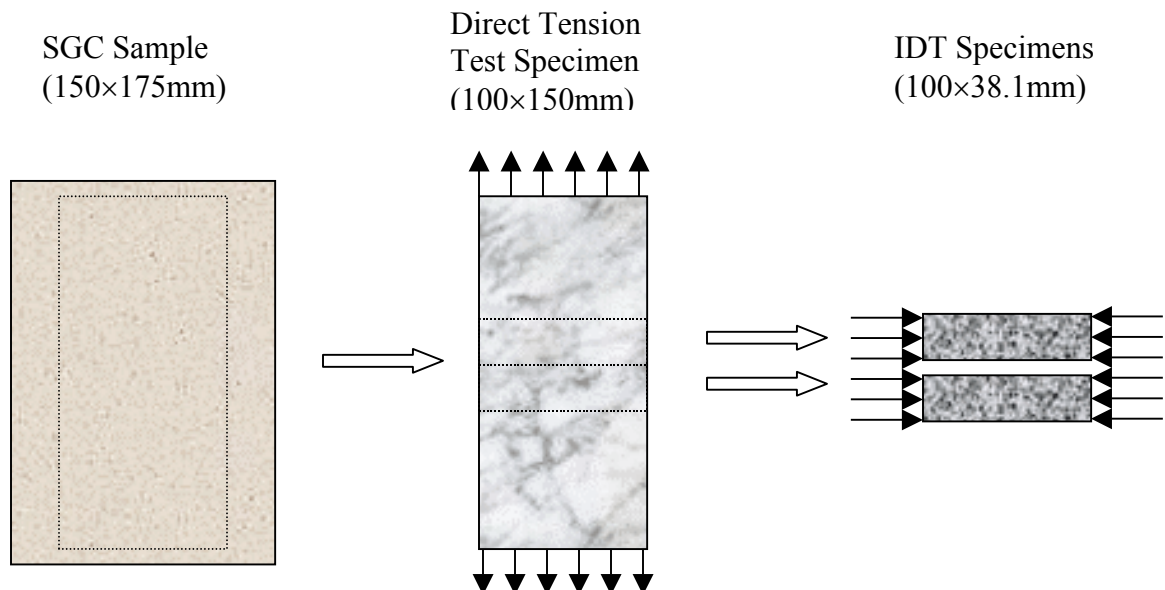


Figure 5.5 Preparation for Direct Tension Specimen and Indirect Tension Specimen

The comparison was based upon the assumption that the sample was homogeneous and isotropic. Therefore, it is presumed that the values of creep compliance obtained from different testing modes and from different parts of the specimen would be close to each other. Three SGC samples were fabricated using the North Carolina mix. An 80 lb load was used in the direct tension test and a 50 lb load was used in the indirect tension test. The durations of both the direct tension and indirect tension tests are 100 seconds. A 50.8mm gauge length at the middle of the specimen was used to measure the vertical deformation. Figure 5.6 presents the comparison between the result from the direct tension test and that from the indirect tension test. It appears that the results are not comparable. Several factors may be attributed to the discrepancy:

(1) The SGC sample could not be considered homogenous, especially due to the air void distribution. Since two indirect tension specimens were cut out of a uniaxial test specimen, the indirect tension creep test was conducted only on part of the uniaxial test specimen, a factor which may have caused the discrepancy.

However, according to Chapter 4, the air void distribution in a direct tension specimen is relatively uniform, indicating that the composition of the IDT test specimen is similar to that of the uniaxial test specimen.

(2) The stress/strain state in the direct tension specimen is not uniform. In the uniaxial direct tension test, in order to allow testing in both tensions, the specimen was glued to the end plates which were connected to the loading frame through a load cell. The end plates constrained the ends of the specimen from deforming horizontally, which may result in non-uniform stress/strain distribution in the specimen. Finite element analysis was performed to check the stress/strain

distribution in the direct tension specimen. Figure 5.7 presents the results of the finite element analysis. It was observed that the strain distribution along the axis of the cylindrical specimen is not uniform, but curved. This is ascribed to the effects of the end plates. However, within the range of the 50.8mm gauge length, the non-uniform strain distribution could be negligible. Therefore, the non-uniformity of stress/strain distribution has an insignificant effect on the test result of the direct tension specimen.

- (3) Asphalt concrete compacted by the Superpave Gyrotory Compactor may be anisotropic. As stated in Chapter 2, the direction of tensile stress in an indirect tension test is perpendicular to that in a uniaxial direct tension test. According to Kennedy, it is highly possible that asphalt concrete is not an isotropic material. Therefore, it seems that the anisotropy of asphalt concrete may cause the difference of results from the indirect tension test and the uniaxial direct tension creep test.

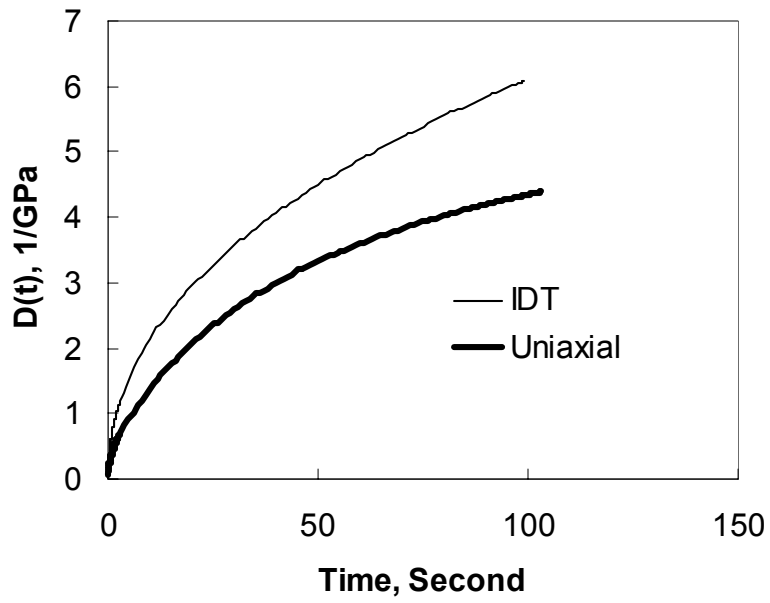


Figure 5.6 Comparison of Creep Compliance from IDT and Uniaxial Test

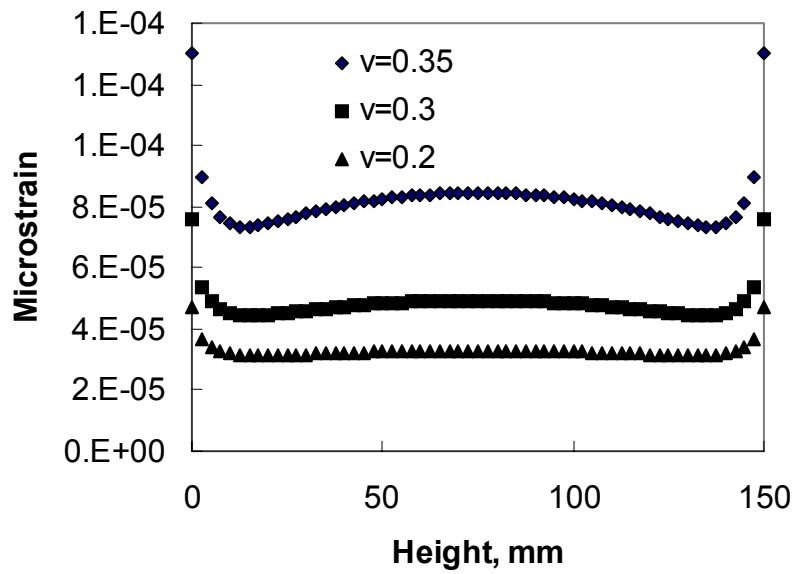


Figure 5.7 Strain Distribution along Axis of Uniaxial Direct Tension Specimen with End Plates

5.4 Application of Correspondence Principle to Indirect Tension Specimen

A series of tests was conducted to check the applicability of the correspondence principle to asphalt concrete in an indirect tension testing mode. Creep tests at different temperatures were performed to obtain a creep compliance master curve. The methods to convert creep compliance into the relaxation modulus were described. Cyclic tests were conducted to study the hysteretic behavior of the stress-strain relationship and applicability of the correspondence principle.

5.4.1 Creep Compliance Test

Creep Compliance Master Curve Construction

Since asphalt concrete is a thermorheologically simple material, the time and temperature dependent creep response may be represented by a single parameter, reduced time, through the time-temperature superposition principle. Creep compliance tests were performed at -10 , 0 , 10 , 20 , and 30°C to obtain thermoviscoelastic properties of the material. The creep compliance master curve was constructed by horizontally shifting the creep curves at various temperatures to the creep curve at a reference temperature of 20°C . The specimens were conditioned to the testing temperatures for a minimum of two hours before the test. Detailed test parameters are given in Table 5.4.

Table 5.4 Creep Test Parameters

Temperature ($^{\circ}\text{C}$)	-10	0	10	20	30
Load (lbs)	500	300	200	80	30

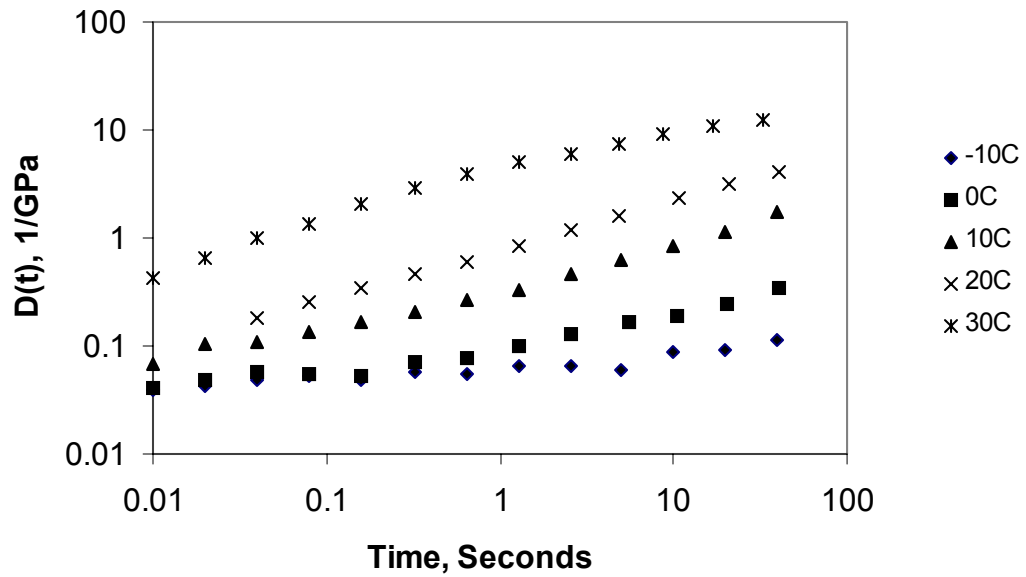


Figure 5.8 Creep Compliance at Different Temperatures before Shifting

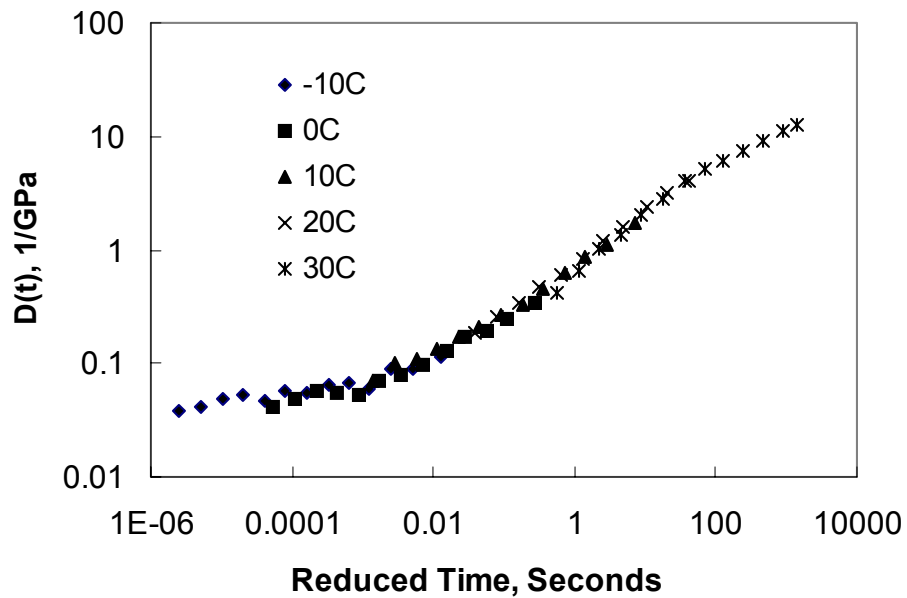


Figure 5.9 Creep Compliance Master Curve after Shifting on IDT Specimens

The creep curves at various temperatures are plotted in Figure 5.8, with a log-log scale, before shifting. The master curve was constructed and is presented in Figure 5.9. Time-temperature shift factors at different temperatures were obtained from the above shifting process; their dependency on temperature is illustrated in Figure 5.10. The data of the master curve were firstly smoothed by representing them using the power law series (PLS), as follows:

$$D(t) = D_0 + \sum_{i=1}^N \frac{D_i}{\left(1 + \frac{\tau_i}{t}\right)^n} \quad (5.27)$$

where $D(t)$ = creep compliance,
 t = time,
 D_0 = short time (glassy) compliance,
 D_i = retardation strengths, and
 τ_i = retardation times.

Here, n is the slope of the linear portion of the creep compliance master curve with a log-log scale. A one-decade interval of τ_i was used for the $N=5$ and $N=11$ series. The coefficients D_i 's were found by solving a system of linear algebraic equations based on a weighted least squares fitting scheme. The reciprocal of the value of each data point was used as the weight. Figure 5.11 shows the raw data of creep compliance and PLS fitting. It seems that using an 11-term series results in a wavy fitting for largely scattered data, whereas the waviness is not found when using a 5-term series. Therefore, it was

proposed to use a 5-term PLS series. A MATLAB code was written to accomplish the curvefitting (see Appendix B).

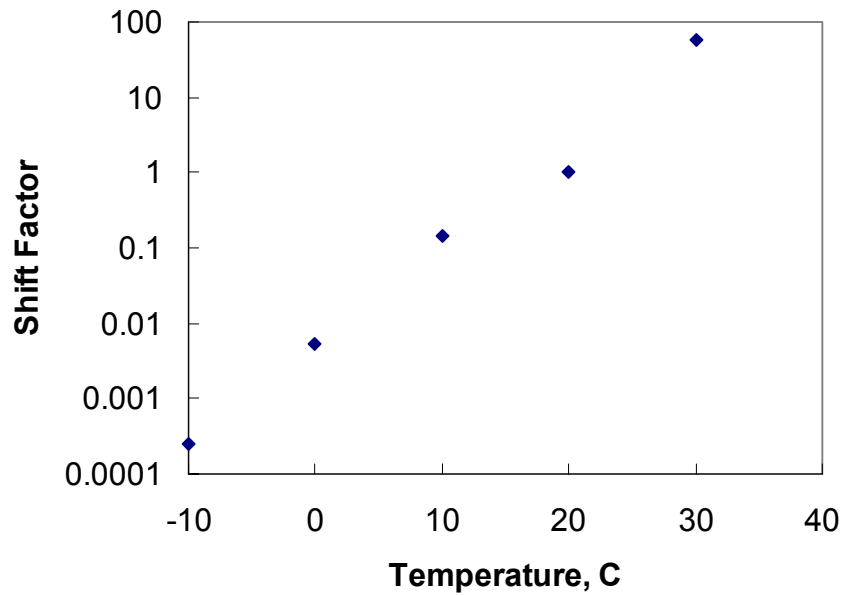


Figure 5.10 Relationship between Shift Factor and Temperature

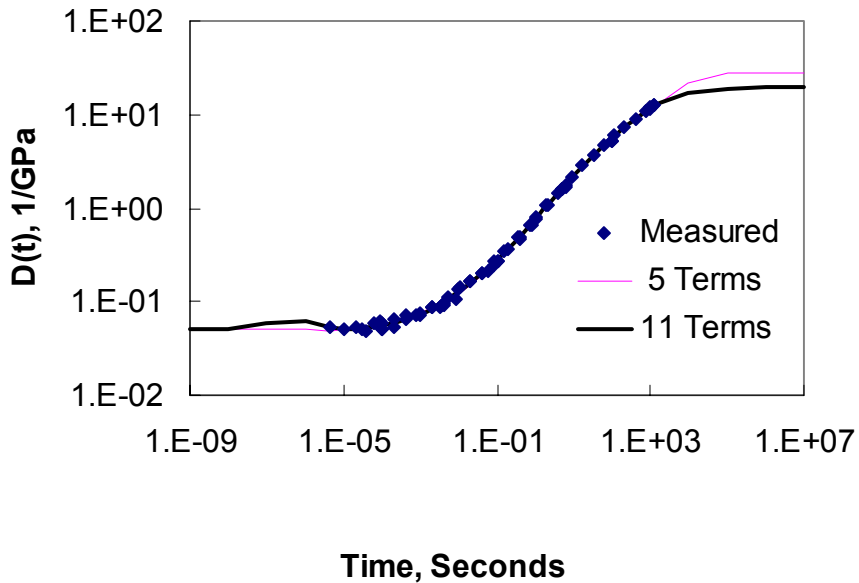


Figure 5.11 Curvefitting of Creep Compliance Using PLS

Interconversion Between Creep Compliance and Relaxation Modulus:

A power law series comprising multiple power law terms is capable of portraying a globally smooth, broadband viscoelastic behavior with minimal impact from local variance of data. However, from the viewpoint of computation, a Prony series representation is preferable to a power law series because of the computational efficiency associated with the exponential basis function of a Prony series. Therefore, the Prony series was fitted to the reconstructed data by the now-established power law series representation. The five-term power law series was used to generate data. Figure 5.12 shows the resultant Prony series fit (with N=11), as shown in Equation (5.28), as well as the parent power law series fit together with the experimental data.

$$D(t) = D_g + \sum_{i=1}^N D_i (1 - e^{-\frac{t}{\tau_i}}) \quad (5.28)$$

The relaxation modulus and creep compliance are related by a convolution integral, as follows:

$$\int_0^t E(t - \tau) D(\tau) d\tau = t \text{ for } t > 0 \quad (5.29)$$

where $D(t)$ is represented by a Prony series.

Equation (5.29) was solved numerically using an appropriate numerical integration scheme. Another MATLAB code was written to obtain an approximate relaxation modulus. The converted relaxation data were fitted into a Prony series in

Equation (5.30). The relaxation modulus predicted from creep compliance is graphically presented in Figure 5.12.

$$E(t) = E_{\infty} + \sum_{i=1}^N E_i e^{-\frac{t}{\rho_i}} \quad (5.30)$$

where $E(t)$ = relaxation modulus,
 t = time,
 E_{∞} = long time (rubbery) modulus,
 E_i = relaxation strengths, and
 ρ_i = relaxation times.

A common numerical approach normally requires that the integral be decomposed into a great number of intervals because of the spread of function over many decades of time; this may render inaccurate results and cause computational difficulties unless the intervals are carefully selected. Therefore, another approach was explored to convert creep compliance into the relaxation modulus, the so-called piecewise method. The PLS model was used to generate a series of data over a range that is divided into multiple intervals. The generated data within each interval were locally fitted into a pure power law (PPL) model. The relaxation modulus within one interval was predicted using the following equation:

$$E(t) = \frac{\sin(n\pi)}{n\pi D(t)} \quad (5.31)$$

where n = power value of local pure power law expression, and
 $D(t)$ = creep compliance within one interval.

The relaxation modulus data predicted were fitted into a Prony series model. In general, the approach is effective in obtaining desirable relaxation modulus representation.

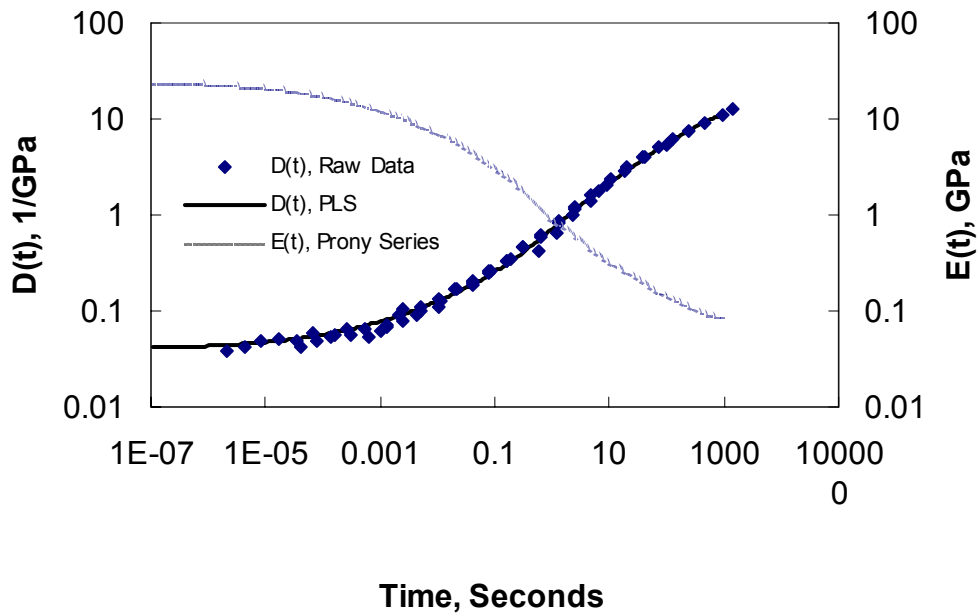


Figure 5.12 Creep Compliance and Converted Relaxation Modulus

5.4.2 Cyclic Test and Pseudo-strain Calculation

In the cyclic loading tests performed at 20°C, a loading amplitude of 50 lbs was used so as not to induce any significant damage. The horizontal displacement response under constant amplitude of cyclic loading without rest periods is represented as:

$$U_x = A + \sum_{i=1}^{10} B_i e^{-\frac{t}{\tau_i}} + C \cos(2\pi ft + \phi) \quad (5.32)$$

where A, B_i, C and φ are non-linear regression constants and are shown in Table 5.5 for a particular mix. The coefficients will change for different specimens, depending on their individual response to the loading. The regression must be done for each test to represent the strain felt by the specimen.

Table 5.5 Non-linear Regression Results of Equation (5.32) Coefficients of a Particular Mix.

Parameter	Value
A	-0.0133
B ₁	0.0116
B ₂	-0.0117
B ₃	0.0002
B ₄	-0.0003
B ₅	-0.0004
B ₆	-0.0015
B ₇	-0.0126
B ₈	0.0561
B ₉	-0.0041
B ₁₀	-0.0113
B ₁₁	-0.0125
C	-0.0003
φ	-0.3673

The measured and regressed horizontal displacements for a particular mix are shown in Figure 5.13. The regressed displacement values are then used to calculate a center strain.

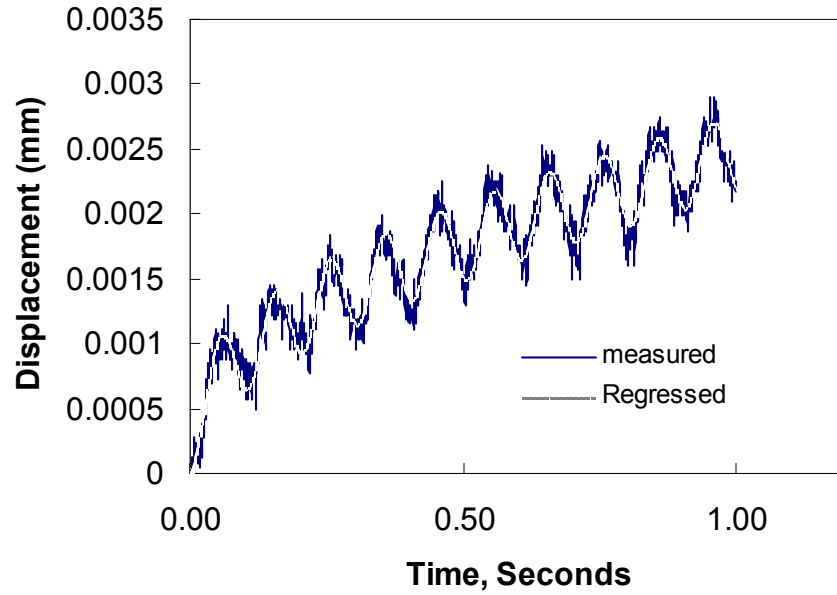


Figure 5.13 Measured and Regressed Horizontal Displacements

From Equation (5.3), the horizontal stress at the center point of the specimen is:

$$\sigma = \sigma_x - \nu\sigma_y = \frac{2P}{\pi td} [1 - \cos(t)](1 + 3\nu) \quad (5.33)$$

The stress in Equation (5.33), $\sigma_x - \nu\sigma_y$, which is representative of the actual stress state in the indirect tension specimen, is called biaxial stress, distinguishing it from the tensile stress, $\sigma_x = \frac{2P}{\pi td}$.

From Equation (5.19), the center point strain is obtained, as follows:

$$\varepsilon_{x=0} = \left[A + \sum_{i=1}^{10} B_i e^{-\frac{t}{\tau_i}} + C \cos(2\pi ft + \phi) \right] \frac{(a + b\nu)}{c + d\nu} \quad (5.34)$$

Pseudo strain is an essential parameter for applying Schapery's correspondence principle to the hysteretic stress-strain behavior of asphalt concrete. According to the theory of viscoelasticity, pseudo strain is represented as:

$$\varepsilon^R = \frac{1}{E^R} \int_0^t E(t-\tau) \frac{\partial \varepsilon}{\partial \tau} d\tau \quad (5.34)$$

where $E(t)$ = relaxation modulus, and
 E^R = reference modulus, 1.0 in this research.

The relaxation modulus is predicted from the master creep compliance curve as described previously and represented as:

$$E(t) = E_g + \sum_{i=1}^{11} E_i \left(1 - e^{-\frac{t}{\tau_i}}\right) \quad (5.35)$$

where E_g , E_i and τ_i are the constants and are shown in Table 5.6 for a particular mix. Figures 5.14 and 5.15 show the biaxial stress against time. Hysteretic stress-strain behavior is presented in Figure 5.16. As expected, the stress-strain loops shift to the right-hand side with increasing permanent strain accumulation. The area inside each stress-strain loop decreases over time as the energy dissipated from each subsequent cycle is reduced. In Figure 5.17, the same stresses are plotted against pseudo-strains. Hysteretic behavior due to loading-unloading and repetitive loading has disappeared using pseudo-strain. The 45° straight line in Figure 5.17 indicates that no damage was induced inside

the specimen and that the theory of linear viscoelasticity is applicable to the characterization of asphalt concrete in an indirect tension testing mode. On the other hand, it demonstrates that the derivations for creep compliance and center strain are accurate and applicable to characterizing asphalt concrete. Otherwise, if either of the developments for creep compliance and for center strain were invalid, the correspondence principle applied to asphalt concrete would not be validated

Table 5.6 Prony Series Coefficients of Relaxation Modulus for a Particular Mix

i	$E_i(\text{Gpa})$	τ_i
1	-0.7501	1E-5
2	2.1726	1E-4
3	-5.3908	1E-3
4	8.4669	1E-2
5	4.0806	1E-1
6	1.0472	1
7	0.1158	1E+1
8	0.0506	1E+2
9	0.0031	1E+3
10	0.0017	1E+4
11	-0.0002	1E+5
$E_g=0.099 \text{ GPa}$		

The correspondence principle has been theoretically and experimentally proven to be an effective tool for characterizing the fatigue behavior of asphalt concrete in a uniaxial direct tension testing mode which is a one-dimensional problem. The validation of the applicability of the correspondence principle to asphalt concrete in an indirect tension testing mode demonstrates that the approach used to investigate asphalt concrete in a one-dimensional problem has the potential to be utilized in a two-dimensional problem.

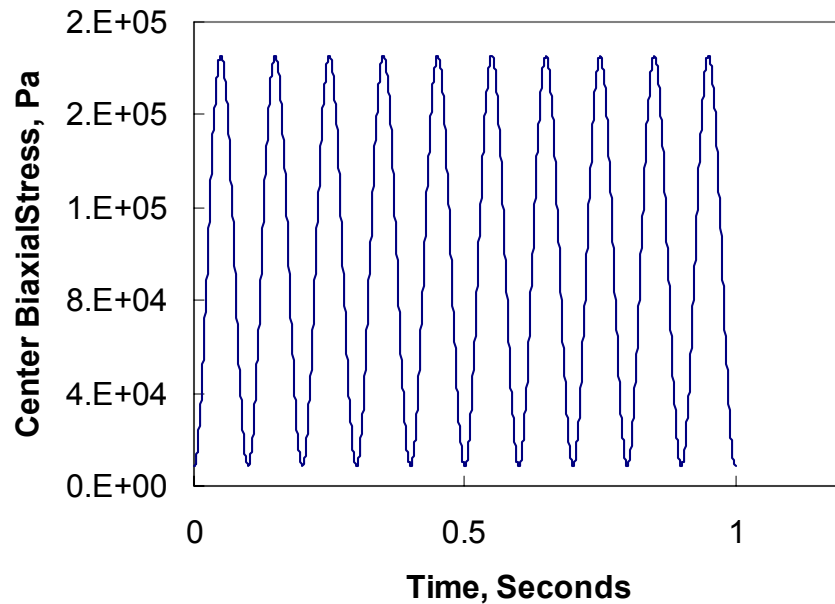


Figure 5.14 Stress vs. Time for Cyclic Tests

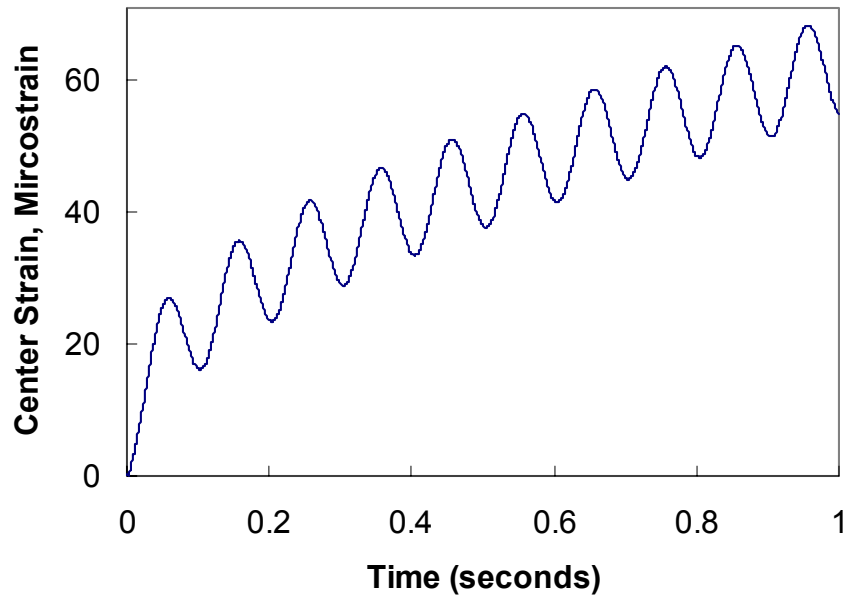


Figure 5.15 Smoothed Center Strain vs. Time

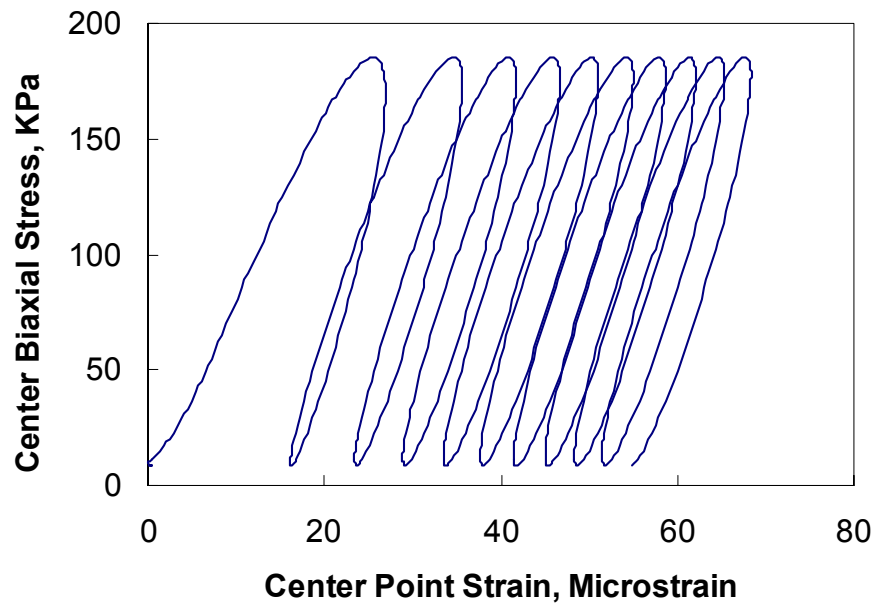


Figure 5.16 Biaxial Stress vs. Center Strain

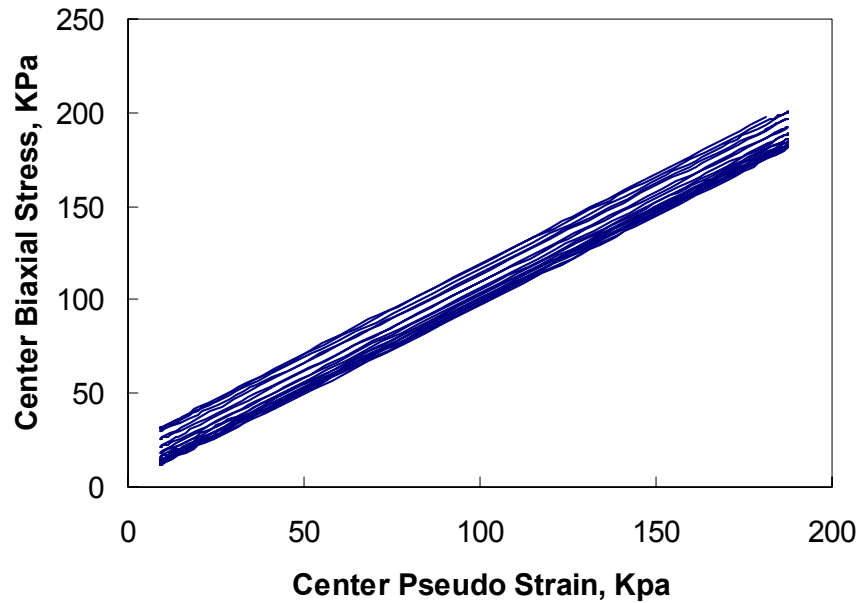


Figure 5.17 Biaxial Stress vs. Pseudo Strain

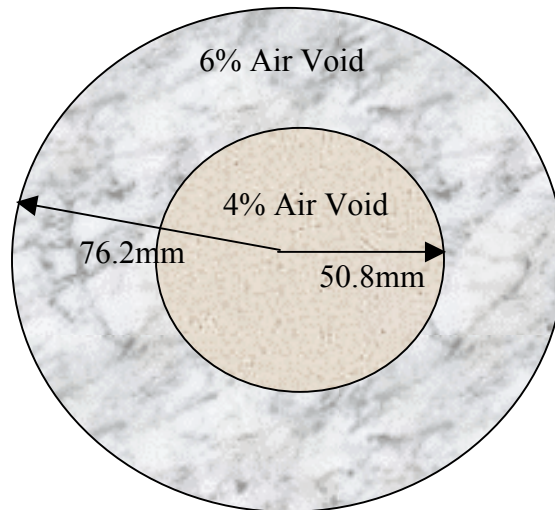
5.5 Effect of Specimen Geometry

In this study, the samples compacted by the IPC Servopac Gyrotory Compactor were 150 mm in diameter by 115 mm in height. Air void contents in the samples vary along the height and diameter. The air void contents in the outer ring and at both ends of the sample are higher than that of the core of the sample. Thus, the samples were cored and cut to obtain two replicates 100 mm in diameter by a 38.1 mm thickness. However, uncored specimens are preferred from the viewpoint of practical operation. Moreover, a field core specimen used to investigate field performance has a 150 mm diameter.

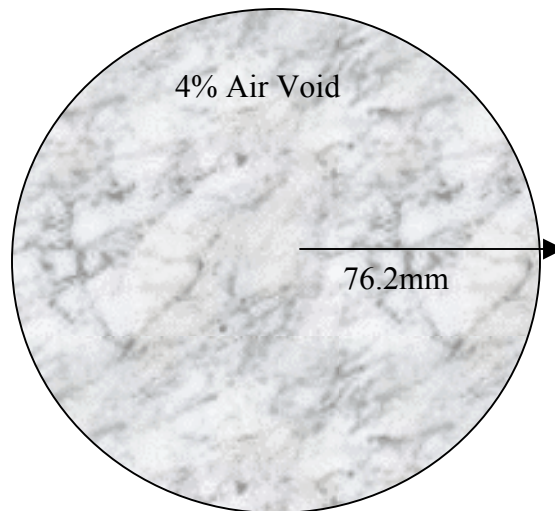
One of the disadvantages of using uncured specimens with a 150 mm diameter is that the rough lateral surface of the specimens makes it hard to position and to align them. Another critical consideration is the air void variation inside the uncured specimen: the air void in the outer ring is more than 2% higher than that of the core. The air void non-uniformity inside the uncured specimen complicates the study of asphalt concrete because during testing load is directly applied to the outer ring, while the measurements across the gauge length are taken from the deformation of the specimen core. Considering the above observations, the effects of geometry and air void variation on asphalt properties were studied using viscoelastic finite element viscoelastic analysis.

Two SGC samples, 150 mm diameter by 115 mm height, were fabricated such that the indirect tension specimens, 100 mm diameter by 38.1 mm thickness, have a 4% air void from one sample and a 6% air void from the other. Creep tests at different temperatures of 0, 13, and 20°C were conducted to obtain the creep compliance master curves of specimens with 4% and 6% air void, respectively. Creep compliances were converted into the relaxation modulus.

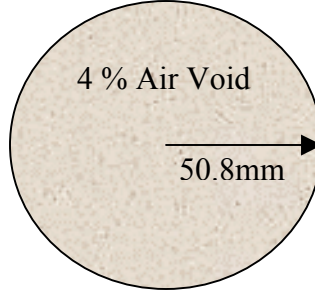
Three cases were studied using finite element viscoelastic analysis, as shown in Figure 5.18.



Case I: Combined Air Void Distribution and 152.4mm Diameter



Case II: Uniform Air Void Distribution and 152.4mm Diameter



Case III: Uniform Air Void Distribution and 101.6mm Diameter

Figure 5.18 Three Cases Studied Using Finite Element Method

The three cases studied here are representative of three kinds of specimens typically used to characterize asphalt concrete in the laboratory.

- a. Case I has a 152.4mm diameter and non-uniform air void distribution. The air void content of the core is 4% while that of the outer ring is 6%. It simulates the laboratory fabricated specimen which is cut from the SGC sample, 150 mm in diameter by a 38.1 mm thickness.
- b. Case II has a 152.4mm diameter and uniform air void distribution. It simulates the field cores taken out of the pavement, especially those of the WesTrack sections used in this study.
- c. Case III has a 101.6mm diameter and uniform air void distribution. It is similar to the laboratory fabricated specimen which is cut and cored from the SGC sample.

The parameters of the relaxation modulus were input for the finite element models of the three cases. The horizontal and vertical displacements across three gauge lengths (25.4, 50.8, and 76.2mm) were obtained. Creep compliances were calculated according to

the viscoelastic solution using Equation (5.17) and/or the ASSHTO TP9-96 method. The results are shown in Figures 5.19, 5.20, and 5.21, respectively, where LVE is the linear viscoelastic solution, $D, AV4\%$ is the experimentally measured creep compliance of the specimen with a 4% air void, and $D, AV6\%$ is the experimentally measured creep compliance with a 6% air void.

For all three cases the linear viscoelastic solutions for a 25.4mm, 50.8mm, and 76.2mm gauge length agree well with the properties of the material. Also, the curves are graphically indistinguishable. The TP9 method, however, underestimates the creep compliance. This finding indicates that the linear viscoelastic solutions give the actual material property of the specimen core on which the LVDTs were mounted and that the effect of the outer ring with the higher air void content on creep compliance is negligible. The results of Case II indicate that an indirect tension specimen can be cut from a field core without coring, which may save significant time in preparing the specimen.

It is noteworthy that the field cores have smooth lateral surfaces while the surfaces of uncored laboratory specimens are rough. Therefore, cored specimens are preferred to avoid experimental errors and reduce variability. Moreover, the above investigation focused on the behavior of asphalt concrete within the linear viscoelastic range. The effects of a higher level of air void in the outer ring on the results of a monotonic test remain unknown. Based upon these observations, the specimen, with cores 100 mm in diameter by a 38.1 mm thickness, will be used to model the asphalt concrete in an indirect tension test while field cores will be cut to obtain a 152.4mm diameter indirect tension specimen without coring.

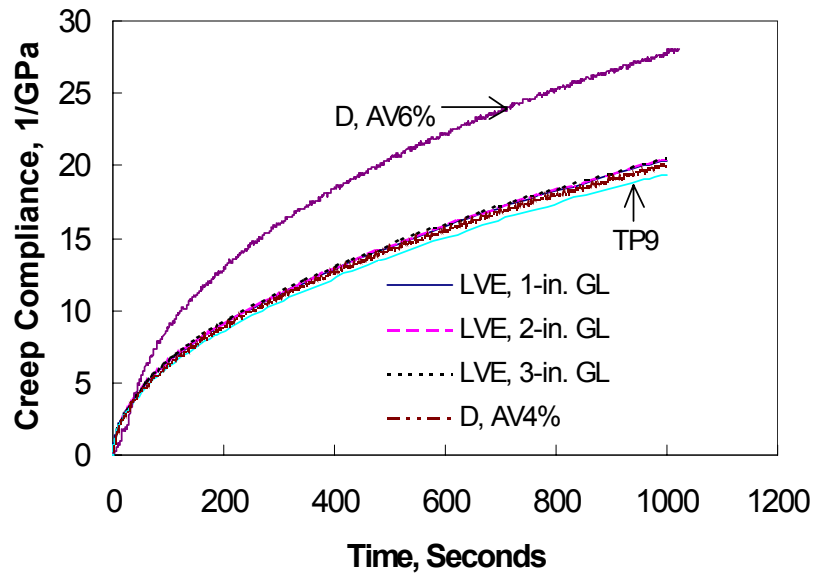


Figure 5.19 Finite Element Analysis Results for Case I

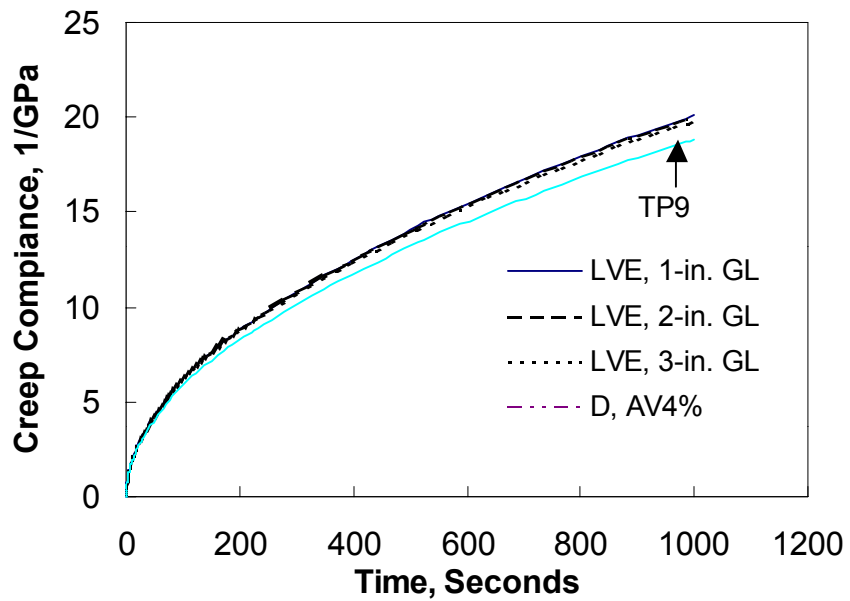


Figure 5.20 Finite Element Analysis Result for Case II

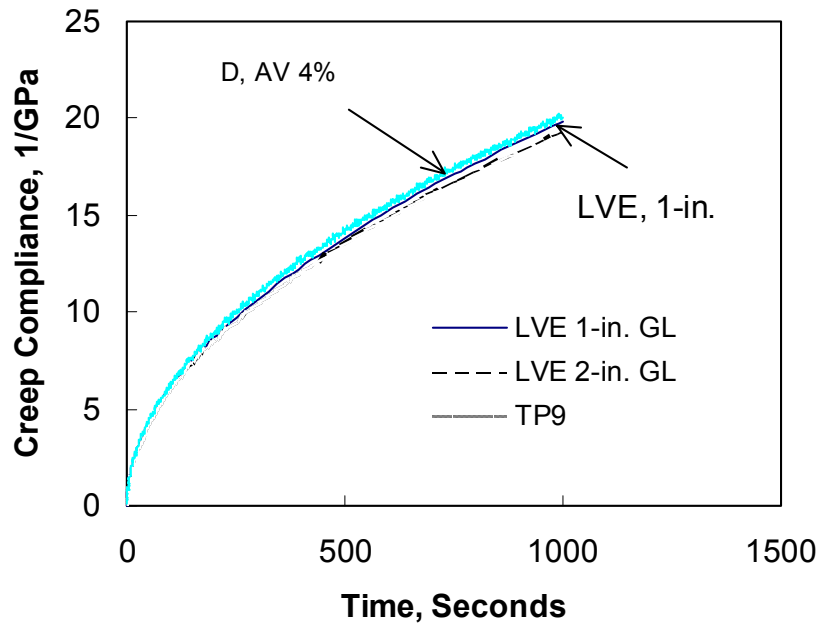


Figure 5.21 Finite Element Results for Case III

The displacement measurement accuracy may be affected by the bulging of the indirect tension specimen. Figure 5.22 illustrates the bulging that occurred during the test. The effects of bulging on measurement are dependent on the gauge length and test temperature. The bulging effects on the measurement were studied for different gauge lengths at temperatures of 0, 13, and 20°C, respectively, as shown in Figures 5.23 and 5.24. It appears that, for horizontal measurement, the error due to bulging increases with the decrease of gauge length, as opposed to that for vertical measurement. Temperature has a minor effect on both the horizontal and vertical measurements. It was found that the maximum error due to bulging for either vertical or horizontal measurements is less than 5%. Thus, the bulging effect in this study was not considered.

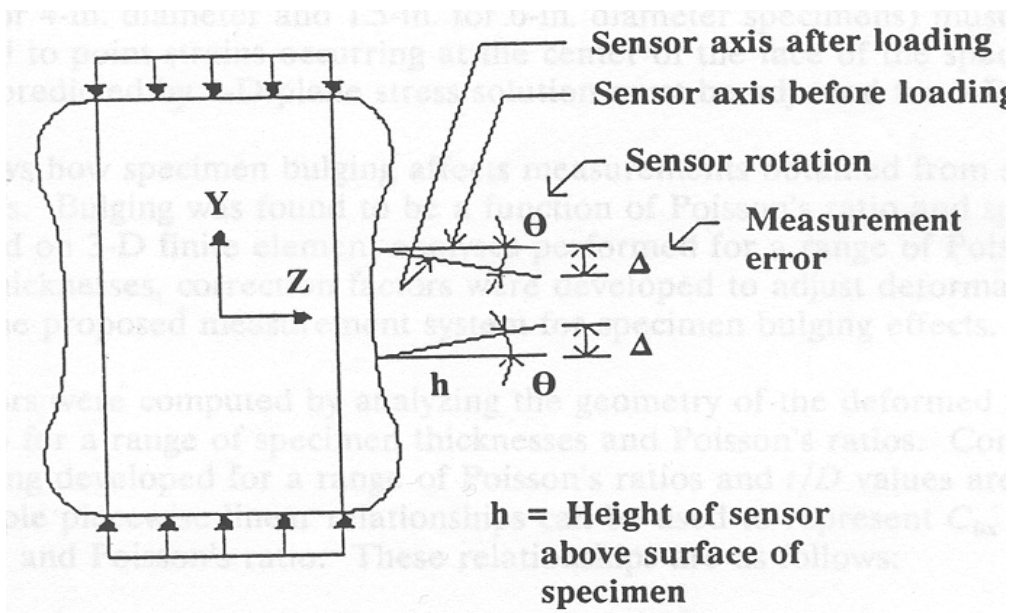
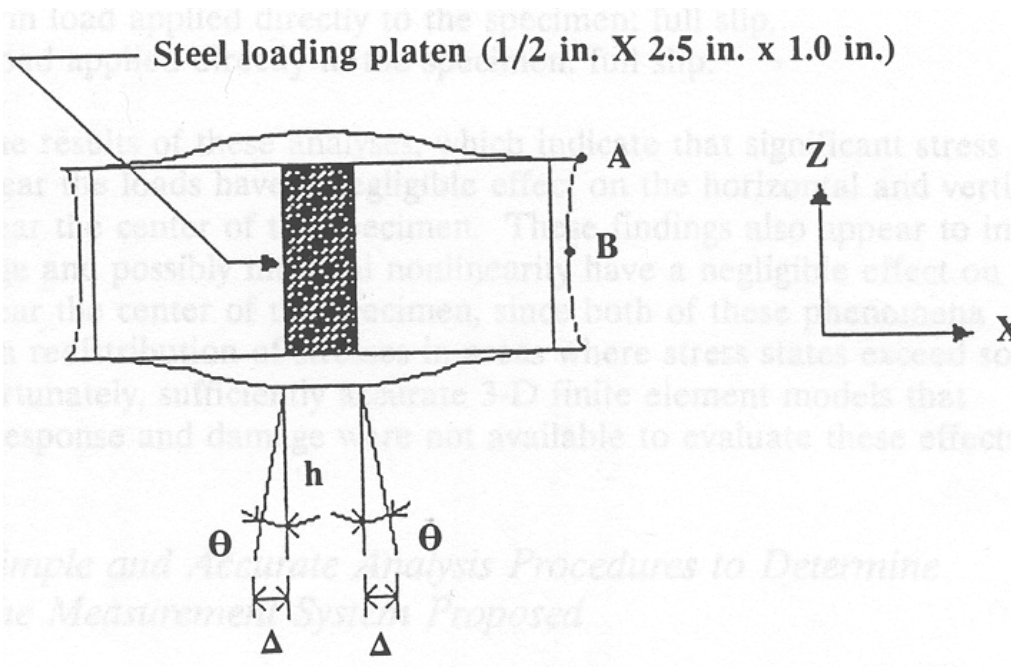


Figure 5.22 Illustration of Bulging Effect (after Roque et. al., 1992)

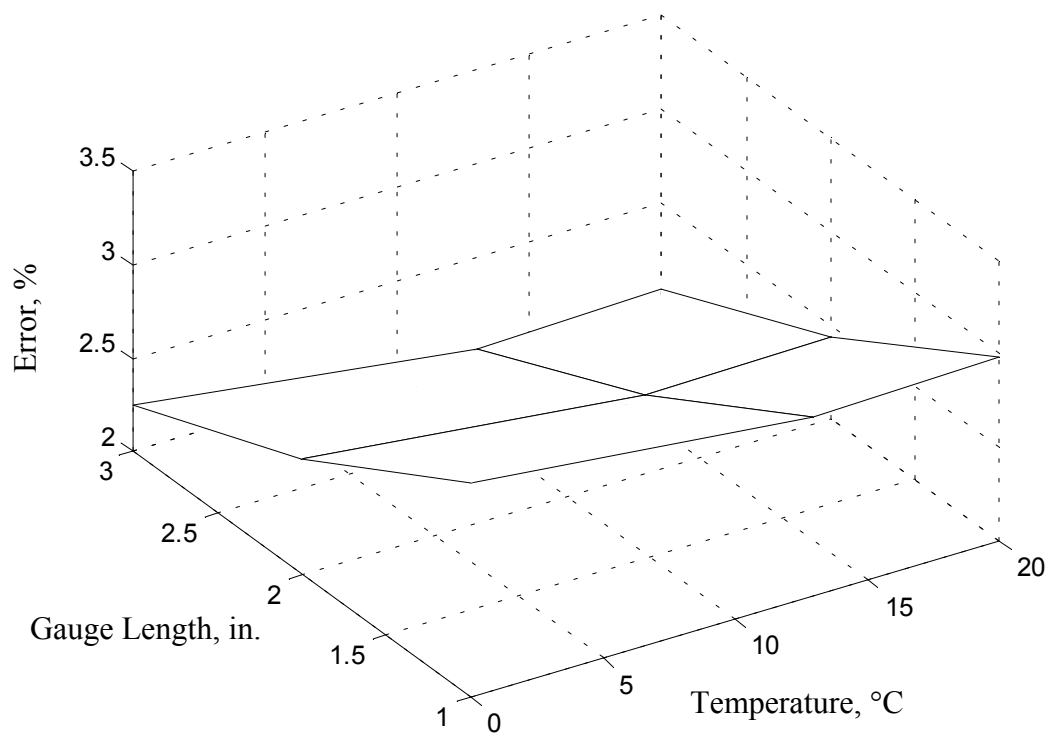


Figure 5.23 Effect of Bulging on Horizontal Measurement

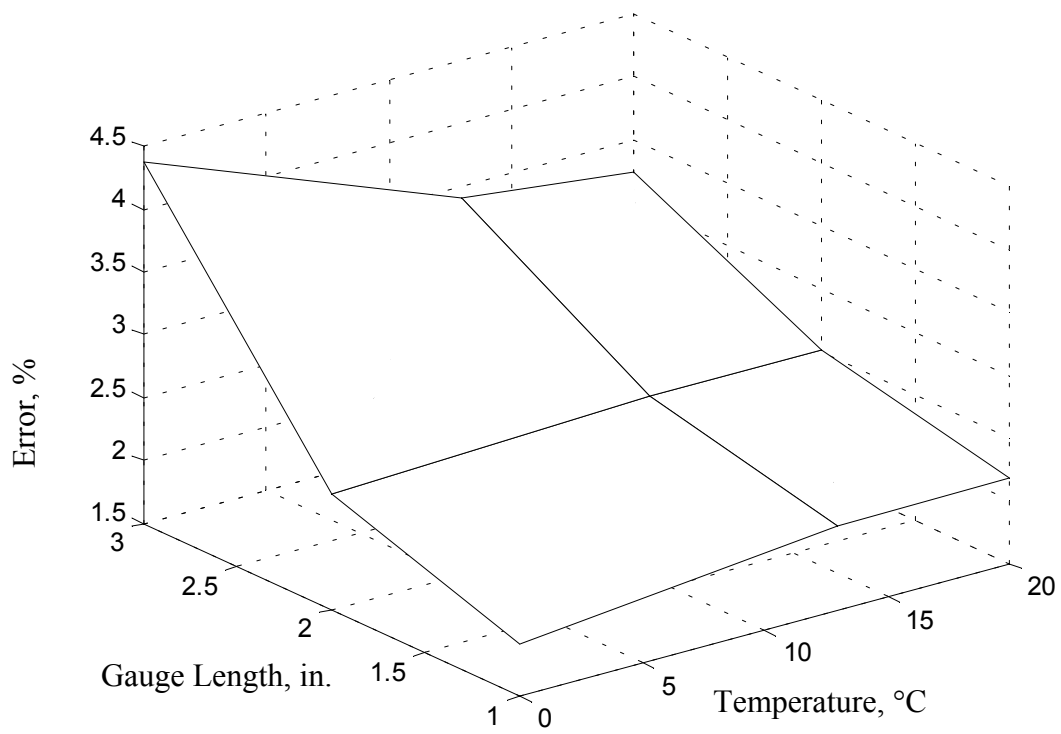


Figure 5.24 Effect of Bulging on Vertical Measurement

CHAPTER 6

DEVELOPMENT OF A SIMPLE PERFORMANCE TEST AND VALIDATION

Schapery's work potential theory was employed to investigate the characteristics of asphalt concrete and to obtain parameters from a simple performance test that is highly correlated with a field performance test. A stepwise approach was adopted to develop the simple performance test. A simple performance test was expected to provide reliable information on the performance of asphalt concrete during the volumetric mixture design process using SGC. Therefore, laboratory mixed-laboratory compacted (LMLC) specimens were used to check the applicability of the work potential theory first. However, it is imperative that field cores of pavement be used in order to verify the simple performance test in the laboratory because the laboratory mixing and compacting processes are only intended to simulate field mixing and field compaction. Therefore, field cores sampled from several sections of WesTrack were evaluated using the approach developed in the laboratory.

6.1 WesTrack Field Performance

WesTrack pavement traffic loading was performed using four (driverless) tractor/triple trailer combinations. The weights per single axle were 89 kN (2,000 lb). Each pass of the truck-trailer combination applied 10.49 equivalent single-axle loads (ESALs). The trucks were equipped with 700 kPa (100 psi), 295/75R22.5 radial tires.

The truck speed was 64 km/hr (40 mph). A schematic diagram of the truck is shown in Figure 6.1 (WesTrack report).

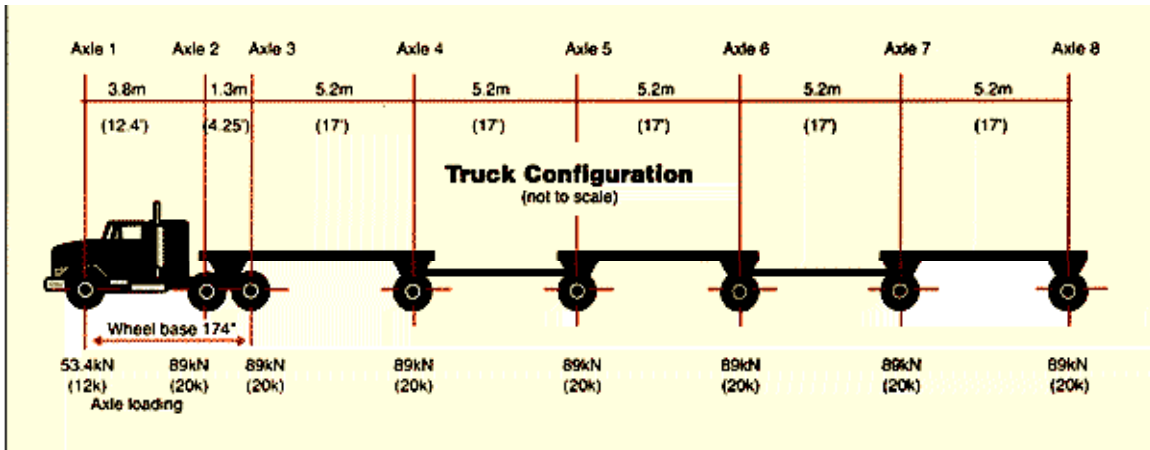


Figure 6.1 Schematic Diagram of the Truck (WesTrack Website)

Over a period of two and a half years, the driverless trucks applied 4.9 million EASLs. By the application of 2.8 million ESALs (May 1997), excessive rutting or fatigue cracking in some of the sections necessitated the replacement of ten of the original test sections, eight of which were coarse graded Superpave mixtures developed from a locally available (Lockwood, Nevada) crushed aggregate and a neat PG64-22 binder. Asphalt content, in-place air void, and gradation (minus 0.075 mm only) were systematically varied among the replacement test sections to simulate typical construction variability.

The presence of fatigue cracking was recorded during the visual condition survey in accordance with the LTPP Distress Identification Manual. The frequency of determining the presence of fatigue cracking was once every two weeks when the track

was subjected to traffic. During periods of rapid development of fatigue cracking, the frequency was increased. During certain periods of the year, (summer primarily) fatigue cracking is often difficult to observe because healing of the cracks can occur.

A review of fatigue cracking development indicates that the majority of the fatigue cracking occurred during the winter months when temperatures were relatively low and crack propagation was relatively rapid. In addition, the difference in the development of fatigue cracking in the left wheelpath versus the right wheelpath on many of the sections is ascribed to the fact that the left side of the truck had slightly more weight than the right side of the truck because of the truck components, loading shifting on the truck, and the pavement cross-slope.

6.2 Laboratory Investigation of WesTrack Mixtures

Eight mixtures were selected to fabricate the specimens in the laboratory, four coarse gradation mixtures and four fine gradation mixtures. The four coarse gradation mixtures are CLO, CML, CMO, and CMH and the four fine gradation mixtures are FLO, FML, FMO, and FMH. Some mixtures can not be realized in the laboratory, such as high air void with high asphalt content or low air void with low asphalt content. First, compaction efforts for the mixtures were investigated to fabricate the specimens in the laboratory at the target air void contents. The heights of samples were adjusted to obtain the target air void levels while the weights of each batch of mixture were constant. Secondly, the samples were cored, using a 100 mm diameter masonry bit, and then were cut into two indirect tension.

Thirdly, indirect tension creep tests were conducted. After a rest period of half an hour, a tensile strength test was performed with a rate of ram movement at 50.8 mm per minute until the failure of the specimen. Both the creep test and strength test were conducted at a temperature of 20°C. Creep compliance was computed in accordance with Equation (5.17), while Poisson's ratio was calculated using Equation (5.16). Figure 6.2 shows creep compliances of four coarse gradation mixtures. Figure 6.3 presents creep compliance of four fine gradation mixtures. It is seen that at 200 seconds (the end of the creep test), the mixture with high asphalt content has a high creep compliance value and that the creep compliance value increases with the increase of air void content.

Poisson's ratio was used to check whether damage occurred during the creep test. In a creep test, the load applied should be small enough so that no damage occurs and so that Poisson's ratio is constant for a particular mixture. However, in a tensile strength test, the crack induced within the range of the gauge length could result in greater horizontal deformation and, hence, a higher Poisson's ratio. Fairhurst et al. (1990) found that Poisson's ratio increases with an increase in temperature and concluded that Poisson's ratio serves as an indicator of excessive damage to a specimen. Figures 6.4 and 6.5 present Poisson's ratio in a creep test and a tensile strength test, respectively. In Figure 6.4, the initial value of Poisson's ratio is highly fluctuating, due to the electrical noise of LVDT and small initial deformation of specimen, and then gradually stabilizes at a certain value, while in Figure 6.5, Poisson's ratio increases with the increase of time. Therefore, for a tensile strength test, it seems that Poisson's ratio could be utilized to quantify the amounts and size of cracks within the range of gauge length.

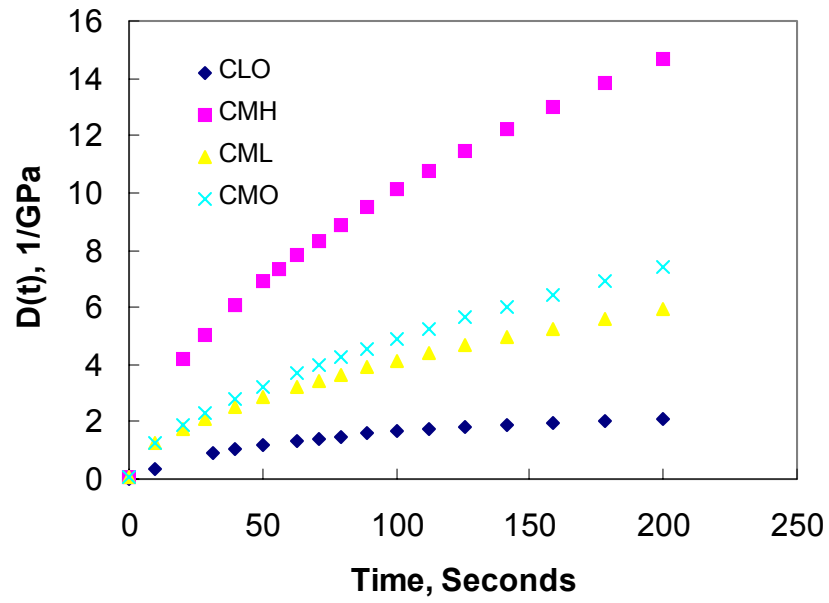


Figure 6.2 Creep Compliance of Four Coarse Gradation Mixtures

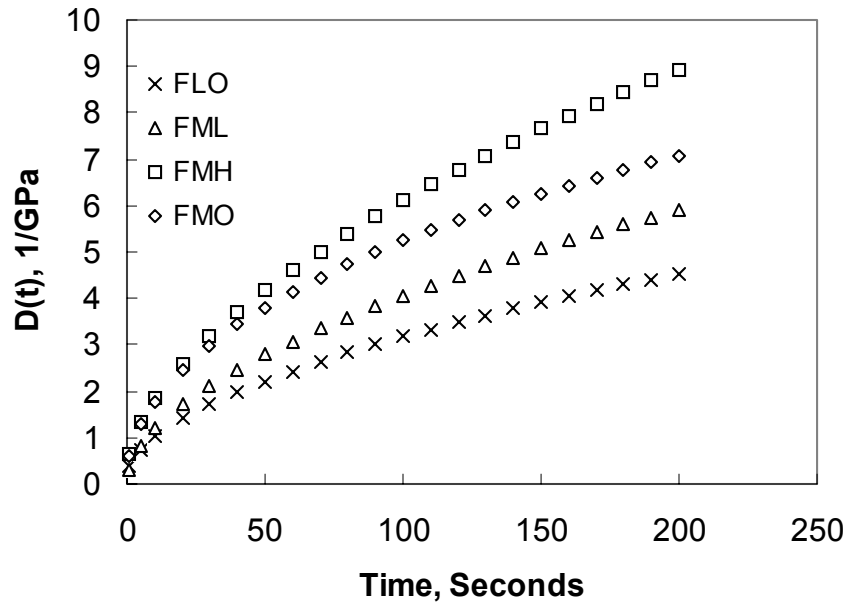


Figure 6.3 Creep Compliance of Four Fine Gradation Mixtures

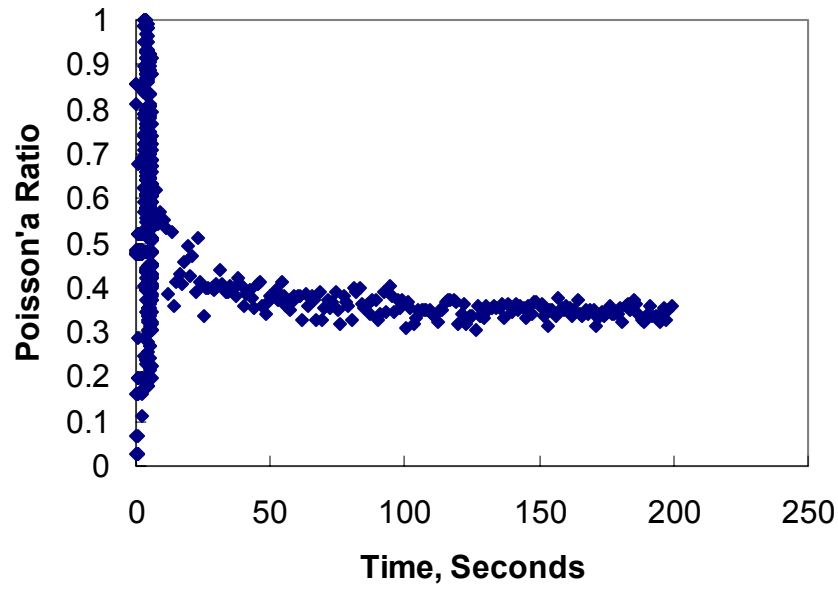


Figure 6.4 Poisson's Ratio in Creep Test

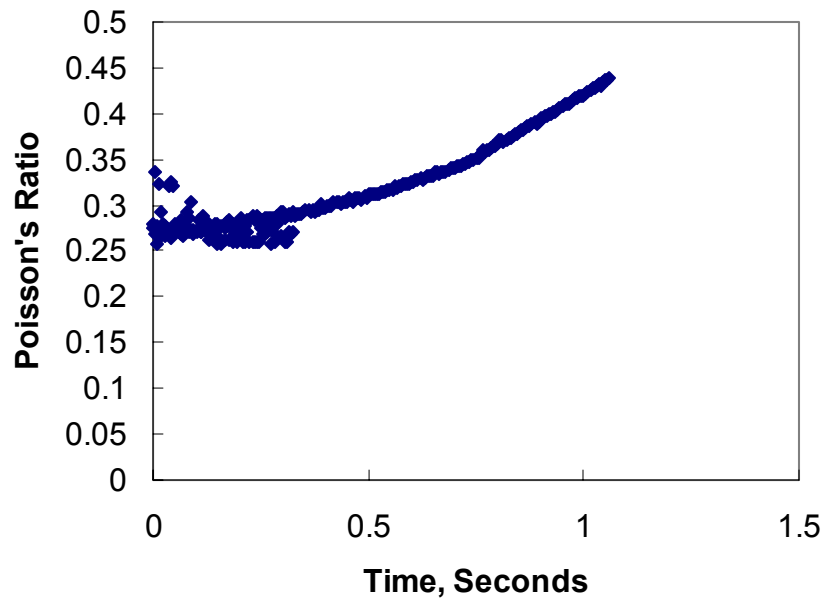


Figure 6.5 Poisson's Ratio in Tensile Strength Test

In the work potential theory based on irreversible thermodynamic process, the total work done by force on an elastic media is the sum of the strain energy and the dissipated energy which contributes to changes in the structure, as follows:

$$W_T = W + W_s \quad (6.1)$$

where W is strain energy and W_s is dissipated energy.

The total work applied to an element is equal to the work of deformation W plus the work of structural change W_s , as shown in Figure 6.6.

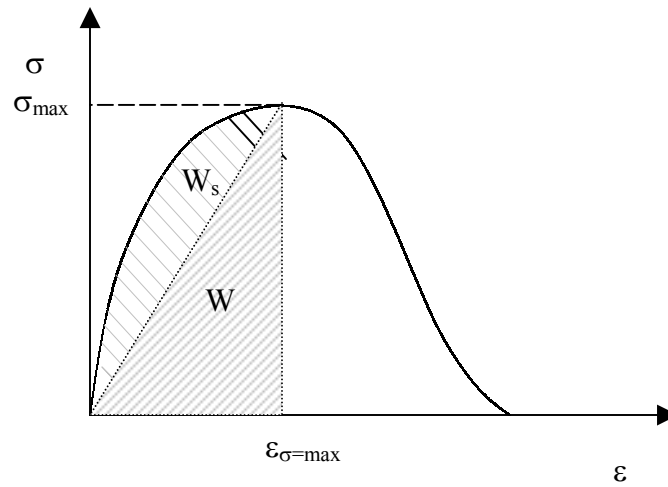


Figure 6.6 Stress-Strain Relationship in Indirect Tensile Strength Test

The total work done on the body by stress during an actual process is denoted by W_T :

$$W_T = \int Qdq = \sum_{i=1}^M Q_i q_i \quad (6.2)$$

The work of deformation W is represented as:

$$W = \frac{1}{2} \sigma_{\max} \varepsilon_{\sigma=\max} \quad (6.3)$$

Thus, the work of structural change, W_s , could be obtained:

$$W_s = W_T - W_s = \int_0^\varepsilon \sigma d\varepsilon - \frac{1}{2} \sigma \varepsilon = \sum_{i=1}^M \sigma_i \varepsilon_i - \frac{1}{2} \sigma_{\max} \varepsilon_{\sigma=\max} \quad (6.4)$$

where M is the number of intervals to calculate total work.

As described in Chapter 3, the work of structural change is a state function of the internal state variable S_m and strain ε . The relationship between thermodynamic forces which produce change of structure and work of structural change is represented as:

$$f_m = \frac{\partial W_s}{\partial S_m} \quad (6.5)$$

The key to obtaining thermodynamic force is the selection of the internal state variable S_m . As described above, if Poisson's ratio could be considered as a parameter quantifying the structural change, for example, cracks distributed within the range of gauge length, then the value of thermodynamic force f_m is the tangent slope of the curve of W_s and Poisson's ratio.

It must be pointed out that the resistance of asphalt concrete to fatigue cracking must be quantified by considering both resistance to deformation and resistance to damage. That is, the work applied by a vehicle on a pavement in the field is consumed by deforming the material as well as by creating damage in the material. For example, the resistance to fatigue cracking of a highly elastic material is good because much work is involved in deforming the material before it initiates damage. Therefore, in this type of material, much more work is involved in straining the material before significant damage is initiated. This observation suggests that the fracture energy, the sum of strain energy and damage energy, is the proper indicator for the resistance of asphalt concrete to fatigue cracking.

Figure 6.7 shows the fatigue cracking of these mixtures at 2.8 million ESALs. It is seen that only three of the eight mixtures showed fatigue cracking, CML, CMO, and FML. No fatigue cracking was observed for other mixtures. After approximately 2.8 million ESALs, most of the coarse gradation sections were removed and replaced by new coarse gradation sections. The fine gradation sections were subjected to traffic until the end of the project and experienced approximately 5 million ESALs. The left lane of each section had more fatigue cracking than the right lane. It is seen that CML has the most severe fatigue cracking in the eight mixes, followed by CMO and FML, in sequence. Fatigue cracking percentages of less than five percent are considered insignificant; at this level the cracking could be due to the initiation of fatigue cracking or to a flawed construction area. Once fatigue cracking exceeds five percent, it generally progresses rapidly.

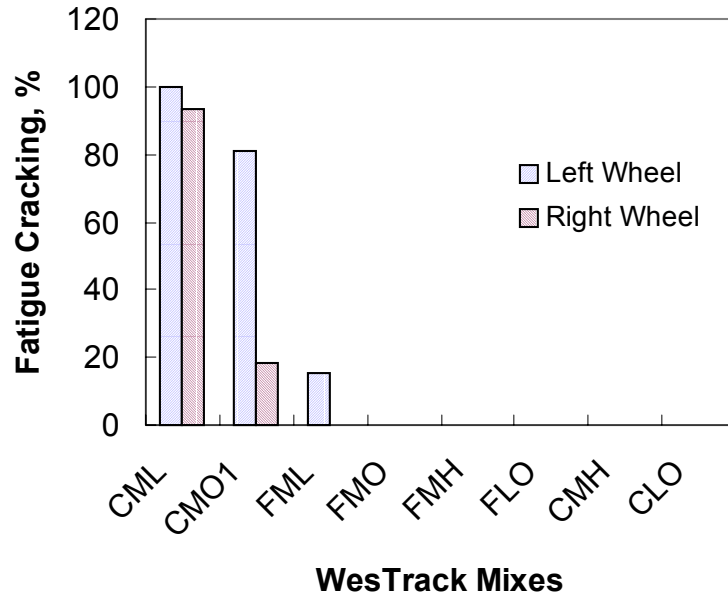


Figure 6.7 Field Performance of WesTrack Mixtures Selected (2.8M EASLs)

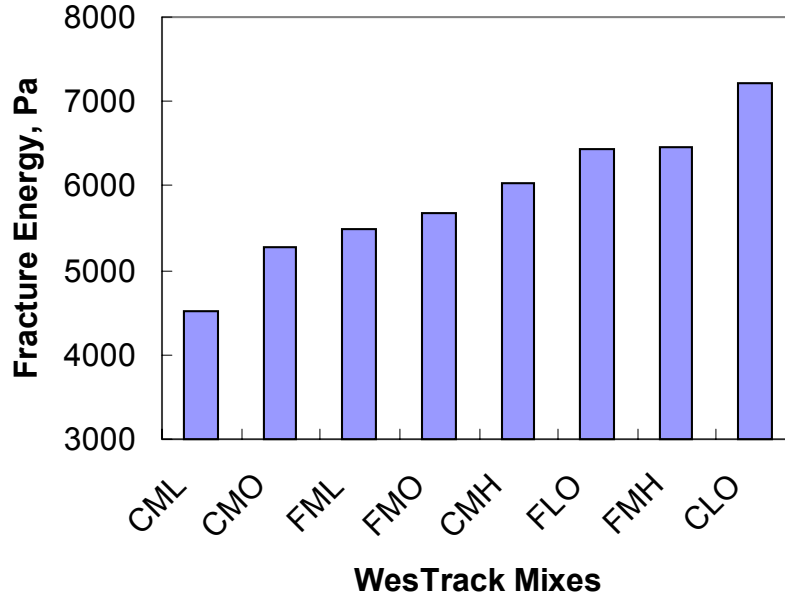


Figure 6.8 Fracture Energies of WesTrack Mixtures Selected

The fracture energies of fine and coarse gradation mixtures, as well as strain energy and damage energy, were calculated to correlate with field performance. As shown in Figure 6.8, CML has the lowest fracture energy, then CMO and FML, from low to high. It appears that, for CML, CMO, and FML, fracture energy very closely correlates with the amount of fatigue cracking; that is, the mixture with high fracture energy shows less fatigue cracking. Since other mixtures have no fatigue cracking at 2 million ESALs, these mixtures can not be used to clearly demonstrate the ability of fracture energy for ranking asphalt mixtures with varying factors.

However, well-known effects of asphalt content and air voids content on fatigue performance of asphalt mixtures may be used to assess the validity of fracture energy as an indicator for ranking the mixtures. It was reported (Epps 1998) that for both fine and coarse gradation sections at WesTrack, fatigue cracking increases significantly as air void content goes from low to high at certain binder content levels, and that an increase in the amount of fatigue cracking is evident as the binder content decreases. It was also pointed out that the coarse gradation section had the most extensive fatigue cracking. It is seen in Figure 6.8 that the fracture energy decreases as air void content goes from low to high, while an increase of fracture energy is observed as binder content increases. These observations agree well with the report from Epps. Based on the above description and the ranking of fracture energies, it was concluded that fracture energy could be a good indicator of the resistance of asphalt concrete to fatigue cracking.

Creep compliance is an essential property of asphalt concrete, a viscoelastic material. Creep compliances of mixtures at 200 seconds are presented in Figure 6.9. The mixture with a high asphalt content has a large creep compliance. Creep compliance

increases with the increase of air void content. The effect of aggregate gradation on creep compliance is not evident. It appears that the ranking of creep compliance does not match that of fatigue cracking. It is inferred that the “stiffness” of mixture itself does not contain enough information to predict the resistance of the mix to fatigue cracking.

Theoretical and empirical work by Jacobs (1995) has indicated that the crack propagation is related to the m-value (the slope of the linear portion of the creep compliance-time curve on a logarithmic scale). Figure 6.10 shows the m-value of eight mixtures. No direct relationship between m-value and the amount of fatigue cracking was observed.

Another two typically used parameters in indirect tensile strength testing are the maximum tensile stress and the horizontal strain at failure. Figures 6.11 and 6.12 show the two parameters of the eight mixes, respectively. Neither the maximum tensile stress nor the horizontal strain at failure could serve as the indicator of resistance to fatigue cracking.

In summary, fracture energy has been theoretically and experimentally proven to be a good indicator for resistance to cracking. Fracture energies of laboratory mixed-laboratory compacted (LMLC) samples are highly correlated with the amount of fatigue cracking for the mixtures that have shown fatigue cracking. Thus, indirect tensile strength testing, with tensile creep testing, is suggested as the simple performance test for fatigue cracking.

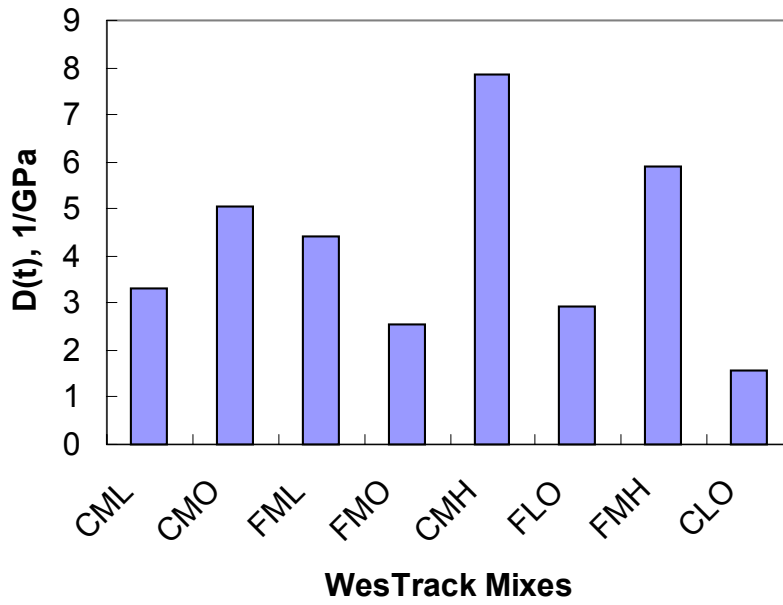


Figure 6.9 Creep Compliance of WesTrack Mixtures at 200 Seconds

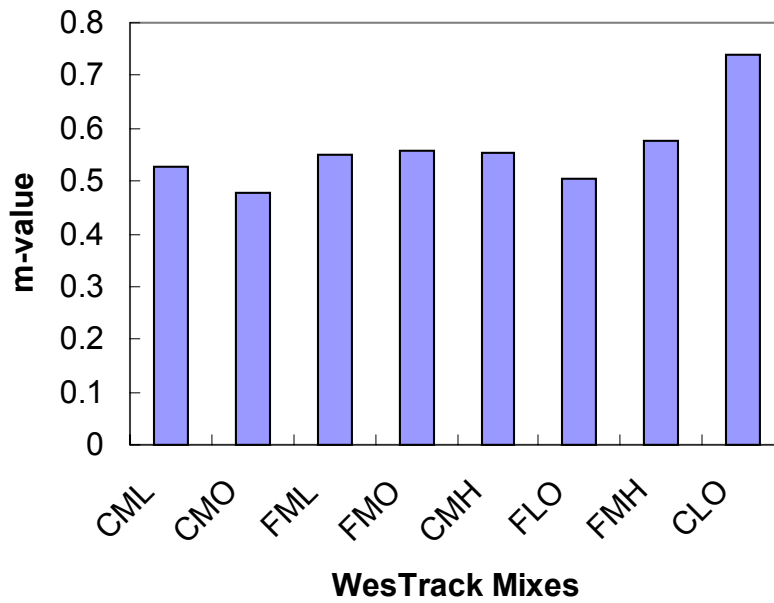


Figure 6.10 m-value of WesTrack Mixtures

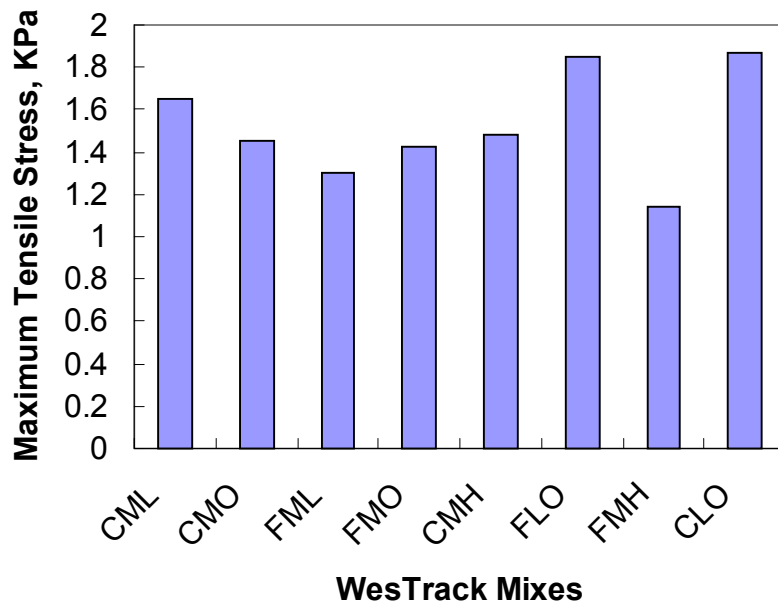


Figure 6.11 Maximum Tensile Stress of WesTrack Mixtures

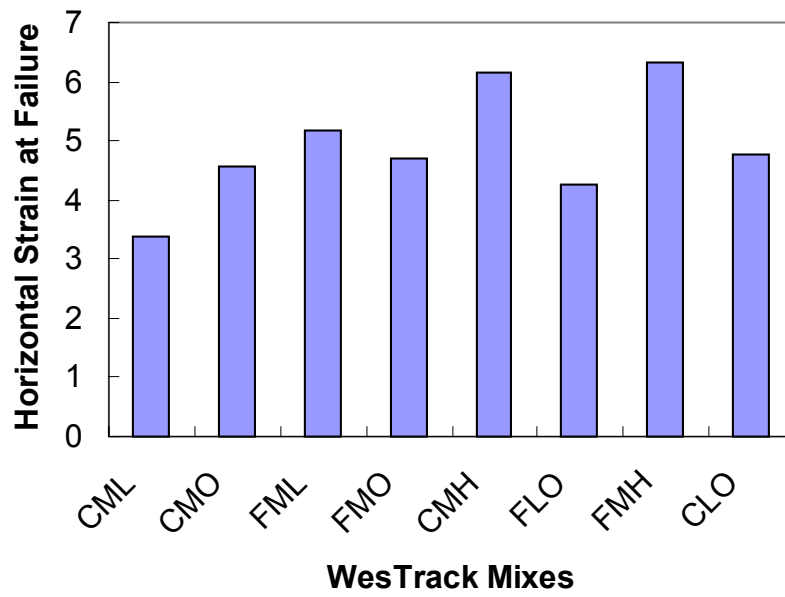


Figure 6.12 Horizontal Strain of WesTrack Mixtures at Failure

6.3 Validation of the Simple Performance Test

LMLC samples are both mixed and compacted in the laboratory and are typically used for mixture design purposes. The laboratory mixing and compacting processes are intended to simulate field mixing and field compaction processes. However, due to different equipment and conditions, there is discrepancy between LMLC mix and actual field mix. Therefore, field mixed-field compacted (FMFC) samples were obtained by coring and removing slabs of pavement. The samples were mixed and compacted with field equipment during construction and represent the actual pavement material in place. It was expected that the best correlation between material properties and field performance of the mixtures could be obtained with the FMFC samples.

Test procedure for the field cores was the same as that for LMLC samples, except that the field core has a 150 mm diameter. Field cores from ten sections were available for testing. Since they were obtained between two wheelpaths, field cores were not subjected to traffic, but had been aged. CHL, CHO, and CMO were from replacement sections and are designated as *CHLr*, *CHOr*, and *CMOr*, respectively. It is noteworthy that at the end of project, replacement sections experienced only 2.18 million ESALs while fine gradation sections experienced approximately 5 millions ESALs. Table 6.1 summarizes the fatigue cracking and ESALs of these sections where field cores used in this study were obtained. Unlike LMLC mixtures selected, these mixtures provide a diverse range of fatigue cracking.

Table 6.1 Traffic Volume Experienced by the Mixtures

Mixture	Traffic (million ESALs)		
	5	3.3	2.18
	Fatigue Cracking (%)		
CHLr			90
CHOr			45.05
FHL1	57.6	1.95	0.9
FML	37.5	9.45	0
FHO	8.9	2.8	1.1
CMO2r			0
FMO1	0.85	0.1	0
CLO		0	0
FLO	0.1	0	0
FMH	1	0	0

6.3.1 Fine Gradation Mixtures

Six fine gradation mixtures were studied using field cores: FMH, FHL, FML, FLO, FMO, and FHO. All the fine gradation sections experienced 5 millions ESALs. Figure 6.13 shows the fatigue cracking of these fine mixtures. The fracture energies of the fine gradation mixtures are shown in Figure 6.14.

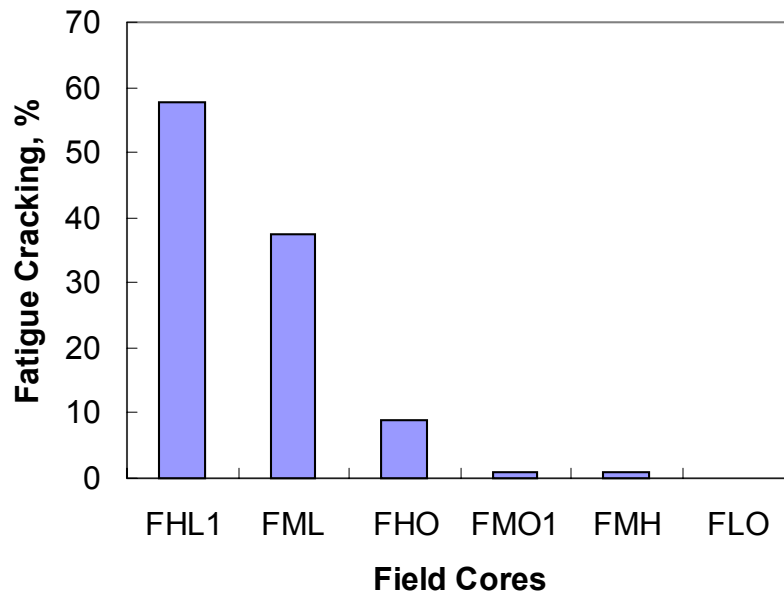


Figure 6.13 Field Performance of WesTrack Sections (Fine) at 5M EASLs

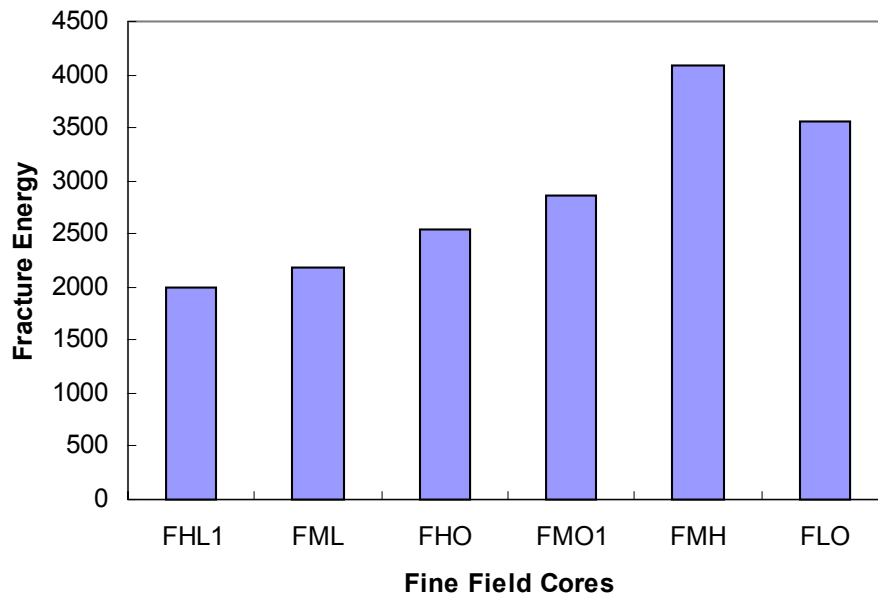


Figure 6.14 Fracture Energies of WesTrack Field Cores (Fine)

The same relationship between the extent of fatigue cracking and the fracture energy of indirect tension specimens was observed: that is, high fracture energy, less fatigue cracking. FHL has a low asphalt content and high air void level and, hence, has the largest amount of fatigue cracking. Accordingly, FHL has the lowest fracture energy. Since FML has a lower air void level compared to FHL, it has less fatigue cracking and higher fracture energy. FHO with a higher air void level and asphalt content shows less cracking, compared to FML, indicating that the beneficial effect of increasing asphalt content from low to optimum on resistance to cracking predominates the deleterious effects of increasing air void level from medium to high.

6.3.2 Coarse Gradation Mixture

Field cores from four coarse gradation sections were tested. The percentage of the instances of fatigue cracking of these sections is presented in Figure 6.15. The fracture energies of the mixtures in indirect tensile strength testing are shown in Figure 6.16. It is seen that fracture energy and field performance is closely correlated.

6.3.3 Fine and Coarse Gradation Mixtures

The effect of gradation on the performance of the mixtures could be evaluated when the fine gradation mixture and coarse gradation mixture were studied together. Figure 6.17 shows the fatigue cracking of both fine gradation and coarse gradation mixtures at 5 million ESALs. Figure 6.18 presents the fracture energies of both fine and

coarse gradation mixtures. Again, fracture energy is a good indicator of resistance to fatigue cracking. It is seen that fracture energy takes into account the effects of aggregate gradation, asphalt content, and air void level of the mixture on resistance to fatigue cracking.

The relationship between fracture energy and fatigue cracking is presented in Figure 6.19. Many researchers attempt to use linear or power type to regress the curve of fracture energy and fatigue cracking percentages. This effort may lead to an erroneous relationship, however, because linear or power regression may become an unrealistic (negative or larger than 100%) prediction of fatigue cracking. A modified logit model is proposed in this study to fit the data in Figure 6.19:

$$F = \exp\left(\frac{\ln \frac{100-C}{C} - b}{a}\right) \quad (6.5)$$

where F = fracture energy,
 C = fatigue cracking percentage, and
 a, b = regression coefficients.

The advantage of making use of the logit model is that it limits the value C to fall within the range of 0-100 percent and the “S” shape is similar to realistic fatigue cracking development. A modified logit model that provides better curvefitting was used to represent the relationship between fracture energy and fatigue cracking:

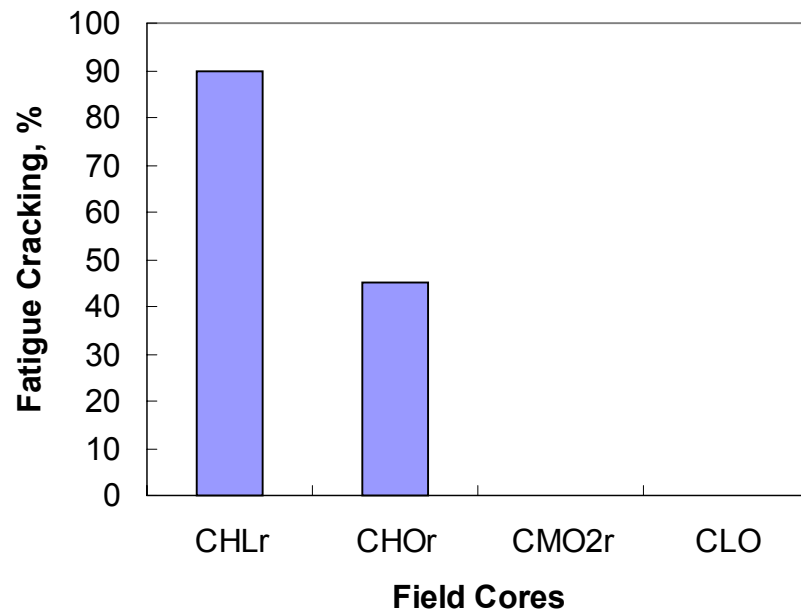


Figure 6.15 Field Performance of Coarse Gradation Sections at 2M EASLs

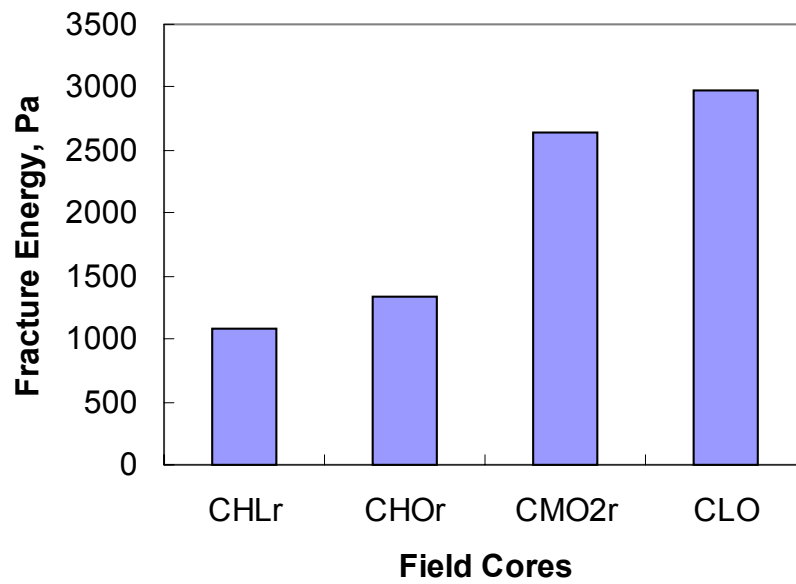


Figure 6.16 Fracture Energies of Coarse Gradation Mixtures

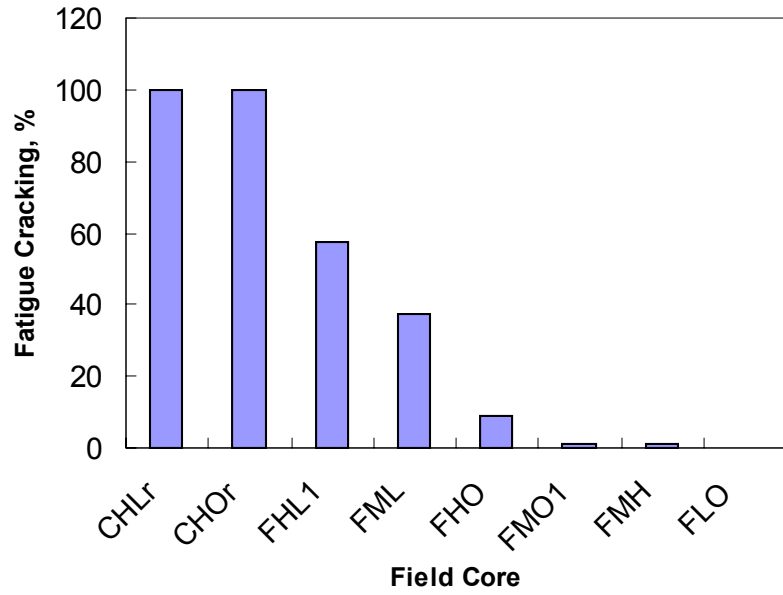


Figure 6.17 Field Performance of Both Fine and Coarse Gradation Sections at 5M EASLs

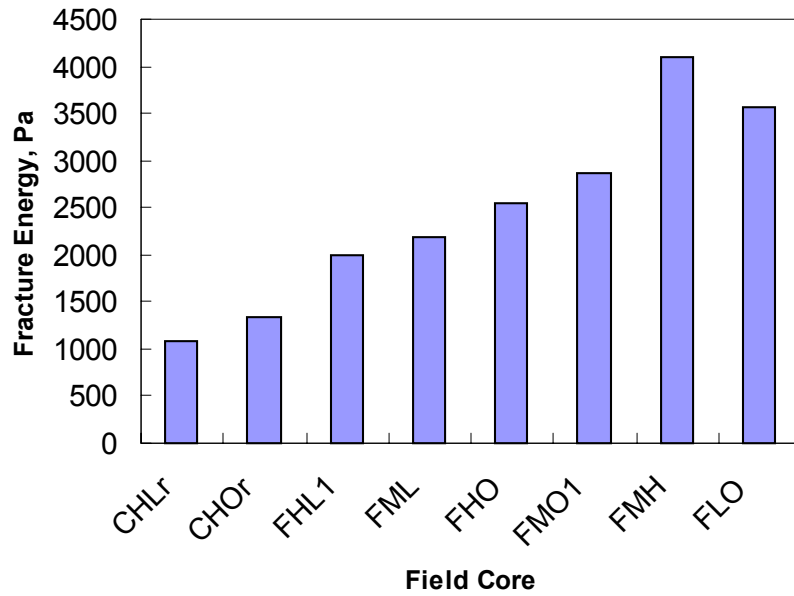


Figure 6.18 Fracture Energies of Both Fine and Coarse Gradation Mixtures

Figure 6.19 shows the direction of regression using a modified logit model. A fairly high correlation was obtained ($R^2=0.94$). It is noteworthy that the regression is based on the amount of fatigue cracking at 5 million ESALs and that fracture energy is obtained from indirect tensile strength testing at a rate of ram movement 50.8 mm per minute at 20°C. Therefore, the relationship in Equation (6.5) is a function of traffic volume, test temperature, and rate of ram movement in indirect tensile strength testing.

As previously stated, fracture energy consists of strain energy and damage energy, as shown in Figure 6.6. Figures 6.20 and 6.21 show the relationship between fatigue cracking and strain energy and damage energy, respectively. Both strain energy and strain energy could be highly correlated to the amount of fatigue cracking.

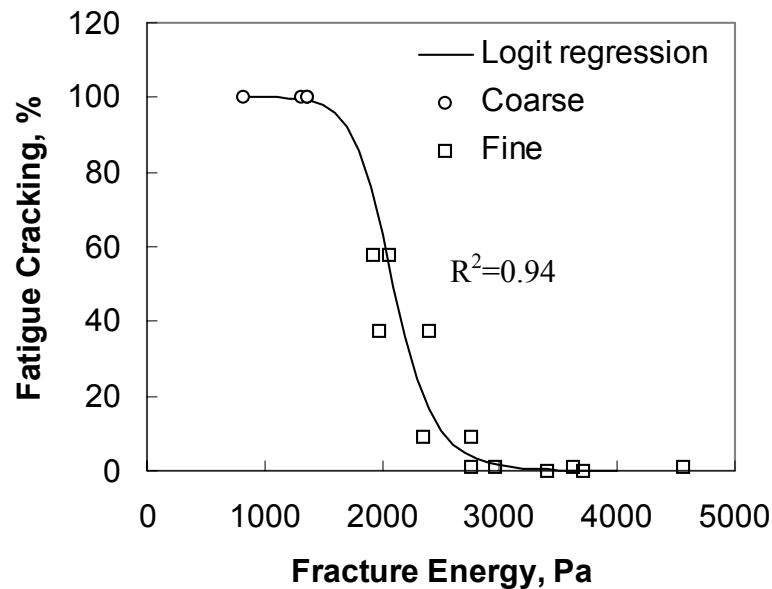


Figure 6.19 Relationship between Field Performance and Fracture Energy

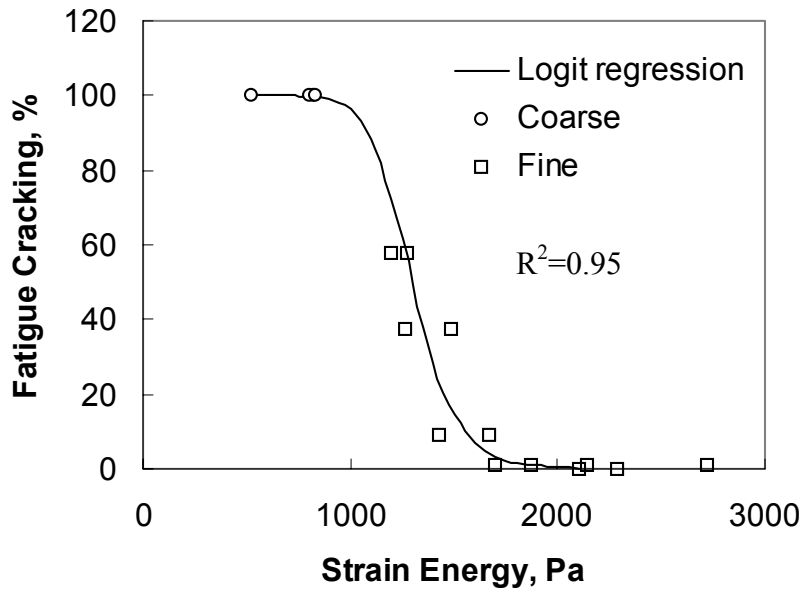


Figure 6.20 Relationship between Strain Energy and Field Performance

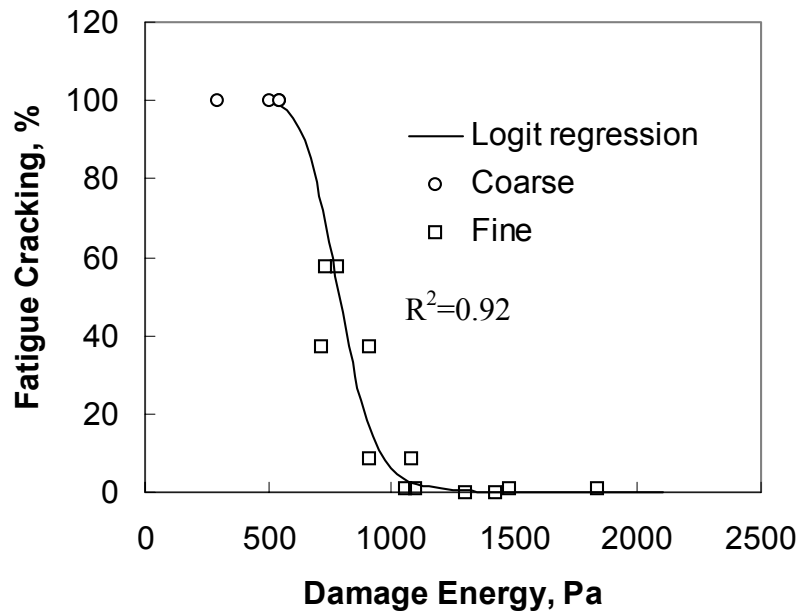


Figure 6.21 Relationship between Damage Energy and Field Performance

The regression coefficients, a and b, in Equation (6.5) are listed in Table 6.2, as follows:

Table 6.2 Regression Coefficients in Equation (6.2)

	TE	SE	DE
a	11.9	12.39	11.29
b	91	88.8	75.3

CHAPTER 7

CONCLUSION AND RECOMMENDATIONS

Fracture energy obtained from both LMLC samples and FMFC samples is proven to be an excellent indicator of the resistance of mixture to fatigue cracking. The fracture energy is calculated using the strain at the center of the specimen, which is determined from displacements with 50.8mm gauge length using the linear viscoelastic solutions. Before indirect tensile strength testing, indirect tensile creep testing must be conducted to obtain Poisson's ratio to calculate center strain. The combination of the indirect tensile creep test and strength test serve as an ideal simple performance test, for the following reasons:

1. Fracture energy from an indirect tensile creep test and strength test is a fundamental mechanical property that is associated with work potential theory based on the thermodynamic of irreversible process, thus satisfying the requirement of a simple performance test; that is, to measure an engineering property that may be linked to advanced material characterization methods.
2. A mixture response parameter, fracture energy, may be an accurately and reliably measured property that is highly correlated to the occurrence of pavement fatigue cracking.
3. Samples compacted by the Superpave Gyratory Compactor may be used in indirect tensile creep and strength testing, providing reliable information about the performance of the HMA mixture during the volumetric design process using SGC.

4. Indirect tensile creep and strength testing may be readily used and are time-saving. Indirect tensile creep testing needs 200 seconds while strength testing takes only several seconds with a rate of ram movement 50.8 mm per minute.

Some additional important findings from this study are as follows:

1. The method to calculate creep compliance based upon the theory of viscoelasticity was developed and was proven to be accurate by 3-D finite element viscoelastic analysis and other tests. Equation (5.17) is applicable to specimens with different diameter and gauge lengths.
2. The method to convert the measured displacements across the gauge length into the center strain was developed and was verified by 3-D finite element viscoelastic analysis. Equation (5.19) is applicable to specimens with different diameter and gauge lengths.
3. The theory of viscoelasticity was applied to indirect tension specimens successfully. The hysteretic stress-strain relationship disappeared when physical strain was replaced by pseudo-strain, thus indicating that the theory of viscoelasticity is applicable to a biaxial stress state.
4. Schapery's work potential theory provides the fundamental principles necessary to characterize the fatigue behavior of asphalt concrete.

Although this study was successful in developing a simple performance test based upon Schapery's work potential theory, further research is recommended to validate the developments, as follows:

1. A greater variety of mixtures, besides WesTrack mixtures, should be used to validate the development of a simple performance test. WesTrack mixtures are the

combinations of different aggregate gradations, asphalt contents, and air void contents. However, only one binder was used. Different binders, including modified, should be used to expand the range of applicability of the simple performance test developed here.

2. The relationship between fracture energy and field performance was established based on the WesTrack pavement field performance only. Indirect tensile strength testing at different test temperatures and different rates of ram movement is recommended to build a stronger model. In addition, more field performance data from other pavement sections should be used.

Reference

- Epps, J. (1998) Performance of HMA Test Sections at WesTrack. *Proceedings, The Association of Asphalt Paving Technologist*, pp738-782
- Chehab, G., E.N., Q'Quinn, and Y.R. Kim (2000). Specimen Geometry Study for Direct Tension Test Based on Mechanical Tests and Air Void Variation in Asphalt Concrete Specimens Compacted by Superpave Gyrotory Compactor. *Transportation Research Record*, TRB, No, 1723, pp. 125-132
- Hand, A. (1998). Relationship Between Laboratory-Measured HMA Material and Mixture Properties and Pavement Performance at WesTrack. PhD Dissertation, University of Nevada, Reno, NV
- Hondros, G. (1959). Evaluation of Poisson's Ratio and the Modulus of Materials of a Low Tensile Resistance by the Brazilian (Indirect Tensile) Test with Particular Reference to Concrete. *Austr. J. Appl. Sci.*, Vol. 10, No. 3, 243-268.
- Huang, Y. H. (1993). Pavement Analysis and Design. Prentice Hall, New Jersey
- Jacobs, M. M. J, P. C. Hopman, and A.A.A. Molenaar (1996). Application of Fracture Mechanics Principles to Analyze Cracking in Asphalt Concrete.
- Jacobs, M.M.J., P.C. Hopman, & A.A.A. Molenaar, (1996) "Application of Fracture mechanics Principles to Analyze in Asphalt Concrete." *Journal of the Association of Asphalt Paving Technologists*, Vol. Pp. 1-39.
- Kennedy, T. (1977). Characterization of Asphalt Pavement Materials Using the Indirect Tensile Test. *Proceedings, The Association of Asphalt Paving Technologist*, pp. 321-150
- Kim, Y.R. and D.N. Little (1990). One-dimensional constitutive modeling of asphalt concrete, *Journal of Engineering Mechanics*, ASCE, Vol. 116, No. 4, pp. 751-772.
- Kim, N. (1994). Development of Performance Prediction Models for Asphalt Concrete Layers, Ph.D. Dissertation, North Carolina State University, Raleigh, NC.
- Kim, Y.R., Y.C. Lee, H.J. Lee (1995). Correspondence Principle for Characterization of Asphalt Concrete, *ASCE Journal of Materials in Civil Engineering*, Vol. 7, No. 1, pp. 59-68.
- Kim, Y.R., H.J. Lee, and D.N. Little (1997). Fatigue Characterization of Asphalt Concrete Using Viscoelasticity and Continuum Damage Theory, *Journal of the*

Association of Asphalt Paving Technologists, Vol. 66, pp. 520-569.

- Lee, H.J. (1996) Uniaxial Constitutive Modeling of Asphalt Concrete Using Viscoelasticity and Continuum Damage Theory, PhD Dissertation, North Carolina State University, Raleigh, NC.
- Lee, H.J. and Y.R. Kim (1997). A Uniaxial Viscoelastic Constitutive Model for Asphalt Concrete under Cyclic Loading, *ASCE Journal of Engineering Mechanics*, Vol. 124, No. 1, pp. 32-40.
- Lee, H.J. and Y.R. Kim (1998). A Viscoelastic Continuum Damage Model of Asphalt Concrete with Healing, *Journal of Engineering Mechanics*, ASCE
- McGraw, E.O. (2000). Quality Control in Fabricating and Testing Laboratory Asphalt Concrete Specimens, M.S. Thesis, North Carolina State University, Raleigh, NC.
- M.L. Williams, R.F. Landal, and J.D. Ferry, "The Temperature Dependence of Relaxation Mechanisms in Amorphous Polymers and Other Glass Forming Liquid", *The Journal Of The American Chemical Society*, Vol. 77 (1955).
- Park, S.W., Y.R. Kim, and R.A. Schapery (1996). A Viscoelastic Continuum Damage Model and Its Application to Uniaxial Behavior of Asphalt Concrete, *Mechanics and Materials*, Vol. 24, No. 4, pp. 241-255.
- Park, S.W. and R.A. Schapery (1997). A Viscoelastic Constitutive Model for Particulate Composites with Growing Damage, *International Journal of Solids and Structures*, Vol. 34, No. 8, pp. 931-947.
- Roque, R. and Buttlar W.G. (1992). The Development of a Measurement and Analysis System to Accurately Determine Asphalt Concrete Properties Using the Indirect Tensile Mode, *Proceedings, The Association of Asphalt Paving Technologist*, pp. 304-333.
- Roque, R. and Zhang, Z.W. and Sankar, B. (1999) Determination of Crack Growth Rate Parameters of Asphalt Mixtures Using the Superpave IDT, *Proceedings, The Association of Asphalt Paving Technologist*, pp. 404-434.
- Schapery, R.A. (1975). A Theory of Crack Initiation and Growth in Viscoelastic Media, Part I: Theoretical Development, Part II: Approximate Methods of Analysis, Part III: Analysis of Continuous Growth, *Int. J. Fracture*, 11, 141-159, 369-388, pp. 549-562.
- Schapery, R.A. (1984). Correspondence Principles and a Generalized J Integral for Large Deformation and Fracture Analysis of Viscoelastic Media, *Int. J. Fracture*, 25, pp. 195-223.

- Schapery, R.A. (1987a). Deformation and Fracture Characterization of Inelastic Composite Materials Using Potentials, *Polymer Eng. and Sci.*, 27, pp. 63-76.
- Schapery, R.A. (1990). A Theory of Mechanical Behavior of Elastic Media with Growing Damage and Other Changes in Structure. *J. Mech. Phys. Solids*, 38, pp.215-253, 1990
- WesTrack (2000). WesTrack Project Overview, Part III. Draft 1: February 1.
- Wijk, G. (1978). Some New Theoretical Aspects of Indirect Measurements of the Tensile Strength of Rocks. *Int. J. Rock Mech. Min. Sci. & Geomech. Abstr.* Vol 15, pp 149-160
- Wen H.(2001). Fatigue Performance Evaluation of WesTrack Asphalt Mixtures Based on Viscoelastic Analysis of Indirect Tensile Test, submitted to Association of America Paving Technologist (2002).
- Zhang, Z.W. and Roque, R. and Birgisson, B. (2001). Evaluation of Laboratory Measured Crack Growth Rate for Asphalt Mixtures, *Transportation Research Board*, Washington, D.C. 2001

Appendix A

Specimen Fabrication

Mixing

1. Batch aggregate into pan. Make one batch of 4500 grams. Set oven to 12°C higher than mixing temperature. Cover with foil and place in oven overnight.
2. Place asphalt in oven 2 hours prior to desired mixing time. Pry top of asphalt can off to avoid a build-up in pressure. In addition, place specimen mold, spoon, spatula, whip, 4 bowls, end plates, and mixing bowl in oven.
3. Turn compactor on. Make sure to turn power on before turning air pressure on.
4. Place asphalt on heating plate and place in probe. Stir frequently until temperature reads the mixing temperature.
5. Place whip on mixer.
6. Place mixing bowl on scale and tare. Pour aggregates in bowl. Pour asphalt in with aggregate. Cover asphalt with aggregates.
7. Set mixing time to 2 minutes. Begin mixing. After 1 minute scrape bowl and whip. Continue mixing for remaining time.
8. After mixing, place mixture back in the oven. Ensure it is evenly spread out on the pan.
9. Put whip, mixing bowl, and all utensils back in oven. Wait five minutes and repeat 5-8 with second batch.
10. Reduce temperature to curing temperature and stir asphalt every hour for four hours.

11. Place asphalt mixture into bowl. Place back in oven and raise the temperature of the oven to compaction temperature.

Compaction

12. Check to ensure temperature has reached compaction specification.
13. Remove mold from oven and place paper in bottom. Place mixture in bowl in mold and rod material.
14. Place paper on top of material followed by a metal plate
15. Set the compaction effort to achieve a predetermined height. Record number of gyrations and test number.

Remove specimen from mold and allow to cool.

Appendix B

Matlab Code to Convert Creep Compliance into Relaxation Modulus

```
% This cod is to convert creep compliance into relaxation modulus

G=zeros(size(D,1),size(D,1));

D0=0.05;

n=-0.4934

for i=1:size(D,1);
    G(i,i)=(D(i,2))^(n);
end

for i=1:3;

tau(i)=10^(i-0);

for j=1:size(D,1)

A1(i,j)=(1+tau(i)/D(j,1))^n;

end

end

A=A1*G*A1';

C=A1*G*(D(:,2)-D0);

B=A\C;

for i=1:size(D,1)

PLS(i)=D0+sum(B'.*(1+tau/D(i,1)).^n);

end

for i=1:200

TT(i)=10^(i/20-5);

dpls(i)=D0+sum(B'.*(1+tau/TT(i)).^n);

end

for i=1:20
```

```

beta0=[1 1];
beta=Nlinfit_2(TT(1,(i*10-9):i*10),dpls(1,(i*10-
9):i*10),'POWER1',beta0);
Tt(i)=TT(1,(i*10-5));
Dpls(i)=beta(1)*TT(1,i*10-5)^beta(2);
Epls(i)=sin(beta(2)*pi)/(beta(2)*pi)/Dpls(i);
end
loglog(D(:,1),D(:,2),'o',TT,dpls,Tt,Dpls,'*',Tt,Epls,'+')
W=zeros(20,20);
for i=1:20
W(i,i)=1/Epls(i);
for j=1:9
taul(j)=2*10^(j-5);
AA(i,j)=exp(-Tt(i)/taul(j));
end
end
AAA=AA'*W*AA;
CC=AA'*W*(Epls-Epls(20))';
BB=AAA\CC;

for i=1:200;
T(i)=10^(i/10-10);
ppls(i)=Epls(20)+sum(BB'.*(exp(-T(i)./taul)));
end;
hold on;loglog(T,ppls)
E=[Epls(20);BB]

```

Matlab Code to Calculate Pseudo Strain

```
in7_2_2;

N=size(Cyclic(:,1),1)

beta0=[0.001 0.001 -0.001 -0.001];

beta=Nlinfit_2(Cyclic(1:N,1),Cyclic(1:N,3), 'Cyc',beta0);

alpha0=[100 100 1];

alpha=Nlinfit_2(Cyclic(1:N,1),Cyclic(1:N,2), 'Load',alpha0);

LOAD=alpha(1)+alpha(2)*cos(2*pi*10*Cyclic(1:N,1)+alpha(3));

f=beta(1)+beta(2)*Cyclic(1:N,1)+beta(3)*cos(2*pi*10*Cyclic(1:N,1)+beta(
4));

Cyclic(1:N,1)/1e-4)+beta(4)*exp(-Cyclic(1:N,1)/1e-3)+beta(5)*exp(-
Cyclic(1:N,1)/1e-2)+beta(6)*exp(-Cyclic(1:N,1)/1e-1)+beta(7)*exp(-
Cyclic(1:N,1)/1e0)+beta(8)*exp(-Cyclic(1:N,1)/1e1)+beta(9)*exp(-
Cyclic(1:N,1)/1e2)+beta(10)*exp(-Cyclic(1:N,1)/1e3)+beta(11)*exp(-
Cyclic(1:N,1)/1e4)+beta(12)*exp(-
Cyclic(1:N,1)/1e5)+beta(13)*cos(2*pi*10*Cyclic(1:N,1)+beta(14));
```

Code to Convert Relaxation Modulus Numerically

```
function x=fem1(y);
persistent L a;
for m=1:12;
I=1e-10*10^(m-2);
L(m)=I*10000;
for i=1:10000;
y(i)=f(i*I);
end ;
for j=1:10000;
if j==1;
x(1)=(3-y(1)/f(0))/(f(0)+y(1));
else
for i=1:j-1;
if i==1;
g(i)=(x(i)+1/f(0))*(y(j-i)+y(j-i+1))*I;
else
c=(x(i)+x(i-1))*(y(j-i)+y(j-i+1))*I ;
g(i)=g(i-1)+c ;
end
end;
x(j)=-x(j-1)+(4*j*I-g(j-1))/(f(0)+y(1))/I;
end;

end;
a(m)=x(10000);
loglog(L,a,'-');
end
```

```
save a a -ascii
```

```
save L L -ascii
```

```
function a=f(t);
```

```
BB=[-0.0012
```

```
    0.0133
```

```
    0.0247
```

```
    0.0557
```

```
    0.2021
```

```
    0.7873
```

```
    1.7366
```

```
    6.2150
```

```
    6.2454
```

```
    0.4585
```

```
    0.1946];
```

```
tau1=[ 2e-5 2e-4 2e-3 2e-2 2e-1 2 20 200 2000 20000 2e5]' ;
```

```
a=0.05+sum(BB.*(1-exp(-t./tau1)));
```